THERMAL CONDUCTION IN NANOSCALE SYSTEMS

Zeng Nan

NATIONAL UNIVERSITY OF SINGAPORE

2008

THERMAL CONDUCTION IN NANOSCALE SYSTEMS

Zeng Nan

A THESIS SUBMITTED
FOR THE DEGREE OF DOCTOR OF PHILOSOPHY
DEPARTMENT OF PHYSICS
NATIONAL UNIVERSITY OF SINGAPORE

2008

I certify that I have read this dissertation and that, in my opinion, it is fully adequate in scope and quality as a dissertation for the degree of Doctor of Philosophy.

(Wang Jian-Sheng) Principal Adviser

Approved for the University Committee on Graduate Studies.

Acknowledgments

First and foremost, I would like to thank my supervisor, Prof. Jian-Sheng Wang. His insightful opinions and suggestions are most valuable to me. Without him, this thesis can not be completed.

I am indebted to my colleagues, Jian Wang and Jingtao Lü, who have provided a lot of help and suggestions on my research work.

I am grateful to Prof. Baowen Li, who is so kind to write a recommendation letter for me for my postdoc job position.

I would also like to express my gratitude to Yung Shing Gene, our system administrator, for his assistance and prompt response to any problems I met when running programs. I sincerely thank Lim Joo Guan, our hardware administrator, for his kindness and help on various issues.

I would like to thank Department of Physics and all the secretaries for numerous assistance on various issues. Especially, I am obliged to Teo Hwee Cheng, Sng Wee Lee and Teo Hwee Sim.

Finally, I would like to thank my parents. Their constant supports have helped me pass many difficult times.

Abstract

In recent years, the advance of technology has made nanoscale devices possible. Thus there are increasing demands to understand the thermal transport properties of nanoscale materials. Compared to large scale systems, where bulk properties are dominant, nanoscale systems usually have limited dimension in one or two directions. This limitation incurs novel properties which do not present in bulk systems, thus special treatment is required.

In a three-dimensional mass system, the thermal conductivity is temperature dependent and system size independent. However, It is found that in low-dimensional systems, the thermal conductivity is size dependent and there is a power law relation between the thermal conductance and the system size. Various interpretation has been given for this phenomenon and for different models studied, the power index is often different. The first part of this thesis is thus trying to find out the underlying mechanism that determines the value of this power index. Classical molecular dynamics method is used in this part as it is suitable for studying many-body systems at relatively high temperatures. A quasi one-dimensional chain model is chosen to simulate a realistic high density polyethylene chain. The Nosé-Hoover heat baths are applied to the ends of the chain to maintain a temperature gradient across the system. The atoms in the chain move according to Newton's laws with nearest neighbor interactions. The thermal flux is then calculated to give the thermal conductance of

the system. We found that the value of the power index depends on the tension exerted on the chain. With greater tension force, the system approaches a linear chain with increasing thermal conductance. This result suggests a simple way to control the thermal conductance of a low-dimensional system.

In the second part of the thesis, a nonequilibrium Green function method is used to calculate the thermal conductance of a system. This quantum mechanical treatment enables us to deal with systems at both low and high temperatures properly. The Green functions are solved using both equation of motion method and perturbation method. Nonlinear interactions are included in the derivation, which are essential for systems at high temperatures. Feynman diagrams are used to simplify the calculation. The thermal flux is derived and it is similar to the Caroli formula except for the nonlinear term. An effective transmission function is also defined. We have applied this method to investigate the thermal rectification effect of a one-dimensional chain system. This effect is observed for systems with asymmetrical structure and nonlinear interactions. We found that by modifying phonon frequency band in the transmission material, thermal rectification can be achieved. Our results provide a general guide to design real solid state thermal rectifiers.

Contents

List of Figures

List of Publications

J.-S. Wang, J. Wang, N. Zeng, "Nonequilibrium Green's function approach to mesoscopic thermal transport," Phys. Rev. B 74, 033408 (2006).

J.-S. Wang, N. Zeng, J. Wang, C. K. Gan, "Nonequilibrium Green's function method for thermal transport in junctions," Phys. Rev. E 75, 061128 (2007).

N. Zeng, J.-S. Wang "Thermal rectification in one-dimensional chains" (in press)

Chapter 1

Introduction

The advance of nanotechnology has made manufacturing of nanodevices possible. Nanodevices are devices at the scale of nanometers, i.e. $10^{-9}m$. Their potential to be used in various fields, such as the computer industry, medical instrument production and others has invoked an increasing demand to have a deeper understanding of their particular electrical and thermal transport properties.

The thermal transport properties of materials are reflected in their thermal conductivities. Whenever there is a temperature difference across a system, there is thermal flux. Heat energy flows from a region of higher temperature to a region of lower temperature. In an isolated system without heat sources or heat sinks, this process will eventually make it reach thermal equilibrium state. By applying heat baths to the system, the system will instead come to a steady state. In a bulk macroscopic system, the heat flux can be calculated by the phenomenological Fourier's Law $\mathbf{J} = -\kappa \boldsymbol{\nabla} T$. Here $\mathbf{J}$ is the heat current, which is the energy that crosses a unit area in a unit time, $\boldsymbol{\nabla} T$ is the temperature gradient, which specifies a temperature difference between different locations, and κ is the thermal conductivity. κ is usually temperature dependent and is a scalar if the system is isotropic or a tensor otherwise.

To understand the underlying mechanism that governs thermal conductivity, we

need to start from the atomic level, where heat energy is carried by phonons and electrons. For insulators, phonons play a major role in thermal transport, while in metals, electrons' effect is also important. Theoretically, for an infinite crystal with purely harmonic interactions between phonons, as is well known, no temperature gradient exists and the thermal conductivity is infinite. However, for mundane materials, their thermal conductivities are always finite. It has been pointed out already that there are three main factors for this result [1, 2]. Firstly, there are always various defects, like mass differences caused by isotopes, dislocations, impurities and so on, which will cause scattering of the heat carriers, thus reduce the thermal conductivity of the material. Secondly, the size of the material is finite. The surface of the material will cause scattering too. A famous example is Kapitza resistance [3, 4], which causes temperature discontinuities at the interface between different materials. Finally, there are anharmonic interactions, the so called Umklapp processes are usually essential for finite thermal conductivity.

Based on the method being used, currently, research on thermal transport can be divided into two categories. One is the classical point of view, where the dynamics of the system follows Newton's law. Molecular dynamics method is heavily used to simulate the actual system. This method is generally very fast and can be used to solve large many body systems. It is applicable for systems under high temperature. For very low temperatures where quantum effects show up, this method is no longer valid, and we need to resort to the second point of view, using quantum transport theory.

In the following sections, works on low-dimensional thermal transport are first reviewed. Then several quantum mechanical method frequently used in quantum transport are discussed. It is followed by current experimental progress on measuring thermal conductivities of nanowires and nanotubes. Finally, the problems faced in the previous works are discussed and the object of this thesis is given.

1.1 Low-dimensional thermal transport

The thermal transport properties of low-dimensional systems have gained great attention in recent years, due to their abnormal behavior compared with macroscale bulk systems. In certain circumstances, the thermal conductivities of low dimensional systems were found to be divergent with $\kappa \propto L^{\alpha}$, where L is the length of the system and $\alpha > 0$. This is contrary to the thermal conductivities of macroscale three dimensional systems where the thermal conductivities are always finite. A thorough understanding of this abnormality is still lacking up to now.

It has been shown [5] that pure harmonic interactions will result in an infinite thermal conductivity without internal temperature gradient, which is caused by the lacking of scattering mechanism. To obtain an internal temperature gradient, nonlinear interactions must be included [6]. The simplest model of this type is Fermi-Pasta-Ulam (FPU) model [6, 7]. It includes both cubic and quartic interactions. Numerical calculations on FPU model [7] showed that nonlinear interactions alone is not likely to infer normal thermal transport and the power index $\alpha = 0.4$ was obtained. Grassberger et al.[8] studied the thermal conductivity of a one-dimensional hard-particle gas and obtained a 1/3 power law index, while Casati and Prosen [9] found $\alpha = 1/4$ for the same model. Another model with nonlinear interactions is diatomic Toda model, which has an exponential interaction between neighboring sites. Although previous results [10] suggested no system size dependence of thermal conductivity for this model, a more recent study [11] refuted that result and gave α around 0.35. The authors further argued that the abnormal thermal conductivity should be a common feature for a momentum conserved one-dimensional system. This argument is further reinforced analytically [12, 13] and is consistent with some earlier research on momentum conserved systems. However, the work done by Gendelman and Savin [14], Giardiná et al. [15], Garrido et al. [16] showed that even for systems with conserved

momentum, the thermal conductivity can be finite. Hu et al. [17] studied the Frenkel-Kontorova model, which has harmonic interactions between neighboring sites and also has a sinusoidal potential on each site. By including this external potential to the system, they observed finite thermal conductivity. They thus claimed that the interaction between phonons and the external lattice is essential to obtain the Fourier's law. The ϕ^4 model, which includes a quartic on-site potential in the system Hamiltonian, also presents normal thermal conductivity [18, 19]. Pereira and Falcao [20] studied a weakly connected 1D model with on-site harmonic potential. Their results showed that normal thermal conductivity of this model can be obtained at high temperatures. Another model, so called "ding-a-ling" model [21], also has normal conductivity. It includes hard cores in the chain as scattering center which interact with free particles among them. Li et al. [22] studied the anomalous heat conduction in one-dimensional momentum conserved model using an effective phonon method. They attribute the abnormality of the thermal conductivity to a zero-frequency phonon mode which has infinite mean free path. It does seem that momentum conservation plays an important role in obtaining abnormal thermal conductivity, but it is not the single reason for that.

Besides the interest in looking for an explanation for the one-dimensional anomalous thermal transport, there are also interest in understanding what factors affect the divergence. Dhar [23] discovered that the divergence is boundary dependent. Li and Wang [24] established a connection between the abnormal thermal conductivity and the diffusion in one-dimensional systems. Wang and Li [25] shows that transverse motion results in a 1/3 power law index. Li and Li [26] investigated the temperature dependence in the framework of effective phonon theory.

Some more realistic quasi-one-dimensional systems have also been studied, such as carbon nanotubes [27, 28, 29, 30] and silicon nanowires [31, 32]. It is found that when the diameter of nanotubes is small, with a chirality of $(5, 5)$ for example, a power law

index around 1/3 is obtained, which is similar to the pure one-dimensional case; when the diameter is increased with a chirality $(10, 10)$, the power index is about 0.11 [28]. This shows a trend of decreasing thermal conductivity with reduced diameter, or in another word, with reduced transverse movement as the tension between each site is increased.

There are also research on calculating the thermal conductivity of 2D systems [33, 34, 35, 36, 37, 38, 39, 40]. Various models have been studied, such as 2D FPU model, 2D Toda model, etc. Specifically, a logarithmic divergence was discovered in a 2D FPU model [39, 40].

1.2 Quantum Transport

Almost all the non-equilibrium thermal transport theories work on a similar model. The system usually comprises three parts: a left lead, a central conduction region, and a right lead. The two leads are always thermostated with heat baths, thus maintaining a fixed temperature. They are theoretically semi-infinite in length to suppress any temperature fluctuation due to energy change. The central conduction region is the particular molecule whose thermal transport properties we want to study. When the size of the material is comparable to its phonon mean free path, phonons can no longer be considered as free particles. The interference of phonons comes into play and classical treatments are not valid anymore. Thus, we need quantum theory to study the transport phenomenon. Three methods are used commonly in this field, namely Langevin equation, Landauer formula and non-equilibrium Green's function.

1.2.1 Langevin Equation

The Langevin Equation was devised to study stochastic processes, such as Brownian motions, where random force is needed. The equations of motion of the system

with random force can be solved analytically or numerically. This method provides an effective way to construct heat baths, thus it can be applied to non-equilibrium systems. A quantum form general Langevin equation was studied by Ford et al.[41]. They showed that quantum Langevin equation can be derived rigorously based on some basic principles, such as the second law of thermal dynamics and causality. This technique was later used by Segal et al.[42] to study the thermal conductance of harmonic nanowires. They found that harmonic interactions played a major role in the thermal conduction of relatively short molecular chains. A more recent study [43] applied the general Langevin equation combined with molecular dynamics method to study thermal transport problem, which gives an effective way to study quantum systems by traditional calssical method. Even though the Langevin equation can be applied to study quantum systems, the introduction of random force in the equations of motion makes it a phenomenological equation, as experimental inputs are necessary in most of the cases except for very simple models. In order to have a deeper insight into the problem, it would be better to utilize a more fundamental theory.

1.2.2 Landauer Formula

A more fundamental approach is to use Landauer formula, which was first suggested by Landauer [44] in the study of mesoscopic electrical transport with two terminals. Later, it was generalized to multi-terminals by Buttiker [45], which made this formula more suitable for comparing with experimental results. It was also shown that this formula can be derived from linear response theory [46]. In both cases, only non-interacting electrons were considered. The Landauer formula is widely used for calculating electrical conductance. In recent years, it also found its way to thermal transport. With this formula, Rego and Kirczenow [47] discovered that at low temperatures, a universal thermal conductance quantum $\pi^2 k_B^2 T/3h$ existed, which was later verified by experiments [48]. However, The Landauer formula is only valid for ballistic

regions, where no interactions are considered. In general situations, especially when the temperature is much higher than absolute zero, three-phonon interactions and four-phonon interactions are quite common. These nonlinear interactions are major causes of thermal dissipation. In these cases, other theories more suitable for dealing with interactions should be applied.

1.2.3 Green's Function Method

The historical development

Green's function method, which has its root in quantum field theory [49, 50], has been applied to study many body problems since 1950s [51] or even earlier. Its strength in dealing with interactions between particles makes it a very powerful tool in many body physics.

The Green's function method was originally applied to systems under ground state, where the temperature is zero. It was later expanded to calculate the grand partition function by Matsubara [52]. Matsubara's approach makes the calculation of systems with temperature $T > 0$ possible.

While the Green's function is usually a time dependent function to signify the evolution of the system, it can also be solved through Fourier transformation, where the condition for arriving at a unique solution was given [53].

In solving the transport problems, it is necessary to maintain the conservation laws of energy, momentum, angular-momentum and number of particles, which is essential for a quantitative calculation. This becomes especially important when approximations are applied. Several rules were given in Ref. [54, 55] and some widely used approximations were discussed for a system under external perturbation.

Several attempts to solve the Green's functions using the perturbation procedures

have been made [56, 57], while the most accepted method for solving the Green's functions are given by Ref. [58, 59]. Keldysh developed a diagram approach, which uses Feynman diagrams. Kadanoff and Baym created an equations of motion approach. Both methods are well suitable for studying a dynamic system in nonequilibrium state. They have formed the basis for the following works.

Fujita [60] derived a similar formula which is similar to Ref. [59] using the diagram approach. It was shown that the initial correlation of the Green's function is not important. Its effect fades after some time and the Boltzman's equation can be derived [60].

Based on the general contour ordered Green's function [58], Caroli et al. [61] were able to calculate tunnelling current directly for a nonequilibrium system.

Several review articles were available in 1980s dealing with nonequilibrium Green's function method [62, 63, 64].

Wagner [65] generalized NEGF to arbitrary initial density matrix. Niu et al. [66] derived the equations of motion approach from Keldysh formalism, thus unifying the two different approaches. Meir and Wingreen [67] even derived a Landauer type current formula from Keldysh formalism. It seems that NEGF is truly a fundamental method for quantum transport theory. However, up to now, NEGF method has only been used to study harmonic interactions, no investigation on nonlinear interactions has been made.

In Ref. [68], the authors discussed a formalism to get arbitrary order perturbations of Green's functions, which can be used to study anharmonic interactions in solids. Their treatment only works for equilibrium state systems, and maybe useful for spectrum analysis of real solids. However, no actual application has been done in this paper.

Several studies on electrical transport has been done using nonequilibrium Green's function method [69, 70]. A lead-junction-lead model was studied and nonlinear

interactions in the junction part was included.

Since 2000, the potential of wide application of nanoscale system has intrigued extensive studies on the quantum transport of nanodevices. Several groups have studied nanoscale systems using this method [71, 72, 73, 74, 75, 76] and works on thermal transport also began to emerge [77, 78, 79, 80, 78, 81], where nonequilibrium Green's function method is the major tour in these investigations.

The concept

The concept of Green's function is quite simple. Consider a system at equilibrium. We add in a particle at some time t and remove it at time t'. During this period, the new particle will interact with the other particles in the system, thus causes a perturbation. The system at t' will be in different state from the system at time t. This effect can be represented by correlation functions, which is Green's function. Green's function can be used to calculate the expectation values of any single-particle operator, the exciting spectrum and others.

1.3 Experimental measurements

Measuring the nanoscale thermal conduction requires that a suspended nanostructure must be fabricated. Besides, nanoscale thermometers and nanoscale thermal heaters are also required in order to measure the temperature and provide a heat flow, respectively. The technique to fulfill these requirements are only becoming available in recent years.

Electron-beam lithography has been utilized to fabricate nanoscale suspended devices. Tighe et al. [82] are the first to use this technique to measure the thermal conductivity of GaAs beams below 10K. Using the same technique, Fon et al. [83] measured doped and undoped GaAs beams with a temperature up to 40K.

Kim et al. [84] designed a different device to measure the nanoscale thermal conductivity. In their approach, two silicon nitride membrane islands are suspended by silicon nitride beams. The islands are heated by Pt resistors, which also serve as thermometers. The nanowire to be measured is then placed on the suspended islands to make a bridge. Using this method, the thermal conductivities of individual multiwalled carbon nanotubes [84], single-walled carbon nanotubes [85, 86] and silicon nanowires [87] were measured.

Another way is to apply self-heating 3ω method [88, 89, 90, 91, 92]. The sample is placed between two electrodes. An alternate current with frequency ω flows through the sample. This current causes a 3ω voltage fluctuation. The thermal conductivity of the sample can be obtained by measuring the frequency dependence of the voltage amplitude and its phase shift.

Instead of using the microfabrication technique, Dames et al. [93] developed a hot-wire probe. The selected nanowire is placed between the hot-wire probe and the scanning tunneling microscope (STM) tip. The hot-wire also acts as a thermometer. The thermal conductivity of the selected nanowire can be obtained by measuring the temperature rise of the probe corresponding to the power. Compared with previous methods, this approach has greater flexibility and doesn't involve any microfabrication.

Fujii et al. [94] suggested a new method to measure nanowire thermal conductivity using sample-attached T-type nanosensor, and Pop et al. [95] measured the thermal conductivity of a single-wall carbon nanotube above room temperature by Joule self-heating method.

A measurement on a coated nanotube [96] has been worked out recently and thermal rectification effect at such a scale was observed physically for the first time. It was noted that thermal flux transmits better in the direction of mass decrement, which can not be explained by the wave theory and the authors claimed that the

observed rectification should be related to solitons.

The development of these nanoscale thermal conductivity measurements has made it possible to verify theoretical results from molecular dynamics simulations or quantum mechanical calculations.

1.4 Problems

Molecular dynamics simulation has been intensively used to study thermal transport properties of low-dimensional systems, and the thermal conductivities of one-dimensional models with conserved momentum are found to be divergent corresponding to the system length, as we have reviewed above. The problem is that there are still controversies over the exact value of the power index that signifies the divergence. On the other hand, although molecular dynamics method is good for systems at relatively high temperatures which is above the Debye temperature of the system, it is not reliable for systems at or below the Debye temperature where quantum statistics must be considered. Because of this reason, a quantum mechanical way to study nanoscale thermal transport is necessary.

Even though quantum mechanical methods have been successfully applied to electrical transport studies at various scales, an effective way to investigate thermal transport properties of nanoscale systems with nonlinear interactions is still lacking. The problem presented by the nonlinear interactions can be solved using nonequilibrium Green's function method, which has been solidly established in the electrical transport studies. Thus an extension of this method to be used in thermal transport studies is needed.

1.5 Objectives

The purpose of this thesis is to investigate the thermal transport properties of nanoscale systems. Because of the small length scale, the thermal conductivities of nanoscale systems are quite different from those of macroscale systems. The Fourier's Law, which is a good approximation to thermal transport in macroscale systems, does not always give a finite thermal conductivity in low-dimensional systems. The temperature at such a scale is not well defined too. To treat these problems properly, we need to apply quantum mechanical methods. In this thesis, we will focus on the thermal conductance of insulators, where only phonon-phonon interactions are important. In this way, we avoid the complexity caused by electron-phonon interactions and electron-electron interactions.

This thesis will be divided into two parts. In the first part, classical thermal transport is studied. Molecular dynamics simulation is used to study the relationship of thermal conductance and system length in quasi one-dimensional systems. This is an attempt to solve the long existing controversy over this relationship. The effect of different implementations of heat bath to the thermal conductance will also be touched on. As the molecular dynamics method is based on Newton's Laws, this method cannot be applied to systems at very low temperatures, where quantum theory must be applied.

The second part is on quantum transport theory. After comparing different quantum transport theories currently available, the NEGF method is chosen as the starting point, as this method is the most suitable method for solving transport problems with interactions. However, most theoretical work using this method considered only linear interactions, as nonlinear interactions are quite difficult to solve. Thus, a rigorous treatment of nonlinear interactions is still in demand. A derivation of thermal conductance with nonlinear interactions using the NEGF method will be addressed in

this thesis. After extending this method to the nonlinear region, several concrete models will be studied.

This work on the thermal transport of nanoscale systems may deepen our understanding on the thermal transport properties of low dimensional systems. The general NEGF method derived here should be helpful for further investigations of molecular devices.

Part I

Classical Molecular Dynamics and Heat Transport

Chapter 2

Thermal Conductivity of Polyethylene

2.1 Molecular Dynamics Method

For a large classical system comprised of many particles, it is impossible to solve the dynamical properties analytically. Numerical simulations are necessary in such case. Two major methods are widely used. One is the Monte Carlo method (MC) based on statistical physics and random theory. Another is the molecular dynamics method (MD) based on Newton's laws. The former is usually used when the system is in its equilibrium state. The physical quantities are measured by the ensemble average. However, this method is not suitable for nonequilibrium state. The latter can be used both in equilibrium state and nonequilibrium state, which is its great advantage over MC. Its drawback is that it can only be used in the situation where classical mechanics is applicable, while MC can be used both classically or quantum mechanically. As we are trying to study the thermal dynamic properties of a nanoscale system which is nonequilibrium in its nature, we are left with the MD method.

In its concept, MD method is quite simple. From Newton's law, if there is no

external force exerted on an object, the object will remain still or in constant motion. If there are force on the object, the object will move according to Newton's second law

$$\frac{d\mathbf{p}}{dt} = \mathbf{F}, \tag{2.1}$$

where $\mathbf{p}$ is the momentum of the object and $\mathbf{F}$ is the external force. We also know that

$$\mathbf{p} = m\frac{d\mathbf{x}}{dt}, \tag{2.2}$$

where $\mathbf{x}$ is the coordinate of the object and m is the mass. By solving this set of first order differential equations, with proper initial coordinates and momenta, we are able to obtain the coordinates and momenta of a many body system at any time. Once we know these quantities, it is straightforward to calculate other physical quantities from them. This is the basic ideas of molecular dynamics.

2.1.1 Force field

It is always possible to calculate material's properties directly from first-principles quantum mechanics, such as using Hartree-Fock method or density functional theory. However, these methods are quite time consuming for large systems and become practically impossible most of the time. In this situations, it is always desirable to use some kind of empirical force field, which does not require tedious quantum mechanical calculation. There are various force fields available currently. Some of them are widely used, such as Amber, CHARMM, MM2, MM3, MM4, etc. These force fields are geared towards special applications. For example, Amber and CHARMM are good for proteins, and MM2, MM3, MM4 are particularly for small molecules. For different force fields, they may have different function form, and different parameters. It is usually the case that a particular force field should be chosen for a particular implementation to get results as accurate as possible.

For our application, we have chosen DREIDING force field [97]. This force field has the virtue that it is quite general. It has a general set of parameters that do not change across different applications. Once the atom type is given, all the other parameters are fixed. The atom type depends on the chemical element, the hybridization, implicit hydrogens attached and other specific characteristics of the atom.

Four types of force are usually included in a force field. They are bond stretch force, bond angle force, dihedral angle force, and other long-range force, such as Coulomb force or van der Waals force. The bond stretch force between two atoms has two forms. One is the simple harmonic interaction, which has the potential

$$V_b = \frac{1}{2}k_b(R - R_b)^2. \tag{2.3}$$

Here R is the distance between the two atoms and R_b is the equilibrium distance between them. The force on each atom is the derivative of (2.3), which yields

$$\mathbf{F} = -k_b(1 - \frac{R_b}{R})\mathbf{R}. \tag{2.4}$$

Another form of bond stretch interaction is the Morse function, which has the form

$$V_b = D_b(e^{-\alpha n(R-R_b)} - 1)^2. \tag{2.5}$$

Here n is the bond order. For an $sp2$ hybridization, for example, the bond order is 2. α is determined by

$$\alpha = (\frac{k_b}{2D_b})^{1/2}. \tag{2.6}$$

This ensures that after Taylor expansion, the second order term are the same as the harmonic case.

The equilibrium distance between two atoms is determined by

$$R_{ij}^0 = R_i^0 + R_j^0 - \delta, \tag{2.7}$$

where $\delta = 0.01\mathring{A}$. It is simply an addition of the two atom radii and is subtracted by a small value δ.

The bond angle interaction is the interaction potential between two bonds who share a common atom. The change of the angle between these two bonds will affect the bond angle potential. Assuming that there are three atoms i, j, k, which form bond $\mathbf{R}_{ij}$ and $\mathbf{R}_{jk}$, the bond angle potential has the form

$$V_\theta = \frac{1}{2} C_\theta (\cos\theta - \cos\theta_0)^2, \tag{2.8}$$

where θ is the angle between the two bonds, θ_0 is the equilibrium angle, $C_\theta = k_\theta/(\sin\theta_0)^2$ and k_θ is the parameter when the potential is written in a quadratic form of θ

$$V_\theta = \frac{1}{2} k_\theta (\theta - \theta_0)^2. \tag{2.9}$$

For four adjacent atoms i, j, k, l who form planes ijk and jkl, the torsion between the two planes also contribute energy, which is called the dihedral potential. It has the form

$$V_d = \frac{1}{2} k_d \big\{1 - \cos[n(\phi - \phi_0)]\big\}. \tag{2.10}$$

where n is the periodicity, ϕ is the dihedral angle, and ϕ_0 is the equilibrium dihedral angle. k_d determines the flexibility of the rotation of the two planes, and is called rotation barrier. For a CH_3 group which has periodicity of 3, $n = 3$.

No long-range interactions are considered in our simulation.

2.1.2 Numerical integrations

In molecular dynamics simulations, an essential task is to solve the Hamilton's equations

$$\begin{aligned} \frac{d}{dt}p(t) &= -\frac{\partial}{\partial q}H(p(t),q(t),t), \\ \frac{d}{dt}q(t) &= \frac{\partial}{\partial p}H(p(t),q(t),t), \end{aligned} \tag{2.11}$$

where p and q are generalized momentum and coordinate, respectively. With a proper initial condition, the differential equations (2.11) can be solved using various integration numerical methods [98], such as Runge-Kutta method, predictor-corrector method, Verlet method, etc. In our simulation, we have chosen a variant of Verlet method, i.e. velocity Verlet method. Compared with Runge-Kutta method, it conserves the phase space quite good even after a long simulation, and it is easy to implement.

Verlet method

We first do a Taylor expansion of the coordinates at a time slightly later and earlier

$$\begin{aligned} \mathbf{q}(t+h) &= \mathbf{q}(t) + \frac{h}{m}\mathbf{p}(t) + \frac{h^2}{2m}\mathbf{F}(t) + O(h^3), \\ \mathbf{q}(t-h) &= \mathbf{q}(t) - \frac{h}{m}\mathbf{p}(t) + \frac{h^2}{2m}\mathbf{F}(t) - O(h^3). \end{aligned} \tag{2.12}$$

Their subtraction gives

$$\mathbf{q}(t+h) - \mathbf{q}(t-h) = \frac{2h}{m}\mathbf{p}(t) + O(h^3), \tag{2.13}$$

Thus we get the momentum at time t

$$\frac{\mathbf{p}(t)}{m} = \frac{\mathbf{q}(t+h) - \mathbf{q}(t-h)}{2h} + O(h^3) \tag{2.14}$$

Addition of (2.12) gives

$$\mathbf{q}(t+h) = -\mathbf{q}(t-h) + 2\mathbf{q}(t) + \frac{\mathbf{F}(t)}{m}h^2 + O(h^4). \tag{2.15}$$

which shows that this equation is reversible. We can calculate the coordinate at time t' from t, or we can reverse the process to calculate $\mathbf{q}(t)$ from $\mathbf{q}(t')$. This is an advantage of Verlet algorithm over others, such as Runge-Kutta method.

Velocity Verlet method

A draw back of the Verlet algorithm is that we can not get the velocity and the coordinate at the same time. To solve this problem, we use the improved velocity Verlet method.

Increasing the time step by half, we first expand the momentum at time $t + \frac{h}{2}$ to the momentum at time t. Then we calculate the coordinate $\mathbf{q}(t + \frac{h}{2})$ based on $\mathbf{q}(t)$ and the new momentum $\mathbf{p}(t + \frac{h}{2})$, which yields

$$\begin{aligned} \mathbf{p}(t + \frac{h}{2}) &= \mathbf{p}(t) + \frac{h}{2}\mathbf{F}(\mathbf{q}(t)) + O(h^2) \\ \mathbf{q}(t + \frac{h}{2}) &= \mathbf{q}(t) + \frac{h}{2m}\mathbf{p}(t + \frac{h}{2}) + O(h^2). \end{aligned} \tag{2.16}$$

In the second half step, we calculate $\mathbf{q}(t + h)$ based on $\mathbf{q}(t + \frac{h}{2})$ and $\mathbf{p}(t + \frac{h}{2})$, and

$\mathbf{p}(t+h)$ based on $\mathbf{p}(t+\frac{h}{2})$ and $\mathbf{q}(t+h)$. The equations are

$$\begin{aligned}\mathbf{q}(t+h) &= \mathbf{q}(t+\frac{h}{2}) + \frac{h}{2m}\mathbf{p}(t+\frac{h}{2}) + O(h^2) \\ \mathbf{p}(t+h) &= \mathbf{p}(t+\frac{h}{2}) + \frac{h}{2}\mathbf{F}(\mathbf{q}(t+h)) + O(h^2)\end{aligned} \tag{2.17}$$

Combine (2.16) and (2.17), we have

$$\begin{aligned}\mathbf{q}(t+h) &= \mathbf{q}(t) + \frac{h}{m}\mathbf{p}(t) + \frac{h^2}{2m}\mathbf{F}(\mathbf{q}(t)) + O(h^2) \\ \mathbf{p}(t+h) &= \mathbf{p}(t) + \frac{h}{2}\{\mathbf{F}(\mathbf{q}(t)) + \mathbf{F}(\mathbf{q}(t+h))\} + O(h^2).\end{aligned} \tag{2.18}$$

This is the velocity Verlet algorithm. With this algorithm, we can calculate the momentum and the coordinate at the same time step by step. Moreover, this algorithm preserves the phase space volume, which is highly desirable in the numerical simulation.

2.2 Heat Bath

Heat bath, which is also called thermostat, is essential in a constant temperature molecular dynamics simulation, such as NVT or NPT simulation, where the number of particles, the volume or pressure of the system, and the temperature remain constant. The heat bath maintains a fixed temperature for a particular part of the system. It works by adding an additional force term to the system Hamiltonian. This additional force interacts with the system particles. The particle's momentum is adjusted corresponding to the target temperature. If the momentum is too large, it will be reduced. If it is too small, it will be increased.

Generally, there are two kinds of heat bath implementations. They are differentiated by the property of the force term. If the force is random, the heat bath is called

stochastic heat bath, otherwise, deterministic heat bath. Deterministic heat bath is preferred as it is time reversible and the final results can be repeated. A most popular deterministic heat bath is the Nosé-Hoover thermostat.

The original Nosé-Hoover thermostat [99] depends on the assumption that the system is ergodic, i.e. the time average of a physical quantity is the same as its ensemble average. When the system is small enough (only a few particles, for example [100]) that ergodic assumption can not be applied, Nosé-Hoover thermostat can not generate canonical distribution successfully. Thus a modification of Nosé-Hoover thermostat, so called Nosé Hoover chain method, is suggested [101]. It works well for small non-ergodic systems. This is the thermostat we used in our simulation as it is an improvement to the previous Nosé-Hoover thermostat. The Hamiltonian of the system is

$$H = \sum_{i=1}^{N} \frac{\mathbf{p}_i^2}{2m} + \sum_{i=1}^{M} \frac{p_{\zeta_i}^2}{2Q_i} + \phi(\mathbf{r}) + N_f kT\zeta_1 + kT\sum_{i=2}^{M}\zeta_i \tag{2.19}$$

where M is the number of thermostats, p_{ζ_i} and ζ_i are the generalized coordinates of the thermostats. The equations of motion are:

$$\begin{aligned}
\dot{\mathbf{r}}_i &= \frac{\mathbf{p_i}}{m} \\
\dot{\mathbf{p}}_i &= \mathbf{F}_i - \mathbf{p}_i\frac{p_{\zeta_1}}{Q_1} \\
\dot{\zeta}_i &= \frac{p_{\zeta_i}}{Q_i} \\
\dot{p}_{\zeta_1} &= \left[\sum_{i=1}^{N}\frac{\mathbf{p}_i^2}{m} - N_f kT\right] - p_{\zeta_1}\frac{p_{\zeta_2}}{Q_2} \\
\dot{p}_{\zeta_j} &= \left[\frac{p_{\zeta_{j-1}}^2}{Q_{j-1}} - kT\right] - p_{\zeta_j}\frac{p_{\zeta_{j+1}}}{Q_{j+1}} \\
\dot{p}_{\zeta_M} &= \left[\frac{p_{\zeta_{M-1}}^2}{Q_{M-1}} - kT\right]
\end{aligned} \tag{2.20}$$

where $Q_1 = N_f kT$ and $Q_j = kT$.

2.2.1 Heat Flux

In order to obtain the thermal conductivity of the junction, we need to calculate the heat flux first, which is the energy transferred across a unit area in a unit time. We know that the continuity equation is

$$\frac{\partial}{\partial t}\rho(\mathbf{r},t) + \boldsymbol{\nabla}\cdot\mathbf{j}(\mathbf{r},t) = 0, \tag{2.21}$$

where $\rho(\mathbf{r},t)$ is the energy density. Our calculation requires a discrete description of this equation. The energy density and heat flux can be discretized as

$$\begin{aligned}\rho(\mathbf{r},t) &= \sum_n \epsilon_n(t)\delta(\mathbf{r}-\mathbf{r}_n),\\ \mathbf{j}(\mathbf{r},t) &= \sum_n \mathbf{j}_n(t)\delta(\mathbf{r}-\mathbf{r}_n),\end{aligned} \tag{2.22}$$

where ϵ_n is the local energy of each atom and $\mathbf{j}_n$ is the local flux [102].

The Fourier transform of the continuity equation (2.21) gives

$$\frac{\partial}{\partial t}\rho(\mathbf{k},t) + i\mathbf{k}\cdot\mathbf{j}(\mathbf{k},t) = 0, \tag{2.23}$$

with $\rho(\mathbf{r},t) = \int \rho(\mathbf{k},t)e^{i\mathbf{k}\cdot\mathbf{r}}d\mathbf{r}$ and $\mathbf{j}(\mathbf{r},t) = \int \mathbf{j}(\mathbf{k},t)e^{i\mathbf{k}\cdot\mathbf{r}}d\mathbf{r}$. Replacing $\rho(\mathbf{k},t)$ and $\mathbf{j}(\mathbf{k},t)$ by their inverse Fourier transformation $\rho(\mathbf{r},t)$ and $\mathbf{j}(\mathbf{r},t)$ gives

$$\frac{\partial}{\partial t}\int \rho(\mathbf{r},t)e^{-i\mathbf{k}\cdot\mathbf{r}}d\mathbf{r} + i\mathbf{k}\cdot\int \mathbf{j}(\mathbf{r},t)e^{-i\mathbf{k}\cdot\mathbf{r}}d\mathbf{r} = 0. \tag{2.24}$$

Now we can replace the continuous form of energy density and heat flux density by

their discrete form (2.22) and obtain

$$\sum_n \frac{\partial \epsilon_n(t)}{\partial t} e^{-i\mathbf{k}\cdot\mathbf{r}_n} + \sum_n \epsilon_n(t)(-i\mathbf{k}) \cdot \frac{\partial \mathbf{r}_n}{\partial t} e^{-i\mathbf{k}\cdot\mathbf{r}_n} + \sum_n i\mathbf{k}\cdot\mathbf{j}_n(t) e^{-i\mathbf{k}\cdot\mathbf{r}_n} = 0. \quad (2.25)$$

As the energy loss rate for atom n should be equal to the energy gain rate of atom $n+1$, the first term of Eq. (2.25) can be written as

$$\begin{aligned}\sum_n \frac{\partial \epsilon_n(t)}{\partial t} e^{-i\mathbf{k}\cdot\mathbf{r}_n} &= \frac{1}{2}\sum_n (\frac{\partial \epsilon_n(t)}{\partial t} - \frac{\partial \epsilon_{n+1}(t)}{\partial t}) e^{-i\mathbf{k}\cdot\mathbf{r}_n} \\ &= \frac{1}{2}\sum_n \frac{\partial \epsilon_n(t)}{\partial t} e^{-i\mathbf{k}\cdot\mathbf{r}_n}(1 - e^{i\mathbf{k}\cdot(\mathbf{r}_n - \mathbf{r}_{n+1})}).\end{aligned}$$

In the long wave length limit, this can be further reduced to

$$\begin{aligned}&\frac{1}{2}\sum_n \frac{\partial \epsilon_n(t)}{\partial t} e^{-i\mathbf{k}\cdot\mathbf{r}_n}(-i\mathbf{k}\cdot(\mathbf{r}_n - \mathbf{r}_{n+1})) \\ =&\frac{1}{2}\sum_n -i\mathbf{k}\cdot\mathbf{r}_n \frac{\partial \epsilon_n(t)}{\partial t} e^{-i\mathbf{k}\cdot\mathbf{r}_n} + \frac{1}{2}\sum_n i\mathbf{k}\cdot\mathbf{r}_{n+1}\frac{\partial \epsilon_n(t)}{\partial t} e^{-i\mathbf{k}\cdot\mathbf{r}_n} \\ \approx&\sum_n -i\mathbf{k}\cdot\mathbf{r}_n \frac{\partial \epsilon_n(t)}{\partial t} e^{-i\mathbf{k}\cdot\mathbf{r}_n}.\end{aligned}$$

Inserting this result into Eq. (2.25), we have

$$\mathbf{j}_n(t) = \frac{\partial}{\partial t}(\epsilon_n(t)\mathbf{r}_n(t)) = \frac{d}{dt}(\epsilon_n(t)\mathbf{r}_n(t)), \quad (2.26)$$

where we have used the total differential form to reflect the fact that $\epsilon_n(t)$ and $\mathbf{r}_n(t)$ are time dependent only.

The relation between the total flux $\mathbf{J}$, flux density $\mathbf{j}$ and local flux $\mathbf{j}_n$ is

$$\mathbf{J} = \int \mathbf{j}\, d\mathbf{r} = \sum_n \mathbf{j}_n = \sum_n \frac{d}{dt}(\mathbf{r}_n(t)\epsilon_n(t)). \quad (2.27)$$

The system's thermal conductivity is calculated from the local heat flux $\mathbf{j}_n$, which should be equal everywhere in a steady state, i.e.

$$\langle \mathbf{j}_n \rangle = \langle \mathbf{j}_{n+1} \rangle = \frac{\mathbf{J}}{N}, \tag{2.28}$$

where $\langle\ \rangle$ stands for a time average $\lim_{T\to\infty} \frac{1}{T} \int_0^T dt$. Eq. (2.27) and (2.28) give us

$$\mathbf{j} \approx \frac{\mathbf{J}}{V} = \frac{N\langle \mathbf{j}_n \rangle}{NaA} = \frac{\langle \mathbf{j}_n \rangle}{aA}, \tag{2.29}$$

where a is the x axis projection of the distance between two adjacent particles and A is the cross section area. With the Fourier's law, it is straightforward that

$$\frac{\langle \mathbf{j}_n \rangle}{aA} = -\kappa \boldsymbol{\nabla} T = -\kappa \frac{\Delta T}{Na} \hat{\mathbf{x}}, \tag{2.30}$$

where $\hat{\mathbf{x}}$ is a unit vector pointing to the thermal flux flow direction. Eq. (2.30) gives $\langle j_n \rangle \propto N^{\alpha-1}$, thus $\kappa \propto N^{\alpha}$, where α is the power law index.

Chapter 3

Molecular Dynamics: Implementation and Application

3.1 Implementations

In this part, we give the exact formulas to be used in the our molecular dynamics program, such as the three kinds of force exerted on each atom, the thermal flux across the system, etc..

3.1.1 Force

In the molecular dynamics simulation, we need to work out the force on each atom. As we have already known the potential form, we can calculate the force by

$$\mathbf{F} = -\boldsymbol{\nabla} V. \tag{3.1}$$

Bond force

For the bond between atoms i and j, the bond potential is

$$V = \frac{1}{2}k(|\mathbf{r}_{ij}| - R_0)^2, \tag{3.2}$$

where $\mathbf{r}_{ij} = \mathbf{r}_i - \mathbf{r}_j$. The force on atom i is

$$\mathbf{F}_i = -\frac{\partial V}{\partial \mathbf{r}_i} = -k(|\mathbf{r}_{ij}| - R_0)\frac{d|\mathbf{r}_{ij}|}{d\mathbf{r}_i} = -k(|\mathbf{r}_{ij}| - R_0)\hat{\mathbf{r}}_{ij}, \tag{3.3}$$

where $\hat{\mathbf{r}}_{ij}$ is the unit vector. The force on atom j is the opposite of $\mathbf{F}_i$, which yields

$$\mathbf{F}_j = k(|\mathbf{r}_{ij}| - R_0)\hat{\mathbf{r}}_{ij}. \tag{3.4}$$

Bond angle force

For the bond angle interaction between bonds ij and jk, we choose the potential in the harmonic form of angle θ as (2.9), i.e.

$$V_\theta = \frac{1}{2}k_\theta(\theta - \theta_0)^2.$$

The derivative of (2.9) gives the force on each atom. The force on atom i is

$$\mathbf{F}_i = -\frac{\partial V_\theta}{\partial \mathbf{r}_i} = -\frac{dV}{d\theta}\frac{d\theta}{d\cos\theta}\frac{d\cos\theta}{d\mathbf{r}_i} = \frac{k_\theta(\theta - \theta_0)}{\sin\theta}\frac{d\cos\theta}{d\mathbf{r}_i} \tag{3.5}$$

From vector analysis, we know that

$$\cos\theta = \frac{\mathbf{r}_{ij}\cdot\mathbf{r}_{kj}}{|\mathbf{r}_{ij}||\mathbf{r}_{kj}|} = \frac{\mathbf{r}_{ij}\cdot\mathbf{r}_{kj}}{r_{ij}r_{kj}} \tag{3.6}$$

The derivative of $\cos\theta$ to $\mathbf{r}_i$ is

$$\frac{d\cos\theta}{d\mathbf{r}_i} = \frac{r_{ij}^2\mathbf{r}_{kj} - (\mathbf{r}_{ij}\cdot\mathbf{r}_{kj})\mathbf{r}_{ij}}{r_{ij}^3 r_{kj}}. \tag{3.7}$$

The derivative of $\cos\theta$ to $\mathbf{r}_k$ is similar to (3.7), where we only need to exchange the subscript i and k to get

$$\frac{d\cos\theta}{d\mathbf{r}_k} = \frac{r_{kj}^2\mathbf{r}_{ij} - (\mathbf{r}_{kj}\cdot\mathbf{r}_{ij})\mathbf{r}_{kj}}{r_{kj}^3 r_{ij}}. \tag{3.8}$$

The total force on the three atoms from this bond angle potential should be zero, which yields

$$\frac{d\cos\theta}{d\mathbf{r}_j} = -\frac{d\cos\theta}{d\mathbf{r}_i} - \frac{d\cos\theta}{d\mathbf{r}_k}. \tag{3.9}$$

This can easily be verified. Combining (3.5), (3.7), (3.8) and (3.9) together, we can get the forces on each atom that is caused by bond angle interactions, which are

$$\mathbf{F}_i = \frac{k_\theta(\theta-\theta_0)}{\sin\theta}\frac{\mathbf{r}_{kj} - (\hat{\mathbf{r}}_{ij}\cdot\mathbf{r}_{kj})\hat{\mathbf{r}}_{ij}}{r_{ij}r_{kj}}, \tag{3.10}$$

$$\mathbf{F}_j = -\frac{k_\theta(\theta-\theta_0)}{\sin\theta}\frac{\mathbf{r}_{ij} - (\hat{\mathbf{r}}_{kj}\cdot\mathbf{r}_{ij})\hat{\mathbf{r}}_{kj} + \mathbf{r}_{kj} - (\hat{\mathbf{r}}_{ij}\cdot\mathbf{r}_{kj})\hat{\mathbf{r}}_{ij}}{r_{ij}r_{kj}}, \tag{3.11}$$

$$\mathbf{F}_k = \frac{k_\theta(\theta-\theta_0)}{\sin\theta}\frac{\mathbf{r}_{ij} - (\hat{\mathbf{r}}_{kj}\cdot\mathbf{r}_{ij})\hat{\mathbf{r}}_{kj}}{r_{ij}r_{kj}}. \tag{3.12}$$

Dihedral torsion

The dihedral torsion force is more complicated. In Fig.3.1, the atoms i, j, k, l form two planes with an angle ϕ. $\mathbf{m}$ and $\mathbf{n}$ are vectors perpendicular to the joint line on each plane. $\mathbf{M}$ and $\mathbf{N}$ are vectors perpendicular to plane ijk and plane jkl respectively. Thus the dihedral angle can be obtained by

$$\cos\phi = \frac{\mathbf{m}\cdot\mathbf{n}}{|\mathbf{m}||\mathbf{n}|}, \tag{3.13}$$

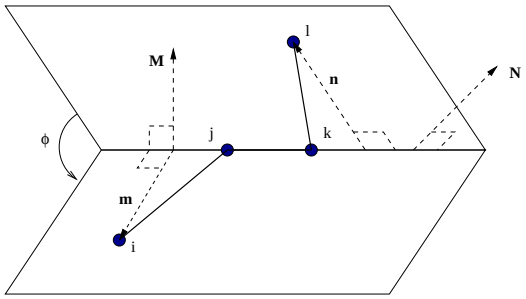

Figure 3.1: An illustration of the dihedral angle potential among four adjacent atoms

where

$$\mathbf{m} = \mathbf{r}_{ij} - (\mathbf{r}_{ij} \cdot \hat{\mathbf{r}}_{kj})\hat{\mathbf{r}}_{kj},$$
$$\mathbf{n} = -\mathbf{r}_{kl} + (\mathbf{r}_{kl} \cdot \hat{\mathbf{r}}_{kj})\hat{\mathbf{r}}_{kj}.$$

We use (2.10) to calculate the dihedral angle force on each atom, which gives

$$\mathbf{F}_\alpha = -\boldsymbol{\nabla}_\alpha V_d(\phi) = -\frac{dV_d(\phi)}{d\phi}\frac{\partial\phi}{\partial\mathbf{r}_\alpha} \tag{3.14}$$

As particle i can move freely on the plane ijk without changing the potential $V_d(\phi)$, the force caused by the dihedral angle potential must be perpendicular to the plane ijk. Let atom i move in the direction of $\mathbf{M}$ with a distance $\Delta r_i = |\mathbf{r}_i' - \mathbf{r}_i|$. The dihedral angle changes by

$$\Delta\phi = \frac{\Delta r_i}{|\mathbf{m}|} = \frac{\Delta r_i}{|\mathbf{r}_{ij} \times \hat{\mathbf{r}}_{kj}|} = \frac{r_{kj}\Delta r_i}{|\mathbf{M}|}, \tag{3.15}$$

where $\mathbf{M} = \mathbf{r}_{ij} \times \mathbf{r}_{kj}$. Thus the force on atom i is

$$\mathbf{F}_i = -\frac{dV_d(\phi)}{d\phi}\frac{\Delta\phi}{\Delta r_i}\hat{\mathbf{M}} = -\frac{dV_d(\phi)}{d\phi}\frac{r_{kj}}{|\mathbf{M}|}\hat{\mathbf{M}} = -\frac{dV_d(\phi)}{d\phi}\frac{r_{kj}}{|\mathbf{M}|^2}\mathbf{M}, \tag{3.16}$$

where $\hat{\mathbf{M}}$ is a unit vector. Similarly, the force on atom l is

$$\mathbf{F}_l = -\frac{dV_d(\phi)}{d\phi}\frac{r_{kj}}{|\mathbf{N}|^2}\mathbf{N}, \tag{3.17}$$

with $\mathbf{N} = \mathbf{r}_{kj} \times \mathbf{r}_{kl}$. To calculate the forces on the atoms j and k on the hinge, we notice that the dihedral potential $V_d(\phi)$ is translation invariant, which means that the total force on all the atoms involved should be zero, ie.

$$\mathbf{F}_i + \mathbf{F}_j + \mathbf{F}_k + \mathbf{F}_l = 0. \tag{3.18}$$

Now we separate the forces into two groups. Let

$$\begin{aligned} \mathbf{F}_j &= -\mathbf{F}_i + \mathbf{A}, \\ \mathbf{F}_k &= -\mathbf{F}_l - \mathbf{A}. \end{aligned} \tag{3.19}$$

As moving the atoms independently along the hinge doesn't change the potential $V_d(\phi)$, all the forces exerted by the dihedral potential should be perpendicular to $\mathbf{r}_{kj}$, which yields $\mathbf{A} \perp \mathbf{r}_{kj}$. Also notice that the dihedral potential is rotation invariant, there is no total torque, thus

$$\mathbf{r}_i \times \mathbf{F}_i + \mathbf{r}_j \times (-\mathbf{F}_i + \mathbf{A}) + \mathbf{r}_k \times (-\mathbf{F}_l - \mathbf{A}) + \mathbf{r}_l \times \mathbf{F}_l = 0. \tag{3.20}$$

(3.20) can be simplified to

$$\mathbf{r}_{ij} \times \mathbf{F}_i + \mathbf{r}_{jk} \times \mathbf{A} + \mathbf{r}_{lk} \times \mathbf{F}_l = 0. \tag{3.21}$$

Let $\mathbf{r}_{kj} \times \mathbf{A} = \mathbf{r}_{ij} \times \mathbf{F}_i - \mathbf{r}_{kl} \times \mathbf{F}_l = \mathbf{B}$. As $\mathbf{A} \perp \mathbf{r}_{kj}$, $\mathbf{A}$ is in the direction of $\mathbf{B} \times \mathbf{r}_{kj}$ and its value $|\mathbf{A}| = |\mathbf{B}|/|\mathbf{r}_{kj}|$. Thus we have

$$\begin{aligned}\mathbf{A} &= \frac{|\mathbf{B}|}{|\mathbf{r}_{kj}|}\frac{\mathbf{B}\times\mathbf{r}_{kj}}{|\mathbf{B}||\mathbf{r}_{kj}|} = \frac{\mathbf{B}\times\mathbf{r}_{kj}}{r_{kj}^2} \\ &= \frac{1}{r_{kj}^2}(\mathbf{r}_{ij}\times\mathbf{F}_i - \mathbf{r}_{kl}\times\mathbf{F}_l)\times\mathbf{r}_{kj} \\ &= \frac{1}{r_{kj}^2}[(\mathbf{r}_{ij}\cdot\mathbf{r}_{kj})\mathbf{F}_i - (\mathbf{r}_{kl}\cdot\mathbf{r}_{kj})\mathbf{F}_l],\end{aligned} \tag{3.22}$$

where we have used $\mathbf{F}_i, \mathbf{F}_l \perp \mathbf{r}_{kj}$ in the last line to remove two terms. (3.19) and (3.22) give us

$$\begin{aligned}\mathbf{F}_j &= \left[\frac{\mathbf{r}_{ij}\cdot\mathbf{r}_{kj}}{r_{kj}^2} - 1\right]\mathbf{F}_i - \frac{\mathbf{r}_{kl}\cdot\mathbf{r}_{kj}}{r_{kj}^2}\mathbf{F}_l \\ \mathbf{F}_k &= -\frac{\mathbf{r}_{ij}\cdot\mathbf{r}_{kj}}{r_{kj}^2}\mathbf{F}_i + \left[\frac{\mathbf{r}_{kl}\cdot\mathbf{r}_{kj}}{r_{kj}^2} - 1\right]\mathbf{F}_l\end{aligned} \tag{3.23}$$

3.1.2 Thermal Flux

The thermal flux is our main targeted physical quantity to calculate in studying the thermal conductivity of nanowires. In Eq. (2.27), a local energy is required, which is the kinetic energy of the particle plus part of the potential. Writing down the differentiation explicitly, we have

$$\mathbf{J} = \sum_i \frac{d}{dt}(\mathbf{r}_i(t)\epsilon_i(t)) = \sum_i \left(\mathbf{v}_i\epsilon_i(t) + \mathbf{r}_i\frac{d\epsilon_i(t)}{dt}\right). \tag{3.24}$$

The local energy $\epsilon_i(t)$ is contributed by the kinetic energy of the atom and the three kinds of potential as discussed in Sec 2.1.1. The derivative of the kinetic part gives us

$$\frac{d}{dt}\frac{\mathbf{p}_i^2(t)}{2m_i} = \frac{\mathbf{p}_i}{m_i}\cdot\frac{d\mathbf{p}_i}{dt}. = \mathbf{v}_i\cdot\mathbf{F}_i = \mathbf{v}_i\cdot(\mathbf{F}_i^b + \mathbf{F}_i^\theta + \mathbf{F}_i^d), \tag{3.25}$$

where $\mathbf{F}_i$ is the total force on the atom, $\mathbf{F}_i^b$, $\mathbf{F}_i^\theta$, $\mathbf{F}_i^d$ are bond stretch force, bond angle force and dihedral force respectively. In fact, the derivative of the local energy can be written in a form as

$$\frac{d}{dt}\epsilon_i(t) = \sum_\alpha \left(\mathbf{v}_i \cdot \mathbf{F}_i^\alpha + \frac{d}{dt} V^\alpha(t) \right) \equiv \sum_\alpha \frac{d}{dt}\epsilon_i^\alpha(t), \tag{3.26}$$

where α stands for a particular potential involved.

For bond potential between atom i and j, the potential is separated equally into the local energy of them, thus we have

$$\begin{aligned} \mathbf{r}_i \frac{d}{dt}\epsilon_i^{b_{ij}}(t) &= \mathbf{r}_i(\mathbf{v}_i \cdot \mathbf{F}_i^{b_{ij}}) + \frac{1}{2}\frac{dV_{ij}^{b_{ij}}}{dt}\mathbf{r}_i \\ &= \mathbf{r}_i(\mathbf{v}_i \cdot \mathbf{F}_i^{b_{ij}}) + \frac{1}{2}\left(\frac{\partial V_{ij}^{b_{ij}}}{\partial \mathbf{r}_i} \cdot \mathbf{v}_i + \frac{\partial V_{ij}^{b_{ij}}}{\partial \mathbf{r}_j} \cdot \mathbf{v}_j \right) \mathbf{r}_i \\ &= \mathbf{r}_i(\mathbf{v}_i \cdot \mathbf{F}_i^{b_{ij}}) - \frac{1}{2}(\mathbf{F}_i^{b_{ij}} \cdot \mathbf{v}_i + \mathbf{F}_j^{b_{ij}} \cdot \mathbf{v}_j)\mathbf{r}_i \\ &= \frac{1}{2}(\mathbf{F}_i^{b_{ij}} \cdot \mathbf{v}_i - \mathbf{F}_j^{b_{ij}} \cdot \mathbf{v}_j)\mathbf{r}_i \end{aligned} \tag{3.27}$$

The total flux through atoms i and j that is contributed by their bond potential is

$$\begin{aligned} \mathbf{J}^{b_{ij}} &= \mathbf{r}_i \frac{d\epsilon_i^{b_{ij}(t)}}{dt} + \mathbf{r}_j \frac{d\epsilon_j^{b_{ij}}(t)}{dt} \\ &= \frac{1}{2}[(\mathbf{F}_i^{b_{ij}} \cdot \mathbf{v}_i - \mathbf{F}_j^{b_{ij}} \cdot \mathbf{v}_j)\mathbf{r}_i + (\mathbf{F}_j^{b_{ij}} \cdot \mathbf{v}_j - \mathbf{F}_i^{b_{ij}} \cdot \mathbf{v}_i)\mathbf{r}_j] \\ &= \frac{1}{2}\mathbf{F}_i^{b_{ij}} \cdot (\mathbf{v}_i + \mathbf{v}_j)\mathbf{r}_{ij}, \end{aligned} \tag{3.28}$$

where we have used the fact that $\mathbf{F}_i^{b_{ij}} = -\mathbf{F}_j^{b_{ij}}$. For each individual atom, the flux is simply one half of $\mathbf{J}^{b_{ij}}$. To write in this form, we only use a relative distance between $\mathbf{r}_i$ and $\mathbf{r}_j$, thus avoid the possibility that $\mathbf{r}_i$ becomes arbitrarily large which increases numerical errors.

The thermal flux induced by the bond angle interaction can be calculated similarly.

A problem arose here is how shall we divide the potential. We can divide the potential equally, or contribute it more to the joint atom, or the other way around. Here we give a general formula. Let atom j be at the joint, then the total potential V^θ is separated into $V_i^\theta = V_k^\theta = \beta V^\theta$ and $V_j^\theta = \alpha V^\theta = (1-2\beta)V^\theta$. The time derivative of the local energy of atoms i, j, k are

$$\frac{d}{dt}\epsilon_i^\theta(t) = \mathbf{v}_i \cdot \mathbf{F}_i^\theta + \beta\frac{dV^\theta}{dt} = (1-\beta)\mathbf{F}_i^\theta \cdot \mathbf{v}_i - \beta\mathbf{F}_j^\theta \cdot \mathbf{v}_j - \beta\mathbf{F}_k^\theta \cdot \mathbf{v}_k, \tag{3.29}$$

$$\frac{d}{dt}\epsilon_j^\theta(t) = \mathbf{v}_j \cdot \mathbf{F}_j^\theta + \alpha\frac{dV^\theta}{dt} = -\alpha\mathbf{F}_i^\theta \cdot \mathbf{v}_i + (1-\alpha)\mathbf{F}_j^\theta \cdot \mathbf{v}_j - \alpha\mathbf{F}_k^\theta \cdot \mathbf{v}_k, \tag{3.30}$$

$$\frac{d}{dt}\epsilon_k^\theta(t) = \mathbf{v}_k \cdot \mathbf{F}_k^\theta + \beta\frac{dV^\theta}{dt} = -\beta\mathbf{F}_i^\theta \cdot \mathbf{v}_i - \beta\mathbf{F}_j^\theta \cdot \mathbf{v}_j + (1-\beta)\mathbf{F}_k^\theta \cdot \mathbf{v}_k. \tag{3.31}$$

The total thermal flux contributed by the bond angle potential for three atoms is thus

$$\begin{aligned}\mathbf{J}^\theta &= \mathbf{r}_i\frac{d}{dt}\epsilon_i^\theta(t) + \mathbf{r}_j\frac{d}{dt}\epsilon_j^\theta(t) + \mathbf{r}_k\frac{d}{dt}\epsilon_k^\theta(t)\\ &= [\mathbf{r}_i - (\beta\mathbf{r}_i + \alpha\mathbf{r}_j + \beta\mathbf{r}_k)]\mathbf{F}_i^\theta \cdot \mathbf{v}_i\\ &\quad + [\mathbf{r}_j - (\beta\mathbf{r}_i + \alpha\mathbf{r}_j + \beta\mathbf{r}_k)]\mathbf{F}_j^\theta \cdot \mathbf{v}_j\\ &\quad + [\mathbf{r}_k - (\beta\mathbf{r}_i + \alpha\mathbf{r}_j + \beta\mathbf{r}_k)]\mathbf{F}_k^\theta \cdot \mathbf{v}_k,\end{aligned} \tag{3.32}$$

which can be readily separated to three parts in this case.

The thermal flux caused by the dihedral angle is similar. The potential is divided as $V_i^d = V_l^d = \beta V^d$, $V_j^d = V_k^d = \alpha V$, and $\alpha + \beta = 1/2$. It has the form

$$\begin{aligned}\mathbf{J}^d &= [\mathbf{r}_i - (\beta\mathbf{r}_i + \alpha\mathbf{r}_j + \alpha\mathbf{r}_k + \beta\mathbf{r}_l)]\mathbf{F}_i^d \cdot \mathbf{v}_i\\ &\quad + [\mathbf{r}_j - (\beta\mathbf{r}_i + \alpha\mathbf{r}_j + \alpha\mathbf{r}_k + \beta\mathbf{r}_l)]\mathbf{F}_j^d \cdot \mathbf{v}_j\\ &\quad + [\mathbf{r}_k - (\beta\mathbf{r}_i + \alpha\mathbf{r}_j + \alpha\mathbf{r}_k + \beta\mathbf{r}_l)]\mathbf{F}_k^d \cdot \mathbf{v}_k\\ &\quad + [\mathbf{r}_l - (\beta\mathbf{r}_i + \alpha\mathbf{r}_j + \alpha\mathbf{r}_k + \beta\mathbf{r}_l)]\mathbf{F}_l^d \cdot \mathbf{v}_l,\end{aligned} \tag{3.33}$$

3.2 Model

We studied the thermal conductivity of a simplified polyethylene chain model which is comprised of connected CH_2 units. The CH_2 units are treated as unified atoms. The bond interaction force constant is set to $k_b = 700$ (kcal/mol)/Å^2. The force constant of bond angle potential is $k_\theta = 100$ (kcal/mol)/rad^2, with $\theta_0 = 1.91$rad, For the dihedral potential, we set $k_d = 2.0$ kcal/mol, $n_{jk} = 3$, and $\phi_0 = 180°(or\ 60°)$. The values of these parameters are adapted from Mayo et al.[97].

The Hamiltonian of the chain is thus

$$H = \sum_i^N \frac{\mathbf{p}_i^2}{2m} + \sum_i V_{i,i+1} + \sum_i V_{i-1,i,i+1} + \sum_i V_{i,i+1,i+2,i+3}, \tag{3.34}$$

where the second term represents the bond interactions, the third term denotes the bond angle interactions and the last gives the dihedral interactions.

The program is implemented in such a way that the positions, velocities and forces are recorded in every unit step. The time step size is usually set to 0.01, thus a unit step corresponds to $1/dt = 100$ time steps. The units used in the program are kcal for energy, g for mass and Å for length. From these units we can derive a single time step corresponding to 48.8fs. The program usually runs more than 10 nano seconds to obtain sufficiently good statistical average.

Initially, the program runs for a period of time to reach steady state before any data are recorded. The steady state is examined by monitoring the potential energy. Once it stops reducing further and begins to oscillate around a particular value, the steady state is established.

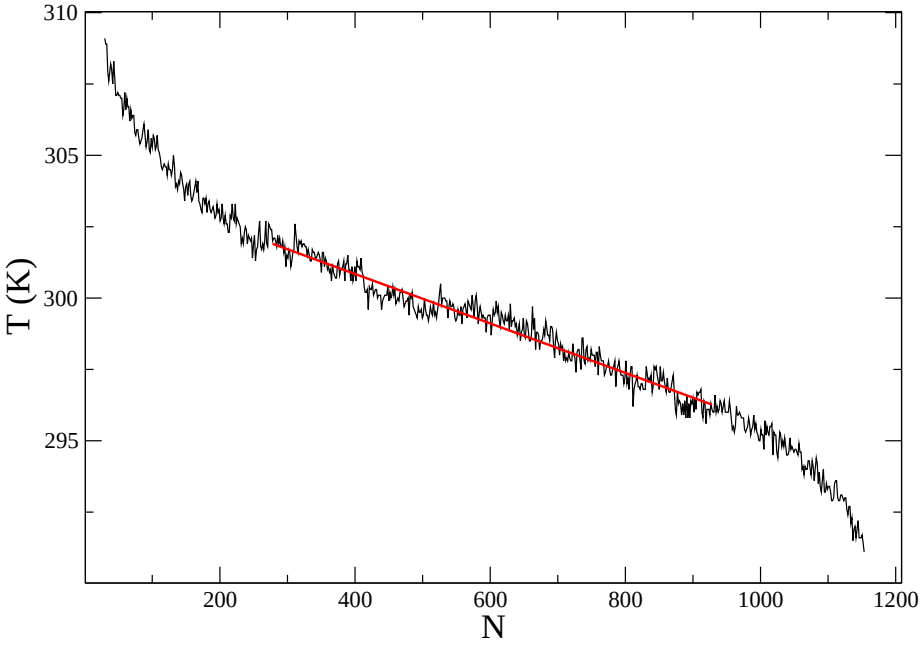

Figure 3.2: Temperature profile of polyethylene with 750 particles in the conduction region with initial separation of 1.50Å. The red solid line is linear fitted. The heat bath parts are omitted.

3.3 Results and Discussion

Figure 3.2 shows a typical temperature profile of the polyethylene chain connected to two heat baths. The local temperature of the chain decreases linearly in the central part, which indicates that a steady state has been well established. The profile near the boundary is nonlinear, which is due to the boundary resistance. The boundary resistance is directly related to the tension on the chain, which is governed by the distance between the ends. For small tensions when the particles locate near their equilibrium positions, the nonlinear effect of the boundary can be ignored and we can simply use Eq. (2.30) for our calculation.

All of our numerical simulations run with the following setup. The chain is coupled to two heat baths, with the left heat bath at 310K and the right one at 290K, thus the heat flux flows along the positive direction of the x axis. Different length of the chain is used in each particular configuration to examine the size effect of the thermal conductivity. The particle number runs through 100 to 800, with a step increase of 40 or 50. All the simulations in general run up to 50 nanoseconds after the steady state has been reached. Particles in the chain can move freely in three-dimensional space. Twenty additional particles on each side of the chain are in the heat baths. We noticed that this number of particles will generate a well behaved heat bath with the canonical distribution. The particles at the ends of the system are fixed.

Our aim in the simulation is to obtain the asymptotic power law relation between the thermal conductivity and the system length. There are two things which are particularly set in focus. One is the power index difference between a linear chain and a nonlinear chain. Another is the effect of the chain extension on the index number. These two foci determine the choice of parameters in the simulation.

Firstly, we studied the model with only harmonic interactions. The potentials of the bond angle interactions and the dihedral interactions are set to zero. The particles are initially distributed on the x axis with a specified separation range from 1.2Å to 1.5Å. A small position offset and an initial momentum according to the Maxwell distribution are given to each particle. The results with different initial separations are shown in Fig. 3.3. We note that with the increment of the system size, the average thermal flux reduces. More over, by fitting the curve to the formula $y = Ax^B$, we got a power law relation between the thermal conductivity and the system size. When the chain is relatively flexible, i.e., the average separation is less than 1.4Å, the power index $\alpha = B + 1$ is around 0.55. With greater tension at 1.5Å, this number increases sharply to 0.65. This shows a trend of increasing thermal conductivity with reduced transverse motion. Previous analytical result [5] on a pure one-dimensional harmonic

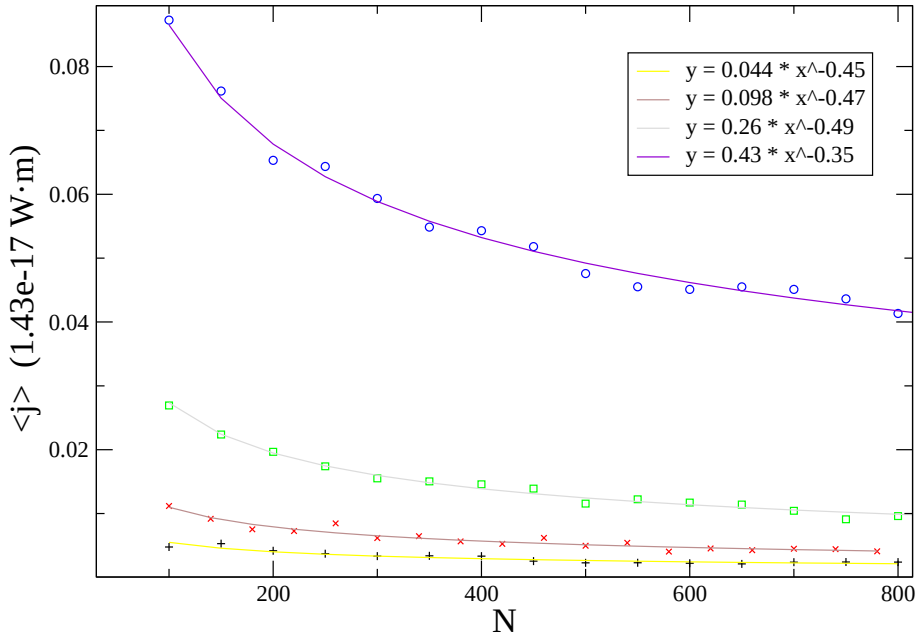

Figure 3.3: Dependence of average flux $\langle j \rangle$ on system size N with only linear bond interactions. The samples are calculated with a separation of 1.2Å, 1.3Å, 1.4Å, 1.5Å from the bottom to the top, respectively.

chain shows that one-dimensional thermal conductivity is proportional to the system size, corresponding to a power index of 1. For a pure one-dimensional system, with only harmonic interactions, no temperature gradient will build up in the central region. Thus the system has infinite thermal conductivity. However, for a quasi one-dimensional system, because of the additional freedom perpendicular to the thermal flux direction, some energy is used by the particle to maintain a local vibration, thus a temperature gradient always exists. For this reason, the thermal conductivity is smaller compared with one-dimensional system. However, the increment of the power index shows that the power index will gradually approaches 1 with increased tension

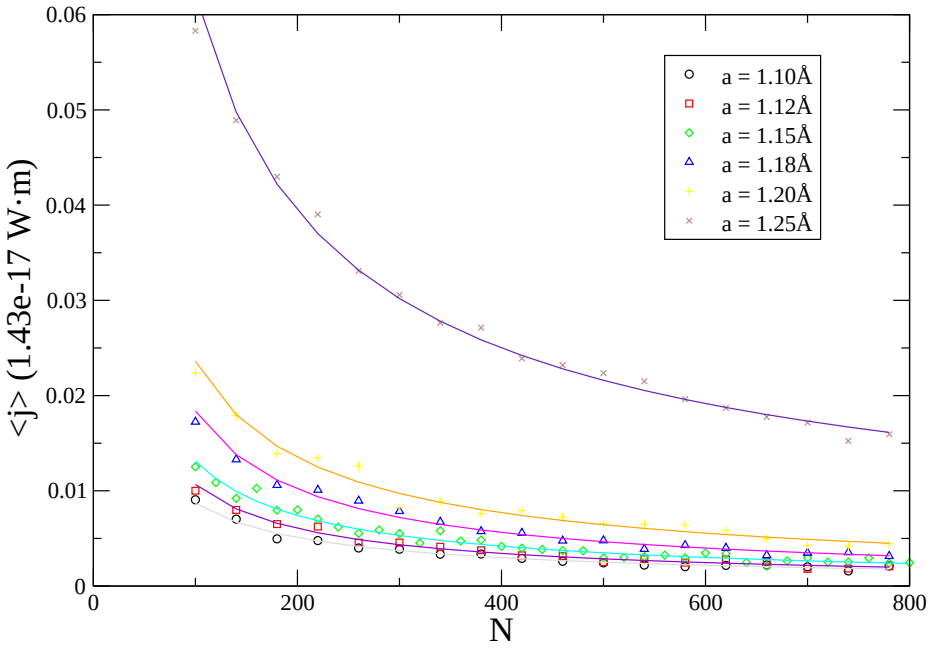

Figure 3.4: Dependence of average flux $\langle j \rangle$ on system size N with additional bond angle interactions and dihedral interactions.

and reduced freedom in the plane perpendicular to the flow direction, which is in agreement with our intuitive.

Secondly, we turn on all the nearest neighboring interactions, i.e., including the bond angle interactions and the dihedral interactions. Initial separations range from 1.10Å to 1.25Å. We obtain a similar pattern like Fig. 3.3 in Fig. 3.4. The relation between the power index α and the average separation a of neighboring particles on the x axis is shown in Fig. 3.5. We note that the power index number is significantly smaller than the linear case, which means that nonlinear interactions reduce the thermal conductivity through the chain. Additionally, there is a minimum value around $a = 1.18$Å. For separation distances larger than 1.18Å, the power index goes

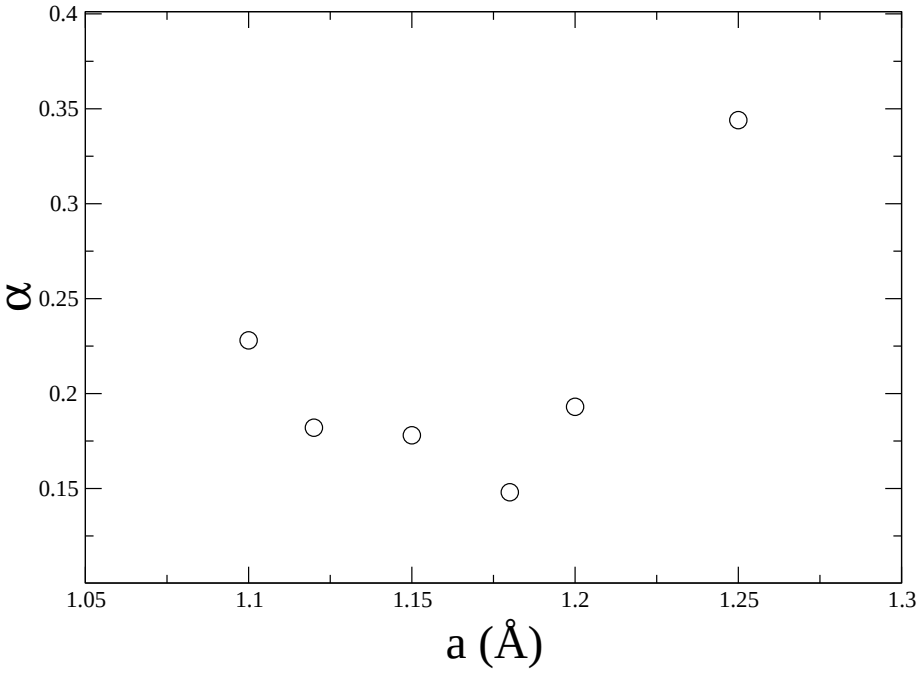

Figure 3.5: relation between the power index α and the average separation a of adjacent particles on the x axis

up, signifies the effect of tension. For separation distance smaller than 1.18Å, the power index slowly reduced from a limit value. It should be noted that the distance between adjacent particles should not be too small, as this will cause the folding of the chain, which is not properly simulated for a chain model. Analytical analysis using mode coupling theory [25] shows that the power index should be 1/3. However, this is under the condition that no tension is exerted on the chain. When a small tension exists in the chain, the power index is smaller, as shown in Fig. 3.5. Studies on nanotubes [29, 28] also show smaller power index around 0.15 for large radius, in which case the atoms are less confined, thus it is consistent with our study.

3.4 Conclusion

We have studied the thermal conductive properties of a realistic polyethylene model using molecular dynamics method. The chain is coupled to Nosé-Hoover heat baths and the particles can move in three-dimensional space. We found that in general there is a power law relation between the thermal conductivity and the system length. Inclusion of nonlinear interactions give a smaller power index than purely linear interactions. The power index is also connected with the transverse flexibility of the chain. A small tension will reduce the power index, while a much larger tension will transform the chain effectively to a harmonic chain.

Part II

Quantum Heat Transport and Application

Chapter 4

Non-equilibrium Green's Functions

Thermal transport in nanoscale systems has gained more attention in recent years. The transport properties at low temperatures are quite different from the properties at high temperatures. When the temperature is high, we can study the system using classical method, as what have been done in the first part of this thesis, where we have studied thermal conductivity of quasi one-dimensional chains using molecular dynamics method. However, this method cannot be used when the temperature is sufficiently low, as the assumption of equal partition is no longer valid in that case, and the Boltzmann's distribution cannot be used. Instead, we need to apply quantum mechanical method to the problem. For many body systems with interactions, Green's functions method is a standard method. This method has been thoroughly studied in equilibrium systems and there is a great deal of literature on this subject. However, for thermal transport problems in non-equilibrium state, little work has been done. Because of the complexity of interactions in a many body system, there is still a vast scope for investigation. In the following sections, we are trying to study the thermal transport properties of one-dimensional systems using the non-equilibrium Green's function method.

In this chapter, we firstly discuss the interaction representation, which is essential

for our study on many body systems with interactions. Then the adiabatic switching-on concept is introduced, which is the basis for further derivation. We then present a general non-equilibrium Green's functions approach to the quantum transport theory, which is our major tool. This is followed by an explanation of Feynman diagram and mean field theory.

Sec. 4.1 – Sec. 4.5 and Sec. 4.8 except for the generalization of the Langreth theorem are standard textbook materials. They are included here to make the discussion complete.

4.1 Model

Our model consists of three parts. The right and left parts are semi-infinite linear leads which act as heat baths. The central junction part is coupled to the leads through linear interactions. It can be in any structure and it also includes nonlinear interactions, which are our major interest. The Hamiltonian of the system is written as

$$\begin{aligned} \mathcal{H} &= \sum_{\alpha=L,C,R} H_\alpha + (u^L)^T V^{LC} u^C + (u^C)^T V^{CR} u^R + H_n, \\ H_\alpha &= \frac{1}{2}(\dot{u}^\alpha)^T \dot{u}^\alpha + \frac{1}{2}(u^\alpha)^T K^\alpha u^\alpha, \\ H_n &= \sum_{ijk} \frac{1}{3} k_{ijk} u_i^C u_j^C u_k^C + \sum_{ijkl} \frac{1}{4} k_{ijkl} u_i^C u_j^C u_k^C u_l^C, \end{aligned} \tag{4.1}$$

where $u_i = x_i\sqrt{m_i}$ is the normalized displacement for atom i. H_α is the harmonic Hamiltonian of each part, V_{LC} and V_{RC} are the interactions between the junction and the lead, and H_n is the nonlinear interaction in the junction.

Thermal energy can be carried by electrons, or through the lattice vibrations, which is abstracted as phonons. We have only considered phonons in our study

as most of the time, thermal transport is dominated by phonons. When the system is linear, the phonon mean free path is infinite, and phonons propagate freely. When nonlinear interactions are involved, the phonon mean free path becomes finite. Phonons get scattered with each other. In order to study the phonon-phonon interactions effectively, we need to work in the interaction representation, which is the topic of next section.

4.2 The interaction representation

In quantum mechanics, when dealing with systems with interactions, it is usually preferred to work in the interaction representation. Thus in the following text, we will present all the basic definitions and formulas for this representation. The text in this and the next section has followed Ref. [103].

We begin with a Hamiltonian

$$\hat{H} = \hat{H}_0 + \hat{H}_1, \tag{4.2}$$

where $\hat{H}_0$ is the Hamiltonian without interactions and $\hat{H}_1$ is the interaction term. In the Schrödinger's representation, we have

$$i\hbar\frac{\partial}{\partial t}|\Psi_S(t)\rangle = \hat{H}|\Psi_S(t)\rangle, \tag{4.3}$$

where $|\Psi_S(t)\rangle$ is the state vector. This equation can be solved formally and gives

$$|\Psi_S(t)\rangle = e^{-\frac{i}{\hbar}\hat{H}t}|\Psi_S(0)\rangle. \tag{4.4}$$

Thus the state vector at a later time can be calculated from the state vector at an initial time $t = 0$. We define a new interaction state vector based on Schrödinger's

state vector

$$|\Psi_I(t)\rangle \equiv e^{\frac{i}{\hbar}\hat{H}_0 t}|\Psi_S(t)\rangle. \tag{4.5}$$

The time derivative of this state vector is

$$\begin{aligned} i\hbar\frac{\partial}{\partial t}|\Psi_I(t)\rangle &= -\hat{H}_0 e^{\frac{i}{\hbar}\hat{H}_0 t}|\Psi_S(t)\rangle + e^{\frac{i}{\hbar}\hat{H}_0 t}\hat{H}|\Psi_S(t)\rangle \\ &= e^{\frac{i}{\hbar}\hat{H}_0 t}\hat{H}_1 e^{-\frac{i}{\hbar}\hat{H}_0 t}|\Psi_I(t)\rangle \\ &= \hat{H}_1(t)|\Psi_I(t)\rangle, \end{aligned} \tag{4.6}$$

which has the same form as the Schrödinger's equation (4.3) and we have set

$$\hat{H}_1(t) \equiv e^{\frac{i}{\hbar}\hat{H}_0 t}\hat{H}_1 e^{-\frac{i}{\hbar}\hat{H}_0 t}. \tag{4.7}$$

For an arbitrary operator in the interaction representation, we define

$$\hat{O}_I(t) \equiv e^{\frac{i}{\hbar}\hat{H}_0 t}\hat{O}_S e^{-\frac{i}{\hbar}\hat{H}_0 t}. \tag{4.8}$$

Its equation of motion is

$$\begin{aligned} i\hbar\frac{\partial}{\partial t}\hat{O}_I(t) &= -\hat{H}_0 e^{\frac{i}{\hbar}\hat{H}_0 t}\hat{O}_S e^{-\frac{i}{\hbar}\hat{H}_0 t} + e^{\frac{i}{\hbar}\hat{H}_0 t}\hat{O}_S\hat{H}_0 e^{-\frac{i}{\hbar}\hat{H}_0 t} \\ &= \hat{O}_I(t)\hat{H}_0 - \hat{H}_0\hat{O}_I(t) \\ &= [\hat{O}_I(t), \hat{H}_0]. \end{aligned} \tag{4.9}$$

Apply (4.9) to annihilation operator $\hat{a}(t)$, we have

$$\begin{aligned} i\hbar\frac{\partial}{\partial t}\hat{a}_i(t) &= [\hat{a}_i(t), \hat{H}_0] = e^{i\hat{H}_0 t}[\hat{a}_i, \hat{H}_0]e^{-i\hat{H}_0 t} \\ &= e^{i\hat{H}_0 t}[\hat{a}_i, \sum_j \hbar\omega_j \hat{a}_j^\dagger \hat{a}_j]e^{-i\hat{H}_0 t} \\ &= \hbar\omega_j e^{i\hat{H}_0 t}[\hat{a}_i, \hat{a}_j^\dagger]\hat{a}_j e^{-i\hat{H}_0 t}\delta_{ij} \\ &= \hbar\omega_i e^{i\hat{H}_0 t}\hat{a}_i e^{-i\hat{H}_0 t} \\ &= \hbar\omega_i \hat{a}_i(t) \\ \hat{a}_i(t) &= \hat{a}_i e^{-i\omega_i t}. \end{aligned} \tag{4.10}$$

Let there be a propagator function that propagates the state vector from time t_0 to t

$$|\Psi_I(t)\rangle = \hat{U}(t, t_0)|\Psi_I(t_0)\rangle. \tag{4.11}$$

From (4.4) and (4.5), this equation can be written out specifically as

$$|\Psi_I(t)\rangle = e^{\frac{i}{\hbar}\hat{H}_0 t}|\Psi_S(t)\rangle \tag{4.12}$$

$$= e^{\frac{i}{\hbar}\hat{H}_0 t}e^{-\frac{i}{\hbar}\hat{H}t}|\Psi_S(0)\rangle \tag{4.13}$$

$$= e^{\frac{i}{\hbar}\hat{H}_0 t}e^{-\frac{i}{\hbar}\hat{H}t}e^{\frac{i}{\hbar}\hat{H}t_0}|\Psi_S(t_0)\rangle \tag{4.14}$$

$$= e^{\frac{i}{\hbar}\hat{H}_0 t}e^{-\frac{i}{\hbar}\hat{H}t}e^{\frac{i}{\hbar}\hat{H}t_0}e^{-\frac{i}{\hbar}\hat{H}_0 t_0}|\Psi_I(t_0)\rangle, \tag{4.15}$$

hence

$$U(t, t_0) = e^{\frac{i}{\hbar}\hat{H}_0 t}e^{-\frac{i}{\hbar}\hat{H}(t-t_0)}e^{-\frac{i}{\hbar}\hat{H}_0 t_0}. \tag{4.16}$$

Substitute (4.11) into (4.6), we get the equation of motion for the propagator

$$i\hbar\frac{\partial}{\partial t}\hat{U}(t, t_0) = \hat{H}_1(t)\hat{U}(t, t_0). \tag{4.17}$$

After integrating (4.17) from t_0 to t, we have

$$\hat{U}(t,t_0) - \hat{U}(t_0,t_0) = -\frac{i}{\hbar}\int_{t_0}^{t} \hat{H}_1(t')\hat{U}(t',t_0)dt'. \tag{4.18}$$

It is obvious from (4.11) that

$$\hat{U}(t_0,t_0) = 1, \tag{4.19}$$

hence

$$\hat{U}(t,t_0) = 1 - \frac{i}{\hbar}\int_{t_0}^{t} \hat{H}_1(t')\hat{U}(t',t_0)dt', \tag{4.20}$$

which is a self-consistent equation. We replace the propagator at the r.h.s. of the equation recursively, and obtain

$$\begin{aligned}\hat{U}(t,t_0) = 1 &- \frac{i}{\hbar}\int_{t_0}^{t} \hat{H}_1(t_1)dt_1 + (-\frac{i}{\hbar})^2 \int_{t_0}^{t}\int_{t_0}^{t_1} \hat{H}_1(t_1)\hat{H}_1(t_2)dt_1dt_2 + ... \\ &+ (-\frac{i}{\hbar})^n \int_{t_0}^{t}\int_{t_0}^{t_1} ... \int_{t_0}^{t_{n-1}} \hat{H}_1(t_1)\hat{H}_1(t_2)...\hat{H}_1(t_n)dt_1dt_2...dt_n + ... \ .\end{aligned} \tag{4.21}$$

For the multi-variable integration, the time variables are ordered in the way that later time variables are on the left and earlier time variables are on the right. These are dummy variables and there are $n!$ ways of permutation. We then expand each upper limit to t, and attach a step function $\theta(t_i - t)$. The overall effect is to order the variables properly. The propagator thus has the form

$$\begin{aligned}\hat{U}(t,t_0) &= \sum_n (-\frac{i}{\hbar})^n \frac{1}{n!}\int_{t_0}^{t} ... \int_{t_0}^{t} T[\hat{H}_1(t_1)...\hat{H}_1(t_n)]dt_1...dt_n \\ &= T\exp\left\{-\frac{i}{\hbar}\int_{t_0}^{t}\hat{H}_1(t')dt'\right\}.\end{aligned} \tag{4.22}$$

In the Schrödinger's representation, the state vectors are time dependent, while the operators are time independent. In the interaction representation, both state vectors and operators are time dependent. Another representation which is quite useful is the

Heisenberg representation, whose state vectors are time independent. The relation between the Schrödinger's representation and the Heisenberg representation is

$$|\Psi_S(t)\rangle = A(t)|\Psi_H\rangle \quad \text{with} \quad A(0) = 1. \tag{4.23}$$

Insert (4.23) into (4.3)

$$i\hbar\frac{\partial}{\partial t}A(t)|\Psi_H\rangle = \hat{H}A(t)|\Psi_H\rangle, \tag{4.24}$$

hence

$$A(t) = e^{-\frac{i}{\hbar}\hat{H}t}. \tag{4.25}$$

We have

$$|\Psi_S(t)\rangle = e^{-\frac{i}{\hbar}\hat{H}t}|\Psi_H\rangle. \tag{4.26}$$

For an arbitrary operator $\hat{O}_S$, its representation in the Heisenberg representation can be derived from (4.26)

$$\begin{aligned} \langle\Psi_S(t)|\hat{O}_S|\Psi_S(t)\rangle &= \langle\Psi_H|e^{\frac{i}{\hbar}\hat{H}t}\hat{O}_S e^{-\frac{i}{\hbar}\hat{H}t}|\Psi_H\rangle \\ &= \langle\Psi_H|\hat{O}_H|\Psi_H\rangle, \\ \hat{O}_H(t) &= e^{\frac{i}{\hbar}\hat{H}t}\hat{O}_S e^{-\frac{i}{\hbar}\hat{H}t}. \end{aligned} \tag{4.27}$$

The equation of motion of $\hat{O}_H(t)$ is

$$i\hbar\frac{\partial}{\partial t}\hat{O}_H(t) = -\hat{H}\hat{O}_H(t) + \hat{O}_H(t)\hat{H} = [\hat{O}_H(t), \hat{H}]. \tag{4.28}$$

The relation between $\hat{O}_H(t)$ and $\hat{O}_I(t)$ is easily got from (4.8) and (4.27), i.e.

$$\hat{O}_H(t) = e^{\frac{i}{\hbar}\hat{H}t}e^{-\frac{i}{\hbar}\hat{H}_0 t}\hat{O}_I(t)e^{\frac{i}{\hbar}\hat{H}_0 t}e^{-\frac{i}{\hbar}\hat{H}t}. \tag{4.29}$$

With the help of (4.16), (4.29) is simplified to

$$\hat{O}_H(t) = \hat{U}(0,t)\hat{O}_I(t)\hat{U}(t,0). \tag{4.30}$$

4.3 Adiabatic switching-on

In order to calculate the physical quantities at a specific time, we need to know the state vectors first. Because of the effect of interactions, the system state is not known to us. To get the state vectors of the current system, we need to start from some already known intitial state. Then using the equation of motion of the state, we can derive the state vectors at a later time. As the eigenstate with no interactions is completely known, we can start from here and switch on the interactions gradually, so that the interactions become full-fledged at the required time. This technique is called adiabatic switching-on, as at each particular time, the eigenstate can be treated as static and the total Hamiltonian does not change.

We start with the Hamiltonian in the form of Eq. (4.2). Initialy, there is no interactions in the system, thus $\hat{H} = \hat{H}_0$. The system is represented by a complete set of eigenvectors $|\Phi_0\rangle$. The time dependent Hamiltonian can be represented as

$$\hat{H}(t) = \hat{H}_0 + e^{-\epsilon|t|}\hat{H}_1, \tag{4.31}$$

where ϵ is an arbitrarily small positive value. As time $t = \pm\infty$, the system has no interactions. When the time t approaches zero, the interactions are fully switched on.

The state vector at the time t can be calculated from the state vector at the time t_0 through Eq. (4.11), ie. $|\Psi_I(t)\rangle = U_\epsilon(t,t_0)|\Psi_I(t_0)\rangle$, with the subscript ϵ to remind about the extra time dependent factor $e^{-\epsilon|t|}$ in the interaction operator. The equation

of motion of $U_\epsilon(t,t_0)$ is

$$i\hbar\frac{\partial}{\partial t}\hat{U}_\epsilon(t,t_0) = e^{-\epsilon|t|}\hat{H}_1(t)\hat{U}_\epsilon(t,t_0), \tag{4.32}$$

which, after integration, gives

$$U_\epsilon(t,t_0) = T\exp\left\{-\frac{i}{\hbar}\int_{t_0}^{t} e^{-\epsilon|t'|}\hat{H}_1(t')dt'\right\}. \tag{4.33}$$

According to Eqs. (4.5) and (4.8), the state vector $|\Psi_I(t_0)\rangle$ can be written as

$$|\Psi_I(t_0)\rangle = e^{\frac{i}{\hbar}\hat{H}_0 t_0}|\Psi_S(t_0)\rangle. \tag{4.34}$$

Let $t_0 \to -\infty$, so that the total Hamiltonian $\hat{H}$ approaches $\hat{H}_0$. The state vector $|\Psi_S(t_0)\rangle$ can be written as $|\Psi_S(t_0)\rangle = e^{-\frac{i}{\hbar}\hat{H}_0 t_0}|\Phi_0\rangle$, where $|\Phi_0\rangle$ is the initial eigenstate. Thus Eq. (4.34) becomes $|\Psi_I(-\infty)\rangle = |\Phi_0\rangle$. In another word, without interaction, the state vectors will remain in a steady state. As the interaction is turned on gradually, the state vector will change according to Eq. (4.11). At the time $t = 0$, we have the relation that $|\Psi_I(0)\rangle = |\Psi_S(0)\rangle = |\Psi_H\rangle$, which gives

$$|\Psi_H\rangle = U_\epsilon(t,-\infty)|\Phi_0\rangle. \tag{4.35}$$

Let ϵ goes to zero, we then arrive at an state vector with full interaction which can be represented by the state vector without interaction through the propagator $U(t,-\infty)$.

In our model, there are two kinds of interactions. one is the interaction between the leads and the junction, and another is the nonlinear interaction in the junction. Thus, our calculation is also separated into two steps. We first start from an initial state that the three parts of the model are independent. No interactions between the leads and the junction are involved and there are no nonlinear interactions either.

Then we slowly switch on the interaction at the interface, until the interaction is fully turned on at a specific time t_0 and the whole system reaches a steady state. We then let t_0 approaches $-\infty$, thus it becomes a new initial state, which is known now. We begin to switch on the nonlinear interactions in the junction, which are fully turned on at time $t = 0$. Through this two-step switching-on method, we are able to obtain the current eigenstate under nonlinear interactions and surface interactions from the eigenstate without interactions. The Hamiltonian of our model is thus written as

$$H(t) = \sum_{\alpha=L,C,R} H_\alpha + e^{-\epsilon|t-t_0|}(V_{LC} + V_{CR}) + e^{-\xi|t|}H_n. \tag{4.36}$$

With the above information, we are able to calculate any physical quantities if we know the density matrix at the specified time, which is defined as

$$\hat{\rho}_I(t) \equiv \sum_i \omega_i |\Psi_{Ii}(t)\rangle\langle\Psi_{Ii}(t)|. \tag{4.37}$$

Substituting the state vector by Eq. (4.11), we have

$$\begin{aligned}
\hat{\rho}_I(t) &= \sum_i \omega_i \hat{U}(t,t_0)|\Psi_{Ii}(t_0)\rangle\langle\Psi_{Ii}(t_0)|\hat{U}(t_0,t) \\
&= \sum_i \omega_i \hat{U}(t,t_0)\hat{S}(t_0,-\infty)|\Psi_{Ii}(-\infty)\rangle\langle\Psi_{Ii}(-\infty)|\hat{S}(-\infty,t_0)\hat{U}(t_0,t) \\
&= \hat{U}(t,t_0)\hat{S}(t_0,-\infty)\hat{\rho}(-\infty)\hat{S}(-\infty,t_0)\hat{U}(t_0,t),
\end{aligned} \tag{4.38}$$

where

$$\begin{aligned}
\hat{S}(t,t_0) &= T\exp\left\{-\frac{i}{\hbar}\int_{t_0}^{t}\hat{V}(t')dt'\right\}, \\
\hat{U}(t,t_0) &= T\exp\left\{-\frac{i}{\hbar}\int_{t_0}^{t}\hat{H}_n(t')dt'\right\},
\end{aligned}$$

and we have used the relation $\hat{U}^\dagger(t,t_0) = \hat{U}(t_0,t)$.

4.4 Time ordered Green's functions

To start with, we give the definition of a time ordered Green's function

$$G^t(t,t') = -\frac{i}{\hbar}\langle \mathcal{T} u(t)u(t')^T\rangle, \tag{4.39}$$

where $\mathcal{T}$ is the time ordering operator. When t and t' have a specific order, the time ordering operator $\mathcal{T}$ can be removed. $G^t(t,t')$ can be written as

$$G^<(t,t') = -\frac{i}{\hbar}\langle u(t')u(t)^T\rangle^T \qquad t<t', \tag{4.40}$$

$$G^>(t,t') = -\frac{i}{\hbar}\langle u(t)u(t')^T\rangle \qquad t>t', \tag{4.41}$$

i.e.

$$G^t(t,t') = \theta(t-t')G^>(t,t') + \theta(t'-t)G^<(t,t'). \tag{4.42}$$

Sometimes, an anti-time ordered Green's function is useful, which has the form

$$\begin{aligned} G^{\bar{t}}(t,t') &= -\frac{i}{\hbar}\langle \bar{\mathcal{T}} u(t)u(t')^T\rangle \\ &= \theta(t-t')G^<(t,t') + \theta(t'-t)G^>(t,t'). \end{aligned} \tag{4.43}$$

Eq. (4.42) and (4.43) gives us

$$G^t(t,t') + G^{\bar{t}}(t,t') = G^<(t,t') + G^>(t,t'). \tag{4.44}$$

We will also frequently use the retarded Green's function and the advanced Green's function, which are defined as

$$G^r(t,t') = -\frac{i}{\hbar}\theta(t-t')\langle [u(t),u(t')^T]\rangle, \tag{4.45}$$

$$G^a(t,t') = \frac{i}{\hbar}\theta(t'-t)\langle [u(t),u(t')^T]\rangle. \tag{4.46}$$

The relation between $G^r(t,t')$, $G^a(t,t')$ and other Green's functions are

$$G^r(t,t') = \theta(t-t')(G^>(t,t') - G^<(t,t')), \tag{4.47}$$

$$G^a(t,t') = \theta(t'-t)(G^<(t,t') - G^>(t,t')), \tag{4.48}$$

$$G^r(t,t') - G^a(t,t') = G^>(t,t') - G^<(t,t'), \tag{4.49}$$

$$G^r(t,t') + G^a(t,t') = G^t(t,t') - G^{\bar{t}}(t,t'). \tag{4.50}$$

4.5 Equilibrium Green's Functions

In equilibrium state with only harmonic interactions, phonons in the system move freely. In this case, the Green's functions have simple forms. In the followings, we will discuss the Green's functions in equilibrium state. Only one element of the whole matrix is discussed, and as the matrix is diagonalized, the subscript is omitted. The coordinates can be represented by the annihilation and creation operators, i.e.

$$\hat{u} = \sqrt{\frac{\hbar}{2\omega_0}}(\hat{a} + \hat{a}^\dagger) \tag{4.51}$$

Inserting (4.51) into Green's function $g^<(t,t')$ gives

$$\begin{aligned}
g^<(t,t') &= -\frac{i}{\hbar}\langle \hat{u}(t')\hat{u}(t)\rangle \\
&= -\frac{i}{2\omega_0}\langle (\hat{a}(t') + \hat{a}^\dagger(t'))(\hat{a}(t) + \hat{a}^\dagger(t))\rangle \\
&= -\frac{i}{2\omega_0}\langle \hat{a}e^{-i\omega_0 t'}\hat{a}^\dagger e^{i\omega_0 t} + \hat{a}^\dagger e^{i\omega_0 t'}\hat{a}e^{i\omega_0 t}\rangle \\
&= -\frac{i}{2\omega_0}(e^{i\omega_0(t-t')}\langle \hat{a}\hat{a}^\dagger\rangle + e^{i\omega_0(t'-t)}\langle \hat{a}^\dagger\hat{a}\rangle) \\
&= -\frac{i}{2\omega_0}(e^{i\omega_0(t-t')}(1 + \langle \hat{a}^\dagger\hat{a}\rangle) + e^{i\omega_0(t'-t)}\langle \hat{a}^\dagger\hat{a}\rangle) \\
&= -\frac{i}{2\omega_0}[e^{i\omega_0(t-t')}(1 + f(\omega_0)) + e^{i\omega_0(t'-t)}f(\omega_0)]
\end{aligned} \tag{4.52}$$

where we have used (4.10), commutation relation $[\hat{a}, \hat{a}^\dagger] = 1$, and $\langle \hat{a}^\dagger \hat{a} \rangle = \frac{1}{e^{\beta\hbar\omega_0 - 1}} = f(\omega_0)$, which is Bose-Einstein distribution and ω_0 is the eigen frequency corresponding to $\hat{a}$. The Fourier transformation of (4.52) is

$$\begin{aligned} g^<(\omega) &= \int_{-\infty}^{\infty} g^<(t,t') e^{i\omega(t-t')} dt \\ &= -\frac{i}{2\omega_0} \int_{-\infty}^{\infty} [e^{i\omega_0(t-t')}(1+f(\omega_0)) + e^{i\omega_0(t'-t)} f(\omega_0)] e^{i\omega(t-t')} dt \\ &= -\frac{i\pi}{\omega_0} [\delta(\omega+\omega_0)(1+f(\omega_0)) + \delta(\omega-\omega_0) f(\omega_0)], \end{aligned} \tag{4.53}$$

where we have used $\delta(\omega) = \frac{1}{2\pi} \int_{-\infty}^{\infty} e^{i\omega t} dt$. Similarly, we have

$$g^>(t,t') = -\frac{i}{2\omega_0} [e^{i\omega_0(t'-t)}(1+f(\omega_0)) + e^{i\omega_0(t-t')} f(\omega_0)] \tag{4.54}$$

$$g^>(\omega) = -\frac{i\pi}{\omega_0} [\delta(\omega-\omega_0)(1+f(\omega_0)) + \delta(\omega+\omega_0) f(\omega_0)] \tag{4.55}$$

We can also derive the retarded Green's function

$$\begin{aligned} g^r(t,t') &= -\frac{i}{\hbar} \theta(t-t') [\hat{u}(t), \hat{u}(t')] \\ &= -\frac{i}{\hbar} \theta(t-t') \frac{\hbar}{2\omega_0} \langle [\hat{a}(t) + \hat{a}^\dagger(t), \hat{a}(t') + \hat{a}^\dagger(t')] \rangle \\ &= -\theta(t-t') \frac{i}{2\omega_0} \langle [\hat{a}(t), \hat{a}^\dagger(t')] + [\hat{a}^\dagger(t), \hat{a}(t')] \rangle \\ &= -\frac{i}{2\omega_0} \theta(t-t') (e^{i\omega_0(t'-t)} - e^{i\omega_0(t-t')}). \end{aligned} \tag{4.56}$$

In the Fourier space, (4.56) becomes

$$\begin{aligned} g^r(\omega) &= \int_{-\infty}^{\infty} g^r(t,t')e^{i\omega(t-t')}dt \\ &= -\frac{i}{2\omega_0}\int_{-\infty}^{\infty}\theta(t-t')(e^{i\omega_0(t'-t)}-e^{i\omega_0(t-t')})e^{i\omega(t-t')}dt \\ &= -\frac{i}{2\omega_0}\int_{-\infty}^{\infty}\left\{-\int_{-\infty}^{\infty}\frac{d\omega'}{2\pi i}\frac{e^{-i\omega'(t-t')}}{\omega'+i\eta}\right\}(e^{i(\omega-\omega_0)(t'-t)}-e^{i(\omega+\omega_0)(t-t')})dt \\ &= \frac{1}{4\pi\omega_0}\int_{-\infty}^{\infty}d\omega'\frac{2\pi(\delta(\omega-\omega_0-\omega')-\delta(\omega+\omega_0-\omega'))}{\omega'+i\eta} \\ &= \frac{1}{2\omega_0}(\frac{1}{\omega-\omega_0+i\eta}-\frac{1}{\omega+\omega_0+i\eta}) \\ &= \frac{1}{(\omega+i\eta)^2-\omega_0^2}, \end{aligned} \tag{4.57}$$

where we have used $\theta(t-t') = -\int_{-\infty}^{\infty}\frac{d\omega'}{2\pi i}\frac{e^{-i\omega'(t-t')}}{\omega'+i\eta}$ and η is an infinitesimal positive value. Similarly, we have the advanced Green's function

$$g^a(t,t') = \frac{i}{2\omega_0}\theta(t'-t)(e^{i\omega_0(t'-t)}-e^{i\omega_0(t-t')}) \tag{4.58}$$

$$\begin{aligned} g^a(\omega) &= \frac{1}{2\omega_0}(\frac{1}{\omega-\omega_0-i\eta}-\frac{1}{\omega+\omega_0-i\eta}) \\ &= \frac{1}{(\omega-i\eta)^2-\omega_0^2} \end{aligned} \tag{4.59}$$

From (4.57) and (4.59), it is obvious that

$$g^r(\omega) = g^a(\omega)^*. \tag{4.60}$$

Another very useful relation can be derived using the symbolic equation

$$\frac{1}{\omega \pm i\eta} = \mathcal{P}\frac{1}{\omega} \mp i\pi\delta(\omega), \tag{4.61}$$

where $\mathcal{P}$ stands for principle value. Write (4.57) and (4.59) in this form, we have

$$g^r(\omega) = \frac{1}{2\omega_0}(\mathcal{P}\frac{1}{\omega-\omega_0} - i\pi\delta(\omega-\omega_0) - \mathcal{P}\frac{1}{\omega+\omega_0} + i\pi\delta(\omega+\omega_0)$$
$$g^a(\omega) = \frac{1}{2\omega_0}(\mathcal{P}\frac{1}{\omega-\omega_0} + i\pi\delta(\omega-\omega_0) - \mathcal{P}\frac{1}{\omega+\omega_0} - i\pi\delta(\omega+\omega_0).$$

Subtracting $g^r(\omega)$ by $g^a(\omega)$ yields

$$g^r(\omega) - g^a(\omega) = \frac{i\pi}{\omega_0}(\delta(\omega+\omega_0) - \delta(\omega-\omega_0)). \tag{4.62}$$

(4.62) has almost the same form as (4.53), in fact, multiply the Bose-Einstein distribution at both sides of (4.62) gives

$$\begin{aligned} f(\omega)[g^r(\omega) - g^a(\omega)] &= \frac{i\pi}{\omega_0}[f(\omega)\delta(\omega+\omega_0) - f(\omega)\delta(\omega-\omega_0)] \\ &= \frac{i\pi}{\omega_0}[f(-\omega_0)\delta(\omega+\omega_0) - f(\omega_0)\delta(\omega-\omega_0)] \\ &= -\frac{i\pi}{\omega_0}[(1+f(\omega_0))\delta(\omega+\omega_0) + f(\omega_0)\delta(\omega-\omega_0)] \\ &= g^<(\omega), \end{aligned} \tag{4.63}$$

where we have used $f(-\omega_0) = \frac{1}{e^{-\beta\hbar\omega_0}-1} = -(1+\frac{1}{e^{\beta\hbar\omega_0}-1}) = -(1+f(\omega_0))$ in the second last line.

4.6 Contour ordered Green's functions

In nonequilibrium steady state, the eigenstate of the system is derived from its initial state, where the interactions are gradually turned on and become full-fledged at present time. It is not usually guaranteed that the system will return to its initial

state after infinite long time, thus it would be better if the system goes backward to its initial state. This procedure requires the system evolve on a complex path, where a contour ordered Green's function is defined, which is

$$G^{\alpha_1,\alpha_2,\ldots,\alpha_n}_{j_1,j_2,\ldots,j_n}(\tau_1,\tau_2,\ldots,\tau_n) = -i\langle \mathcal{T}_\tau u^{\alpha_1}_{j_1}(\tau_1) u^{\alpha_2}_{j_2}(\tau_2)\ldots u^{\alpha_n}_{j_n}(\tau_n)\rangle, \tag{4.64}$$

where $\alpha = L, C, R$ for different sections and j_i represents the degree of freedom. We have chosen $\hbar = 1$ in the definition of the Green's function and hereafter for simplicity. It can always be easily recovered by dimensional analysis. The contour runs from $\tau = -\infty + i\epsilon$ to $\tau = 0$, then from $\tau = 0$ to $\tau = -\infty - i\epsilon$. We can define an extended step function $\theta(\tau - \tau')$ which equals one if τ is later than τ' on the contour, and equals zero otherwise. An extended δ-function, which is the derivative of $\theta(\tau - \tau')$, is also required. It is defined as $\delta(\tau - \tau') = \sigma\delta_{\sigma,\sigma'}\delta(t - t')$ so that its integral along the contour gives one. Here σ stands for the branch of the contour. If the variable is above the real axis, $\sigma = 1$. If it is below the real axis, $\sigma = -1$.

The contour ordered Green's function can be solved using equations of motion method. Let's consider Green's function $G^{CL}_{jk}(\tau,\tau') = -i\langle \mathcal{T}_\tau u^C_j(\tau) u^L_k(\tau')\rangle$ as an example, which is an important quantity in the following thermal conductance calculation. Its first derivative gives

$$\begin{aligned}
\frac{\partial}{\partial\tau'} G^{CL}_{jk}(\tau,\tau') &= -i\frac{\partial}{\partial\tau'}\langle \mathcal{T}_\tau u^C_j(\tau) u^L_k(\tau')\rangle \\
&= -i\frac{\partial}{\partial\tau'}\langle \theta(\tau-\tau') u^C_j(\tau) u^L_k(\tau') + \theta(\tau'-\tau) u^L_k(\tau') u^C_j(\tau)\rangle \\
&= -i\langle \delta(\tau-\tau')[u^L_k(\tau'), u^C_j(\tau)]\rangle - i\langle \mathcal{T}_\tau u^C_j(\tau)\dot{u}^L_k(\tau')\rangle \\
&= -i\langle \mathcal{T}_\tau u^C_j(\tau)\dot{u}^L_k(\tau')\rangle.
\end{aligned} \tag{4.65}$$

The first term in the second last line equals zero as the two elements with the same time commute.

The second derivative of $G^{CL}_{jk}(\tau,\tau')$ can be calculated the same way as Eq. (4.65), which yields

$$\frac{\partial^2}{\partial\tau'^2}G^{CL}_{jk}(\tau,\tau') = -i\langle\mathcal{T}_\tau u^C_j(\tau)\ddot{u}^L_k(\tau')\rangle. \tag{4.66}$$

The second derivative of $u^L_k(\tau')$ can be further replaced by its equation of motion. Let's derive the formula in the Hamiltonian representation. According to Eq. (4.28), we have

$$\frac{\partial}{\partial\tau}\dot{u}^L_j(\tau) = -i[\dot{u}^L_j(\tau), H]. \tag{4.67}$$

Here τ is equivalent to t as its imaginary part approaches zero. Expanding H into its component form as defined in Eq. (4.1), and considering that only terms with Cartesian coordinates $u^L_j(\tau)$ on the left lead does not commute with $\dot{u}^L_j(\tau)$, we have

$$\begin{aligned}
\ddot{u}^L_k(\tau) &= -ie^{iH\tau}[\dot{u}^L_k, H_L + V_{LC}]e^{-iH\tau} \\
&= -ie^{iH\tau}[\dot{u}^L_k, \sum_{lm}\frac{1}{2}u^L_l K^L_{lm}u^L_m + \sum_{lm}u^L_l V^{LC}_{lm}u^C_m]e^{-iH\tau} \\
&= -ie^{iH\tau}[-i\sum_l K^L_{kl}u^L_l - i\sum_l V^{LC}_{kl}u^C_l]e^{-iH\tau} \\
&= -\sum_l K^L_{kl}u^L_l(\tau) - \sum_l V^{LC}_{kl}u^C_l(\tau),
\end{aligned} \tag{4.68}$$

so that Eq. (4.65) becomes

$$\frac{\partial^2}{\partial\tau'^2}G^{CL}_{jk}(\tau,\tau') = -\sum_l G^{CL}_{jl}(\tau,\tau')K^L_{lk} - \sum_l G^{CC}_{jl}(\tau,\tau')V^{CL}_{lk} \tag{4.69}$$

Eq. (4.69) can be written in a more compact matrix form, which gives

$$\frac{\partial^2}{\partial\tau'^2}G^{CL}(\tau,\tau') + G^{CL}(\tau,\tau')K^L = -G^{CC}(\tau,\tau')V^{CL}. \tag{4.70}$$

This equation can be solved by defining a Green's function of the left lead, which

fulfills

$$\frac{\partial^2}{\partial\tau'^2}g^L(\tau',\tau'') + K^L g^L(\tau',\tau'') = -I\delta(\tau'-\tau''). \tag{4.71}$$

By multiplying Eq. (4.70) by $g^L(\tau',\tau'')$ on the right, and multiplying Eq. (4.71) by $G^{CL}(\tau,\tau')$ on the left, then integrating by parts the subtraction of Eq. (4.70) and Eq. (4.71), we have

$$\begin{aligned} G^{CL}(\tau,\tau'') = \int G^{CC}(\tau,\tau')V^{CL}g^L(\tau',\tau'')d\tau' \\ + \frac{\partial G^{CL}(\tau,\tau')}{\partial\tau'}g^L(\tau',\tau'') - G^{CL}(\tau,\tau')\frac{\partial g^L(\tau',\tau'')}{\partial\tau'}\Big|_{-\infty+i\epsilon}^{-\infty-i\epsilon} \end{aligned} \tag{4.72}$$

At both ends of the contour, the heat bath and the central junction are decoupled and each part maintains at its own equilibrium state. Thus when $\tau' = -\infty \pm i\epsilon$, $G^{CL}(\tau,\tau') = 0$ and $\frac{\partial}{\partial\tau'}G^{CL}(\tau,\tau') = 0$. This becomes obvious if we look at the definition of $G^{CL}_{ij}(\tau,\tau') = -i\langle\mathcal{T}_\tau u_i^C(\tau)u_j^L(\tau')\rangle$. When $\tau' = -\infty \pm i\epsilon$, $u_j^L(\tau')$ can be replaced by $(a_j^{L\dagger} + a_j^L)e^{-i\omega_j t}$ multiplied by a constant. It will change the initial state, but this change can not be recovered by $u_i^C(\tau)$, thus it must be zero. It yields that

$$G^{CL}(\tau,\tau'') = \int G^{CC}(\tau,\tau')V^{CL}g^L(\tau',\tau'')d\tau'. \tag{4.73}$$

We can calculate $G^{CC}_{jk}(\tau,\tau') = -i\langle\mathcal{T}_\tau u_j^C(\tau)u_k^C(\tau')\rangle$ based on the same procedure. As $u_j(\tau)$ and $u_k(\tau')$ commute when $\tau = \tau'$, the first derivative of $G^{CC}_{jk}(\tau,\tau')$ relative to τ' gives

$$\frac{\partial}{\partial\tau'}G^{CC}_{jk}(\tau,\tau') = -i\langle\mathcal{T}_\tau u_j^C(\tau)\dot{u}_k^C(\tau')\rangle. \tag{4.74}$$

For the second derivative, as $[u_j^C, \dot{u}_k^C] = i\delta_{jk}$, we have

$$\frac{\partial^2}{\partial\tau'^2}G^{CC}_{jk}(\tau,\tau') = -i\langle\mathcal{T}_\tau u_j^C(\tau)\ddot{u}_k^C(\tau')\rangle - \delta(\tau-\tau')\delta_{jk}. \tag{4.75}$$

Now we need to replace $\ddot{u}_k^C(\tau')$ by its equation of motion, which is

$$\ddot{u}_k = -\sum_l K_{kl}u_l - \sum_l V_{kl}^{CL}u_l^L - \sum_l V_{kl}^{CR}u_l^R - \sum_{lm} T_{klm}u_l u_m - \sum_{lmn} T_{klmn}u_l u_m u_n, \quad (4.76)$$

where the superscript C has been dropped for the junction part here after.

Things get a bit complicated here. Unlike the lead, where only linear interactions are considered, nonlinear interactions are also involved in the junction, which are the fourth and fifth term in Eq. (4.76). These coordinates are at the same time τ, while in Green's functions, in general, the time maybe different. We need a mechanism to track the time. This can be done by integrating the term with a δ-function. For example, let's consider the third order interaction, which gives

$$\sum_{lm} T_{klm}u_l(\tau)u_m(\tau) = \iint T_{klm}u_l(\tau')\delta(\tau-\tau')u_m(\tau'')\delta(\tau-\tau'')d\tau' d\tau''. \quad (4.77)$$

Define $T_{klm}(\tau,\tau',\tau'') = T_{klm}\delta(\tau-\tau')\delta(\tau-\tau'') = T_{klm}\sigma'\delta_{\sigma,\sigma'}\delta(t-t')\sigma''\delta_{\sigma,\sigma''}\delta(t-t'')$, we have

$$\begin{aligned}\frac{\partial^2}{\partial\tau'^2}G_{jk}^{CC}(\tau,\tau') + \sum_l G_{jl}^{CC}(\tau,\tau')K_{lk}^{CC} &= -\delta_{jk}\delta(\tau-\tau') - \sum_l G_{jl}^{CL}(\tau,\tau')V_{lk}^{LC} \\ &- \sum_l G_{jl}^{CR}(\tau,\tau')V_{lk}^{RC} - \sum_{lm}\iint G_{jlm}^{CCC}(\tau,\tau_1,\tau_2)T_{klm}(\tau',\tau_1,\tau_2)d\tau_1 d\tau_2 \\ &- \sum_{lmn}\iint G_{jlmn}^{CCCC}(\tau,\tau_1,\tau_2,\tau_3)T_{klmn}(\tau',\tau_1,\tau_2,\tau_3)d\tau_1 d\tau_2 d\tau_3. \quad (4.78)\end{aligned}$$

The second derivative of $G^{CC}_{jk}(\tau,\tau')$ to τ is similar, which is

$$\frac{\partial^2}{\partial\tau^2}G^{CC}_{jk}(\tau,\tau')+\sum_l K^{CC}_{jl}G^{CC}_{lk}(\tau,\tau')=-\delta_{jk}\delta(\tau-\tau')-\sum_l V^{CL}_{jl}G^{LC}_{lk}(\tau,\tau')$$
$$-\sum_l V^{CR}_{jl}G^{RC}_{lk}(\tau,\tau')-\sum_{lm}\iint T_{jlm}(\tau,\tau_1,\tau_2)G^{CCC}_{klm}(\tau',\tau_1,\tau_2)d\tau_1 d\tau_2$$
$$-\sum_{lmn}\iint T_{jlmn}(\tau,\tau_1,\tau_2,\tau_3)G^{CCCC}_{klmn}(\tau',\tau_1,\tau_2,\tau_3)d\tau_1 d\tau_2 d\tau_3. \quad (4.79)$$

Without nonlinear interaction, the junction Green's function gives

$$\left(\frac{\partial^2}{\partial\tau^2}+K^{CC}\right)G_0(\tau,\tau')+$$
$$\int(V^{CL}g^L(\tau,\tau'')V^{LC}+V^{CR}g^R(\tau,\tau'')V^{RC})G_0(\tau'',\tau')d\tau''=-I\delta(\tau-\tau'), \quad (4.80)$$

where we have used Eq. (4.73) to replace G^{CL} and G^{CR}. Thus $\frac{\partial^2}{\partial\tau^2}+K^{CC}$ can be represented by $G_0(\tau,\tau')$ as

$$\frac{\partial^2}{\partial\tau^2}+K^{CC}=-I\delta(\tau-\tau')G_0^{-1}(\tau,\tau')$$
$$-\int(V^{CL}g^L(\tau,\tau'')V^{LC}+V^{CR}g^R(\tau,\tau'')V^{RC})\delta(\tau-\tau'')d\tau'' \quad (4.81)$$

Substitute Eq. (4.81) into Eq. (4.79), we have

$$G^{CC}(\tau,\tau')=G_0(\tau,\tau')+\iiint G_0(\tau,\tau_1)T(\tau_1,\tau_2,\tau_3)G^{CCC}(\tau_2,\tau_3,\tau')d\tau_1 d\tau_2 d\tau_3$$
$$\iiiint G_0(\tau,\tau_1)T(\tau_1,\tau_2,\tau_3,\tau_4)G^{CCCC}(\tau_2,\tau_3,\tau_4,\tau')d\tau_1 d\tau_2 d\tau_3 d\tau_4 \quad (4.82)$$

where $\delta(\tau-\tau')G_0(\tau-\tau')$ is multiplied on both side of the equation.

The Eq. (4.82) gives an explicit way to solve arbitrary order Green's functions recursively. Fig. 4.1 shows how this is done. The rules for n-point Green's function

are:

1. For an n-point Green's function, it can be depicted as a vertex having n double-line legs.

2. For an mth order interaction, an m-terminal vertex is enrolled which is connected to one of the leg with a single line represents G_0 and connected to the main vertex with two double lines, thus increase the order of the Green's function by $m-2$. This corresponds to the second term of Eq. (4.82).

3. One leg is paired with one of the remaining $n-1$ legs with G_0, which is then multiplied by the remaining $n-2$ order Green's function. The summation of these terms are then multiplied by i. This corresponds to the first term of Eq. (4.82).

4. The graphs are symmetrized by working on each individual leg using step 2 and 3, then a summation is made and divided by n.

An implementation of above rules with cubic interactions using Mathematica is given in Appendix B.

4.7 Feynman diagrams and Dyson's equation

The equation of motion method is accurate and straight forward. However, a major drawback of it is that the final formalism is too complicated and makes it very hard to calculate. To solve this problem, we can use an equivalent but more intuitive method. That is the Keldysh formalism using Feynman diagrams. We start from the definition of the central junction Green's function

$$\begin{aligned} G_{jk}(\tau,\tau') &= -i\langle \mathcal{T}_\tau u_j^H(\tau) u_k^H(\tau')\rangle \\ &= -i\,\mathrm{Tr}\{\hat{\rho}_H(0)\mathcal{T}_\tau u_j^H(\tau) u_k^H(\tau')\}. \end{aligned} \tag{4.83}$$

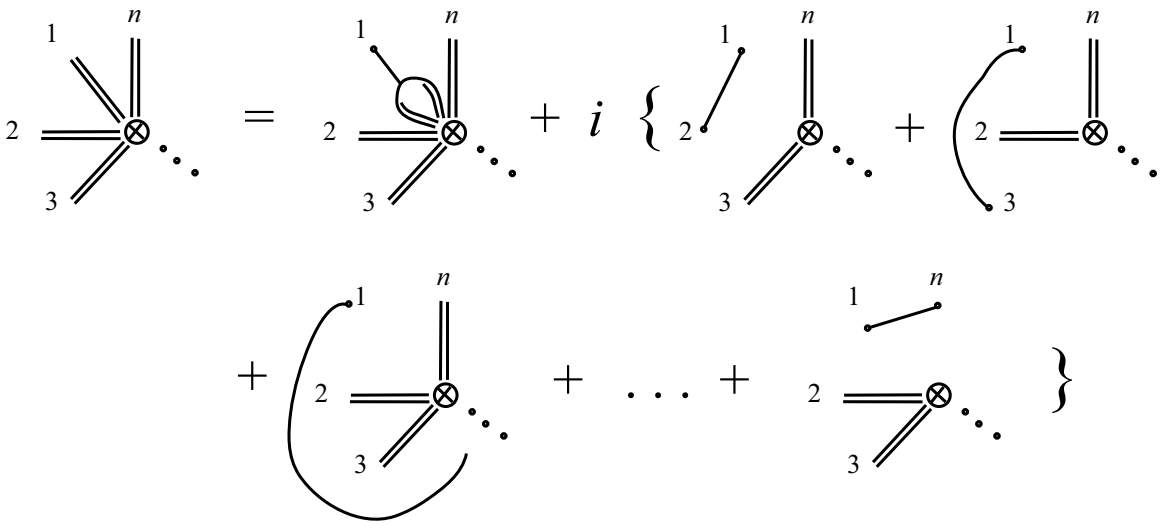

Figure 4.1: Recursive expansion rule for Green's functions.

The operators here are in the Heisenberg representation, and the average is over Heisenberg state characterized by the density matrix $\hat{\rho}_H(0)$. We choose the Heisenberg representation in the definition is because we want a fixed set of eigenstates which does not change over time. However, in order to study a system with interactions, it is better to use the interaction representation.

According to Eq. (4.30), at the time $t = 0$, the operator in the Heisenberg representation is the same as the one in the interaction representation. Thus

$$\hat{\rho}_H(0) = \hat{\rho}_I(0) = S(0, -\infty)\hat{\rho}_0' S(-\infty, 0), \tag{4.84}$$

where $S(\tau, \tau')$ is the evolution operator with nonlinear interactions switched on, and $\hat{\rho}_0'$ is the density matrix at a time before the nonlinear interactions are switched on and the system has already established steady state. It is evolved from the equilibrium state density matrix with the interface interactions turned on. Thus it can be expressed as $\lim_{\tau_0 \to -\infty} U(\tau_0, -\infty)\hat{\rho}_0 U(-\infty, \tau_0)$, where $\hat{\rho}_0$ is the equilibrium state density matrix, $U(\tau, \tau')$ is the evolution operator with interface interactions.

It is more convenient to work in the interaction representation. The displacement $u_i^H(\tau)$ in the Heisenberg representation can be transformed to the interaction representation by

$$u_i^H(\tau) = S(0,\tau)u_i^I(\tau)S(\tau,0). \tag{4.85}$$

Substituting Eq. (4.84) and Eq. (4.85) into Eq. (4.83) gives

$$\begin{aligned} G_{jk}(\tau,\tau') &= -i\,\mathrm{Tr}\{\hat{\rho}_0' S(-\infty,0)\mathcal{T}_\tau S(0,\tau)u_i^I(\tau)S(\tau,0) \\ &\qquad S(0,\tau')u_j^I(\tau')S(\tau',0)S(0,-\infty)\} \\ &= -i\,\mathrm{Tr}\{\hat{\rho}_0'\mathcal{T}_\tau S(-\infty,-\infty)u_i^I(\tau))u_j^I(\tau')\} \\ &= -i\langle\mathcal{T}_\tau e^{-i\int_\tau H_n(\tau'')d\tau''}u_i^I(\tau)u_j^I(\tau')\rangle. \end{aligned} \tag{4.86}$$

The contour integral is from $-\infty$ to τ, to τ' and to $-\infty$. Written in the time domain, we have $\int d\tau = \sum_{\sigma=\pm1}\int_{-\infty}^{+\infty}\sigma dt$. The Taylor expansion of the exponential term of Eq. (4.86) yields

$$G_{jk}(\tau,\tau') = -i\langle\mathcal{T}_\tau\sum_{m=0}^{\infty}(-i)^m\frac{1}{m!}\int_C d\tau_1...\int_C d\tau_m H_n^1(\tau_1)...H_n^m(\tau_m)u_j^I(\tau)u_k^I(\tau')\rangle. \tag{4.87}$$

We will drop the superscript I in the following section for simplicity. All the operators are interpreted in the interaction representation.

When studying the equilibrium Green's function, there is the general Wick's theorem [103], which expands the Green's function to a sum of all the possible pairings of the coordinates. This theorem can be adapted to nonequilibrium case and it gives

$$\langle ABCD\ldots FG\rangle = \langle AB\rangle\langle CD\rangle\ldots\langle FG\rangle + \langle AC\rangle\langle BD\rangle\ldots\langle FG\rangle + \cdots. \tag{4.88}$$

Now we can expand Eq. (4.87) in terms of $G_{0,jk}(\tau,\tau') = -i\langle\mathcal{T}_\tau u_j(\tau)u_k(\tau')\rangle$, which

yields

$$\begin{aligned} G_{jk}(\tau,\tau') = G_{0,jk}(\tau,\tau') + \frac{i}{2}(\frac{1}{3})^2 \sum_{lmn}\sum_{opq} \int\cdots\int d\tau_1 d\tau_2 d\tau_1' d\tau_1'' d\tau_2' d\tau_2'' \\ G_{0,jl}(\tau,\tau_1) T_{lmn}(\tau_1,\tau_1',\tau_1'') G_{0,mp}(\tau_1',\tau_2') \\ G_{0,nq}(\tau_1'',\tau_2'') T_{opq}(\tau_2,\tau_2',\tau_2'') G_{0,nk}(\tau_2,\tau') + \cdots . \end{aligned} \tag{4.89}$$

We have only shows one of the terms in the second order. It is obvious that the result would be quite complicated to consider even a few terms. This is where the Feynman diagram comes to rescue. A Feynman diagram representation of Eq. (4.87) is given in Fig. 4.2. From these diagrams, we are able to write down all the terms as in Eq. (4.89). The rules are as follows:

- Mark each end of a line by a symbol with a particular time τ, then replace each single line by $G_{0,ij}(\tau_i,\tau_j)$ for line ij.
- The vertex is represented by $T_{ijk}(\tau_i,\tau_j,\tau_k)$ or $T_{ijkl}(\tau_i,\tau_j,\tau_k,\tau_l)$, according to its number of legs.
- Integrate over all the internal variables and sum over the internal index, then multiply the prefactor $(-i)^{m+1}/m!$.

Note that there are no disconnected diagrams in Fig. 4.2. These disconnected diagrams only contribute a constant to the formula, thus in frequency domain, it corresponds to $\delta(\omega)$. As we will shown in Eq. (4.113), the thermal flux has a factor ω, which becomes zero with the presence of $\delta(\omega)$. Thus it does not contribute to thermal flux.

Eq. (4.89) can be written in a more compact form. From Fig. 4.2 we notice that the Green's function can be represented by $G = G_0 + \int G_0 \Sigma^* G_0$. Here Σ^* is called self-energy. There are two types of self-energies. One is the proper self-energy, which

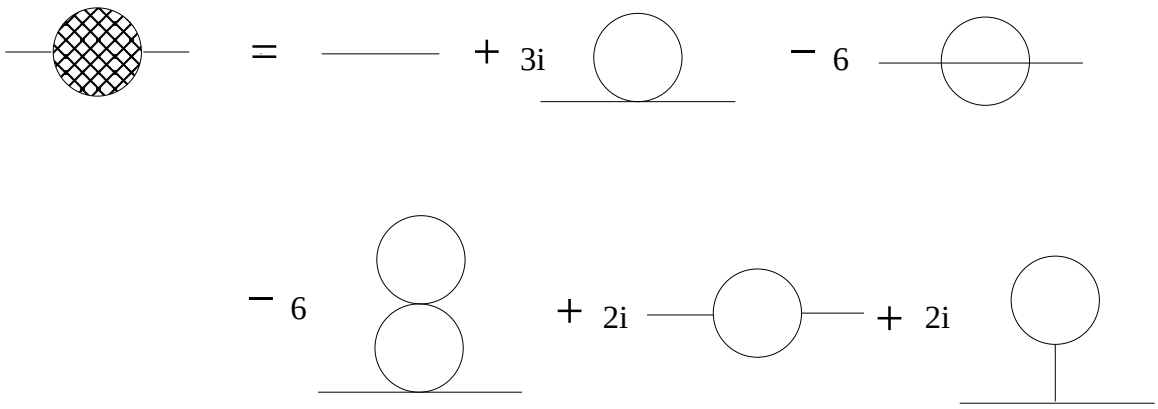

Figure 4.2: Feynman diagram for the Green's function up to the 2nd order with 3rd and 4th order nonlinear interactions.

can not be separated into two parts by dividing a single line. Another is the improper self-energy. Improper self-energy can be represented by a combination of the other proper self-energy by connecting the proper self-energy with G_0. Thus the total self-energy is a combination of all the proper self-energy. Denote the proper self-energy as Σ_n, we have

$$\Sigma^*(\tau,\tau') = \Sigma_n(\tau,\tau') + \iint d\tau_1 d\tau_2 \Sigma_n(\tau,\tau_1) G_0(\tau_1,\tau_2) \Sigma_n(\tau_2,\tau') + \iiiint d\tau_1 d\tau_2 d\tau_3 d\tau_4 \Sigma_n(\tau,\tau_1) G_0(\tau_1,\tau_2) \Sigma_n(\tau_2,\tau_3) G_0(\tau_3,\tau_4) \Sigma_n(\tau_4,\tau') + \cdots . \quad (4.90)$$

Eq. (4.89) becomes

$$G(\tau,\tau') = G_0(\tau,\tau') + \iint d\tau_1 d\tau_2 G_0(\tau,\tau_1) \Sigma_n(\tau_1,\tau_2) G(\tau_2,\tau'). \quad (4.91)$$

This can be easily verified by replacing $G(\tau_2,\tau')$ with the same formula iteratively. Eq. (4.91) is called Dyson's equation. In Eq. (4.91), we notice that the Green's function G is on both sides of the equation. Thus, Dyson's equation is self-consistent. The self-consistent property is very important as it is a requirement for the Green's

function to be convergent.

The Green's function G_0 can be calculated by considering the system without nonlinear interaction, i.e.$H_n = 0$. The Dyson's equation is still valid, and we have

$$G_0(\tau, \tau') = g^C(\tau, \tau') + \iint d\tau_1 d\tau_2 g^C(\tau, \tau_1)\Sigma(\tau_1, \tau_2)G_0(\tau_2, \tau'), \tag{4.92}$$

where $\Sigma = \Sigma_L + \Sigma_R = V^{CL}g^L V^{LC} + V^{CR}g^R V^{RC}$ and can be calculated exactly.

The above formulae are important for the thermal flux calculation. However, before we dive into the calculation of the thermal flux, we need a theory to carry out the contour integration, which will be introduced in the next section.

4.8 Langreth Theorem

The contour integration in the calculation of Green's function is hard to solve, if not impossible. On the other hand, we can transform the contour integration into time integration, thus the integration is calculated along the real axis. In order to do this, we need Langreth theorem [104, 105].

In our calculation, we often encounter integrals in the form

$$A(t, t') = \int_C B(t, \tau)C(\tau, t')d\tau. \tag{4.93}$$

Here τ is a dummy variable on the contour. Assuming that $t < t'$, we separate the contour into two parts, so that t is on the first contour C_1 and t' is on the second contour C_2. We have

$$A^<(t, t') = \int_{C_1} B(t, \tau)C^<(\tau, t')d\tau + \int_{C_2} B^<(t, \tau)C(\tau, t')d\tau, \tag{4.94}$$

as any time τ on contour C_1 is less than t' and any time τ on contour C_2 is greater

than t. We integrate contour C_1 along a path slightly above the real axis from $-\infty$ to ∞ and C_2 along a path slightly below the real axis from ∞ to $-\infty$, thus we have

$$\begin{aligned}
A^<(t,t') &= \int_{-\infty}^{t} B^>(t,\tau)C^<(\tau,t')d\tau + \int_{t}^{-\infty} B^<(t,\tau)C^<(\tau,t')d\tau \\
&\quad + \int_{-\infty}^{t'} B^<(t,\tau)C^<(\tau,t')d\tau + \int_{t'}^{-\infty} B^<(t,\tau)C^>(\tau,t')d\tau \\
&= \int_{-\infty}^{t} \{B^>(t,\tau) - B^<(t,\tau)\}C^<(\tau,t')d\tau \\
&\quad + \int_{-\infty}^{t'} B^<(t,\tau)\{C^<(\tau,t') - C^>(\tau,t')\}d\tau \\
&= \int_{-\infty}^{+\infty} \theta(t-\tau)\{B^>(t,\tau) - B^<(t,\tau)\}C^<(\tau,t')d\tau \\
&\quad + \int_{-\infty}^{+\infty} \theta(t'-\tau)B^<(t,\tau)\{C^<(\tau,t') - C^>(\tau,t')\}d\tau \\
&= \int_{-\infty}^{+\infty} B^r(t,\tau)C^<(\tau,t')d\tau + \int_{-\infty}^{+\infty} B^<(t,\tau)C^a(\tau,t')d\tau.
\end{aligned} \tag{4.95}$$

This can be written symbolically as

$$A^< = B^r C^< + B^< C^a. \tag{4.96}$$

Similarly, we have

$$A^> = B^r C^> + B^> C^a. \tag{4.97}$$

For $A^r(t,t')$, we have

$$\begin{aligned}
A^r(t,t') &= \theta(t-t')(A^>(t,t') - A^<(t,t')) \\
&= \theta(t-t')\Big\{\int_{-\infty}^{+\infty}[(B^r(t,\tau)C^>(\tau,t') + B^>(t,\tau)C^a(\tau,t'))]d\tau \\
&\quad - \int_{-\infty}^{+\infty}[B^r(t,\tau)C^<(\tau,t') + B^<(t,\tau)C^a(\tau,t')]d\tau\Big\} \\
&= \theta(t-t')\Big\{\int_{-\infty}^{+\infty} B^r(t,\tau)\theta(\tau-t')[C^>(\tau,t') - C^<(\tau,t')]d\tau \\
&\quad + \int_{-\infty}^{+\infty} B^r(t,\tau)\theta(t'-\tau)[C^>(\tau,t') - C^<(\tau,t')]d\tau \\
&\quad + \int_{-\infty}^{+\infty} \theta(t-\tau)[B^>(t,\tau) - B^<(t,\tau)]C^a(\tau,t')d\tau \\
&\quad + \int_{-\infty}^{+\infty} \theta(\tau-t)[B^>(t,\tau) - B^<(t,\tau)]C^a(\tau,t')d\tau\Big\} \\
&= \theta(t-t')\int_{-\infty}^{+\infty}[B^r(t,\tau)(C^r(\tau,t') - C^a(\tau,t')) \\
&\quad + (B^r(t,\tau) - B^a(t,\tau))C^a(\tau,t')]d\tau \\
&= \theta(t-t')\int_{-\infty}^{+\infty}[B^r(t,\tau)C^r(\tau,t') - B^a(t,\tau)C^a(\tau,t')]d\tau \\
&= \int_{-\infty}^{+\infty} B^r(t,\tau)C^r(\tau,t')d\tau.
\end{aligned} \tag{4.98}$$

Thus we have

$$A^r = B^r C^r, \tag{4.99}$$

$$A^a = B^a C^a, \tag{4.100}$$

where in the second last line of Eq. (4.98), we have used the fact that $t > t'$ in the retarded Green's function and $t < t'$ in the advanced Green's function. With

Eq. (4.96), (4.97), (4.99) and (4.100), a general formalism can be derived, which is

$$A^{<,>} = A_1^r ... A_{n-1}^r A_n^{<,>} + A_1^r ... A_{n-2}^r A_{n-1}^{<,>} A_n^a + ... + A_1^r ... A_{i-1}^r A_i^{<,>} A_{i+1}^a ... A_n^a + ... + A_1^{<,>} A_2^a ... A_n^a, \quad (n \geq 2), \tag{4.101}$$

$$A^{r,a} = A_1^{r,a} A_2^{r,a} ... A_n^{r,a}. \tag{4.102}$$

We note that at the r.h.s of Eq. (4.101), the $<,>$ component starts from the right end in the first term gradually move to the left end in the following terms. All r components are on the left side of $<,>$ and all a components are on the right side of $<,>$. To prove Eq. (4.101) and (4.102), we use mathematical induction. We have already showed that the formulas Eq. (4.101) and (4.102) is correct at $n = 2$.

It is straightforward to prove Eq. (4.102). Let

$$A = A_1 A_2 ... A_n,$$
$$M = A_1 A_2 ... A_n A_{n+1} = A A_{n+1}.$$

We have

$$A^{r,a} = A_1^{r,a} A_2^{r,a} ... A_n^{r,a},$$
$$M^{r,a} = A^{r,a} A_{n+1}^{r,a} = A_1^{r,a} A_2^{r,a} ... A_n^{r,a} A_{n+1}^{r,a}.$$

Eq. (4.102) is proved. To prove Eq. (4.101), we note that

$$\begin{aligned} M^{<,>} &= A^r A_{n+1}^{<,>} + A^{<,>} A_{n+1}^a \\ &= A_1^r A_2^r ... A_n^r A_{n+1}^{<,>} + (A_1^r ... A_{n-1}^r A_n^{<,>} + ... + A_1^{<,>} A_2^a ... A_n^a) A_{n+1}^a, \end{aligned}$$

which has the same form as Eq. (4.101), thus Eq. (4.101) is proved.

If the correlation function $A(t, t')$ is time independent, i.e. only the time difference is significant, the formulae can be represented in a more compact form in Fourier

space. Let's use Eq. (4.95) as an example. The left hand side gives

$$A^<(t-t') = \int_{-\infty}^{+\infty} e^{-i\omega(t-t')} A^<(\omega) d\omega, \tag{4.103}$$

while the first term on the right hand side is

$$\begin{aligned}
&\int_{-\infty}^{\infty} d\tau \int_{-\infty}^{+\infty} B^r(\omega) e^{-i\omega(t-\tau)} d\omega \int_{-\infty}^{+\infty} C^<(\omega') e^{-i\omega'(\tau-t')} d\omega' \\
&= \int_{-\infty}^{+\infty} e^{i(\omega-\omega')\tau} d\tau \int_{-\infty}^{+\infty} B^r(\omega) e^{-i\omega t} d\omega \int_{-\infty}^{+\infty} C^<(\omega') e^{i\omega' t'} d\omega' \\
&= \int_{-\infty}^{+\infty} B^r(\omega) e^{-i\omega t} d\omega \int_{-\infty}^{+\infty} C^<(\omega') e^{i\omega' t'} \delta(\omega-\omega') d\omega' \\
&= \int_{-\infty}^{+\infty} B^r(\omega) C^<(\omega) e^{-i\omega(t-t')} d\omega.
\end{aligned}$$

The second term can be calculated in the same way, and we have

$$A^<(\omega) = B^r(\omega) C^<(\omega) + B^<(\omega) C^a(\omega).$$

To summarise, the Fourier transform of time invariant contour integral $A(t-t') = \int B(t-\tau) C(\tau-t') d\tau$ has the following relations:

$$A^<(\omega) = B^r(\omega) C^<(\omega) + B^<(\omega) C^a(\omega), \tag{4.104}$$

$$A^>(\omega) = B^r(\omega) C^>(\omega) + B^>(\omega) C^a(\omega), \tag{4.105}$$

$$A^r(\omega) = B^r(\omega) C^r(\omega), \tag{4.106}$$

$$A^a(\omega) = B^a(\omega) C^a(\omega). \tag{4.107}$$

4.9 Thermal flux

With all the previous definitions and derivations, we are able to calculate the thermal flux that passes through the system. The thermal flux is defined as the energy transferred from the heat source to the junction in a unit time, which is equal to the energy transferred from the junction to the heat sink in a unit time, if we assume that no energy is built up in the junction. According to this definition, the thermal flux out of the left lead is

$$J(t) = -\frac{dH_L(t)}{dt} = i[H_L(t), H] = i[H_L(t), V_{LC}(t)], \tag{4.108}$$

where we have used Eq. (4.1). The last term of Eq. (4.108) is obtained because the left lead Hamiltonian H_L commutes with all the terms except V_{LC}. To write this term out explicitly, we have

$$\begin{aligned}
[H_L(t), V_{LC}(t)] &= \frac{1}{2}[\dot{u}_L^T(t)\dot{u}_L(t), u_L^T(t)V^{LC}u_C(t)] \\
&= -\frac{1}{2}[\sum_{jk} u_{Lj}(t)V_{jk}^{LC}u_{Ck}(t), \sum_i \dot{u}_{Li}(t)\dot{u}_{Li}(t)] \\
&= -\frac{1}{2}\sum_{ijk}[u_{Lj}(t), \dot{u}_{Li}(t)\dot{u}_{Li}(t)]V_{jk}^{LC}u_{Ck}(t) \\
&= -i\sum_{ijk}\dot{u}_{Li}(t)\delta_{ij}V_{jk}^{LC}u_{Ck}(t) \\
&= -i\sum_{jk}\dot{u}_{Lj}(t)V_{jk}^{LC}u_{Ck}(t) \\
&= -i\dot{u}_L^T(t)V^{LC}u_C(t).
\end{aligned} \tag{4.109}$$

Substitute Eq. (4.109) into Eq. (4.108), we have

$$J(t) = \dot{u}_L^T(t)V^{LC}u_C(t). \tag{4.110}$$

The average value of the thermal flux is thus given by

$$\begin{aligned}\langle J\rangle &= \langle\sum_{jk}\dot{u}_j^L(\tau)V_{jk}^{LC}u_k^C(\tau)\rangle \\ &= \lim_{\tau'\to\tau^+}\langle\sum_{jk}u_k^C(\tau')\dot{u}_j^L(\tau)V_{jk}^{LC}\rangle \\ &= i\lim_{\tau'\to\tau^+}\mathrm{Tr}[V^{LC}\bar{G}^{CL,<}(\tau,\tau')],\end{aligned} \tag{4.111}$$

where we have used a general complex variable τ to replace the real variable t and defined $\bar{G}_{kj}^{CL,<}(\tau,\tau') = -i\langle\dot{u}_j^L(\tau')u_k^C(\tau)\rangle$.

The calculation of the thermal flux is at the time of steady state, where only the time difference is relevant. Thus we can do a Fourier transform on $\bar{G}_{kj}^{CL,<}(\tau-\tau')$, which gives

$$\begin{aligned}\bar{G}_{kj}^{CL,<}(\tau-\tau') &= \frac{d}{d\tau'}[-i\langle u_j^L(\tau')u_k^C(\tau)\rangle] \\ &= \frac{d}{d\tau'}G_{kj}^{CL,<}(\tau,\tau') \\ &= \frac{d}{d\tau'}G_{kj}^{CL,<}(\tau-\tau') \\ &= \frac{1}{2\pi}\frac{d}{d\tau'}\int_{-\infty}^{+\infty}G_{kj}^{CL,<}(\omega)e^{-i\omega(\tau-\tau')}d\omega \\ &= \frac{1}{2\pi}\int i\omega G_{kj}^{CL,<}(\omega)e^{-i\omega(\tau-\tau')}d\omega\end{aligned} \tag{4.112}$$

Insert (4.112) into (4.111), we have

$$\langle J\rangle = -\frac{1}{2\pi}\int\omega\,\mathrm{Tr}[G^{CL,<}(\omega)V^{LC}]d\omega \tag{4.113}$$

The center-left Green's function G^{CL} can be replaced by the center-center Green's

function G^{CC} using Eq. (4.73) and Eq. (4.104), which yields

$$\begin{aligned}\langle J\rangle &= -\frac{1}{2\pi}\int \omega \,\mathrm{Tr}[G^r_{CC}(\omega)V_{CL}g^<_L(\omega)V_{LC} + G^<_{CC}(\omega)V_{CL}g^a_L(\omega)V_{LC}]d\omega \\ &= -\frac{1}{2\pi}\int \omega \,\mathrm{Tr}[G^r_{CC}(\omega)\Sigma^<_L(\omega) + G^<_{CC}(\omega)\Sigma^a_L(\omega)]d\omega.\end{aligned} \tag{4.114}$$

In the following part, we will omit the subscript CC for simplicity.

In the Fourier space, Eq. (4.91) and Eq. (4.92) become

$$G(\omega) = G_0(\omega) + G_0(\omega)\Sigma_n(\omega)G(\omega) \tag{4.115}$$

$$G_0(\omega) = g(\omega) + g(\omega)\Sigma(\omega)G_0(\omega) \tag{4.116}$$

According to Langreth theorem Eq. (4.99), we have

$$G^r(\omega) = G^r_0(\omega) + G^r_0(\omega)\Sigma^r_n(\omega)G^r(\omega) \tag{4.117}$$

$$G^r_0(\omega) = g^r(\omega) + g^r(\omega)\Sigma^r(\omega)G^r_0(\omega) \tag{4.118}$$

$G^r_0(\omega)$ can be solved by multiplying $g^{r-1}(\omega)$ on both sides, which yields

$$G^r_0 = (g^{r-1} - \Sigma)^{-1} = ((\omega + i\eta)^2 I - K^C - \Sigma^r)^{-1} \tag{4.119}$$

G^r can be solved in the same way, and we have

$$G^r = (G^{r-1}_0 - \Sigma^r_n)^{-1}. \tag{4.120}$$

We can also calculate $G^<_0$ using Eq. (4.96), which gives

$$G^<_0 = g^< + g^r\Sigma^r G^<_0 + g^r\Sigma^< G^a_0 + g^<\Sigma^a G^a_0. \tag{4.121}$$

Eq. (4.121) can be solved by expending $G_0^<$ on the right side iteratively using the same formula, which then yields

$$\begin{aligned}
G_0^< &= g^< + g^r\Sigma^r(g^< + g^r\Sigma^r(g^< + g^r\Sigma^r G_0^< + g^r\Sigma^< G_0^a + g^<\Sigma^a G_0^a) \\
&\quad + g^r\Sigma^< G_0^a + g^<\Sigma^a G_0^a) + g^r\Sigma^< G_0^a + g^<\Sigma^a G_0^a \\
&= (1 + g^r\Sigma^r + (g^r\Sigma^r)^2)(g^< + g^r\Sigma^< G_0^a + g^<\Sigma^a G^a) + (g^r\Sigma^r)^3 G_0^< \\
&= (1 + g^r\Sigma^r + (g^r\Sigma^r)^2 + ...)(g^< + g^r\Sigma^< G_0^a + g^<\Sigma^a G_0^a) \\
&= (1 - g^r\Sigma^r)^{-1}(g^< + g^r\Sigma^< G_0^a + g^<\Sigma^a G_0^a) \\
&= G_0^r g^{r\,-1} g^<(1 + \Sigma^a G_0^a) + G_0^r\Sigma^< G_0^a \\
&= G_0^r g^{r\,-1} g^< g^{a\,-1} G_0^a + G_0^r\Sigma^< G_0^a \\
&= G_0^r g^{r\,-1} f(\omega)(g^r - g^a) g^{a\,-1} G_0^a + G_0^r\Sigma^< G_0^a \\
&= f(\omega) G_0^r(g^{a\,-1} - g^{r\,-1}) G_0^a + G_0^r\Sigma^< G_0^a \\
&= G_0^r\Sigma^< G_0^a,
\end{aligned} \tag{4.122}$$

where we have used (4.57) and (4.59) in the second last line to eliminate the first term. The variable ω is dropped here to make the formula simple.

$G^<$ is calculated in the same procedure until the fourth last line, i.e.

$$G^< = G^r G_0^{r\,-1} G_0^< G_0^{a\,-1} G^a + G^r\Sigma_n^< G^a = G^r(\Sigma^< + \Sigma_n^<) G^a, \tag{4.123}$$

where Eq. (4.122) is used.

Define

$$\begin{aligned}
\Gamma_\alpha(\omega) &= i(\Sigma_\alpha^r(\omega) - \Sigma_\alpha^a(\omega)) = iV_{\alpha C}(g_\alpha^r(\omega) - g_\alpha^a)(\omega)V_{C\alpha} \\
&= if_\alpha(\omega)^{-1} V_{\alpha C} g_\alpha^<(\omega) V_{C\alpha} = \frac{i}{f_\alpha(\omega)}\Sigma_\alpha^<(\omega),
\end{aligned} \tag{4.124}$$

i.e. $\Sigma_\alpha^<(\omega) = -if_\alpha(\omega)\Gamma_\alpha(\omega), \qquad \alpha = L, R.$

$\Gamma(\omega)$ is Hermitian as

$$\Gamma_\alpha^\dagger(\omega) = -i(\Sigma_\alpha^a(\omega) - \Sigma_\alpha^r(\omega)) = \Gamma_\alpha(\omega). \tag{4.125}$$

As the flux (4.114) is a physical quantity, it can be written as half of the sum of itself and its complex conjugate. With the help of Eq. (4.120) (4.123) and (4.124), the thermal flux can be written as

$$\begin{aligned}
\langle J_L\rangle &= -\frac{1}{4\pi}\int \omega\,\mathrm{Tr}[G^r\Sigma_L^< + G^<\Sigma_L^a - G^a\Sigma_L^< - G^<\Sigma_L^r]d\omega \\
&= -\frac{1}{4\pi}\int \omega\,\mathrm{Tr}[-if_L(G^r - G^a)\Gamma_L + G^<(\Sigma_L^a - \Sigma_L^r)]d\omega \\
&= -\frac{1}{4\pi}\int \omega\,\mathrm{Tr}[-if_L(G^r - G^a)\Gamma_L + iG^<\Gamma_L]d\omega \\
&= \frac{1}{4\pi}\int \omega\,\mathrm{Tr}[if_L(G^r - G^a)\Gamma_L - iG^<\Gamma_L]d\omega,
\end{aligned} \tag{4.126}$$

where we have used $G^r = G^{a\dagger}$, $G^{<\dagger} = -G^<$ according to the definition, and $\Sigma^{<\dagger} = V_{C\alpha}(g_\alpha^<)^\dagger V_{\alpha C} = -\Sigma^<$. The flux flows out from the left lead should be the same as the flux flows into the right lead, thus (4.126) can be further symmetrized as

$$\begin{aligned}
\langle J\rangle &= \frac{1}{2}(\langle J_L\rangle - \langle J_R\rangle) \\
&= \frac{1}{8\pi}\int \omega\,\mathrm{Tr}[if_L(G^r - G^a)\Gamma_L - iG^<\Gamma_L - if_R(G^r - G^a)\Gamma_R + iG^<\Gamma_R]d\omega \\
&= \frac{1}{8\pi}\int \omega\,\mathrm{Tr}[i(G^r - G^a)(f_L\Gamma_L - f_R\Gamma_R) - iG^<(\Gamma_L - \Gamma_R)]d\omega.
\end{aligned} \tag{4.127}$$

Note that the integral here is from $-\infty$ to $+\infty$, but we are only interested in the positive frequencies, which gives

$$\langle J\rangle = \frac{1}{4\pi}\int_0^\infty \omega\,\mathrm{Tr}[i(G^r - G^a)(f_L\Gamma_L - f_R\Gamma_R) - iG^<(\Gamma_L - \Gamma_R)]d\omega. \tag{4.128}$$

4.10 Effective transmission function

In electronic transport, the Landauer formula calculates the conductance of the system by defining a transmission function $T[\omega]$, so that

$$\kappa = \frac{1}{2\pi}\int_0^\infty \omega T[\omega]\frac{\partial f(\omega)}{\partial T}d\omega, \tag{4.129}$$

where $f(\omega)$ is the distribution function at temperature T. In thermal transport, with nonlinear interactions present, we would like a formula of the same form.

The thermal conductance is defined as

$$\kappa = \lim_{\Delta T\to 0}\frac{J}{\Delta T} = \frac{\delta J}{\delta T} \tag{4.130}$$

where ΔT is the temperature difference between the two heat baths that are connected to the junction. The temperature of the heat baths are $T_L = T + \Delta T/2$ and $T_R = T - \Delta T/2$. Eq. (4.130) can be calculated using the variational method. The variational derivative is given by

$$\frac{\delta A}{\delta T} = \lim_{\Delta T\to 0}\frac{A(T_L, T_R) - A(T, T)}{T_L - T_R}. \tag{4.131}$$

First we transform Eq. (4.128) to a formula based on G^r, G^a and Γ, which gives

$$\begin{aligned}\langle J\rangle &= \frac{1}{4\pi}\int_0^\infty \omega\,\mathrm{Tr}[i(G^r - G^a)(f_L\Gamma_L - f_R\Gamma_R)\\ &\quad - iG^r(\Sigma^< + \Sigma_n^<)G^a(\Gamma_L - \Gamma_R)]d\omega\\ &= \frac{1}{4\pi}\int_0^\infty \omega\,\mathrm{Tr}[i(G^r - G^a)(f_L\Gamma_L - f_R\Gamma_R)\\ &\quad - G^r(f_L\Gamma_L + f_R\Gamma_R + i\Sigma_n^<)G^a(\Gamma_L - \Gamma_R)]d\omega\end{aligned} \tag{4.132}$$

Note that

$$G^{r-1} - G^{a-1} = (\Sigma_L^a - \Sigma_L^r) + (\Sigma_R^a - \Sigma_R^r) + (\Sigma_n^a - \Sigma_n^r) = i(\Gamma_L + \Gamma_R + \Gamma_n) \quad (4.133)$$

$$G^r(G^{r-1} - G^{a-1})G^a = G^a - G^r = iG^r(\Gamma_L + \Gamma_R + \Gamma_n)G^a, \quad (4.134)$$

$$G^a(G^{r-1} - G^{a-1})G^r = G^a - G^r = iG^a(\Gamma_L + \Gamma_R + \Gamma_n)G^r, \quad (4.135)$$

where we have defined $i\Gamma_n = \Sigma_n^a - \Sigma_n^r$. Inserting Eq. (4.134) into Eq. (4.132) gives

$$\langle J\rangle = \frac{1}{4\pi}\int_0^\infty \omega\,\mathrm{Tr}[(f_L - f_R)(G^r\Gamma_L G^a\Gamma_R + G^r\Gamma_R G^a\Gamma_L) + G^r\Gamma_n G^a(f_L\Gamma_L - f_R\Gamma_R) - iG^r\Sigma_n^< G^a(\Gamma_L - \Gamma_R)]d\omega \quad (4.136)$$

Now let's calculate the variation of $\langle J\rangle$ term by term. The variational derivative of $f_L - f_R$ is

$$\frac{\delta(f_L - f_R)}{\delta T} = \lim_{\Delta T\to 0}\frac{f(T_L) - f(T_R) - (f(T) - f(T))}{\Delta T} = \frac{1}{2}\lim_{\Delta T\to 0}\left(\frac{f(T + \frac{\Delta T}{2}) - f(T)}{\frac{\Delta T}{2}} - \frac{f(T - \frac{\Delta T}{2}) - f(T)}{\frac{\Delta T}{2}}\right) = \frac{\partial f}{\partial T}. \quad (4.137)$$

Because f_L and f_R approaches to the Bose distribution at temperature T as the temperature difference ΔT between the left lead and the right lead goes to zero, the first term in the trace of Eq. (4.136) gives

$$\frac{\partial f}{\partial T}(G^r\Gamma_L G^a\Gamma_R + G^r\Gamma_R G^a\Gamma_L).$$

Noticing that $\Gamma_{L,R}$ is temperature independent, its derivative over T is thus equal to

zero. We can derive the variation of $f_L\Gamma_L - f_R\Gamma_R$ as

$$\begin{aligned}\frac{\delta(f_L\Gamma_L - f_R\Gamma_R)}{\delta T} &= \lim_{\Delta T\to 0}\frac{f(T_L)\Gamma_L - f(T_R)\Gamma_R - [f(T)\Gamma_L - f(T)\Gamma_R]}{\Delta T} \\ &= \frac{1}{2}\frac{\partial f}{\partial T}(\Gamma_L + \Gamma_R).\end{aligned} \tag{4.138}$$

To calculate the variation of Eq. (4.136), we also need to know the value of $\delta G^r/\delta T$, which can be derived from Dyson's equation $G^r = G_0^r + G_0^r\Sigma_n^r G^r$ as

$$\begin{aligned}\delta G^r &= \delta G_0^r + \delta G_0^r\Sigma_n^r G^r + G_0^r\delta\Sigma_n^r G^r + G_0^r\Sigma_n^r\delta G^r \\ &= G_0^r\delta\Sigma_n^r G^r + G_0^r\Sigma_n^r\delta G^r \\ &= G_0^r(\delta\Sigma_n^r G^r + \Sigma_n^r\delta G^r) \\ &= G^r(1+\Sigma_n^r G^r)^{-1}(\delta\Sigma_n^r G^r + \Sigma_n^r\delta G^r),\end{aligned} \tag{4.139}$$

where we have omitted δT for simplicity and used $\delta G_0^r/\delta T = 0$ to eliminate δG_0^r. Multiplying $(G^{r\,-1}+\Sigma_n^r)$ on both sides of Eq. (4.139) with some simple manipulations, we have

$$\delta G^r = G^r\delta\Sigma_n^r G^r, \tag{4.140}$$

which is also valid for δG^a.

The second term in the trace of Eq. (4.136) thus yields

$$\begin{aligned}&(\delta G^r\Gamma_n G^a + G^r\delta\Gamma_n G^a + G^r\Gamma_n\delta G^a)(f_L\Gamma_L - f_R\Gamma_R) + \frac{1}{2}G^r\Gamma_n G^a(\Gamma_L+\Gamma_R)\frac{\partial f}{\partial T} \\ &= (G^r\delta\Sigma_n^r G^r\Gamma_n G^a + G^r\delta\Gamma_n G^a + G^r\Gamma_n G^a\delta\Sigma_n^a G^a)(\Gamma_L-\Gamma_R)f + \frac{1}{2}G^r\Gamma_n G^a(\Gamma_L+\Gamma_R)\frac{\partial f}{\partial T}.\end{aligned}$$

Repeating the same process, the third term in the trace of Eq. (4.136) gives

$$
\begin{aligned}
&- i(\delta G^r \Sigma_n^< G^a + G^r \delta\Sigma_n^< G^a + G^r \Sigma_n^< \delta G^a)(\Gamma_L - \Gamma_R) \\
&\qquad = -i(G^r \delta\Sigma_n^r G^r \Sigma_n^< G^a + G^r \delta\Sigma_n^< G^a + G^r \Sigma_n^< G^a \delta\Sigma_n^a G^a)(\Gamma_L - \Gamma_R).
\end{aligned}
$$

These terms can be further simplified if we replace $\Sigma_n^<$ by $-if\Gamma_n$ and define

$$
S = i\left[f(\frac{\delta\Sigma_n^r}{\delta T} - \frac{\delta\Sigma_n^a}{\delta T}) - \frac{\delta\Sigma_n^<}{\delta T}\right]\left(\frac{\partial f}{\partial T}\right)^{-1}. \tag{4.141}
$$

The final form can then be compared with the Landauer formula and we obtain an effective transmission function [106]

$$
T[\omega] = \frac{1}{2}\,\mathrm{Tr}\{G^r(\Gamma_L + \frac{1}{2}\Gamma_n - S)G^a\Gamma_R\} + \frac{1}{2}\,\mathrm{Tr}\{G^a\Gamma_L G^r(\Gamma_R + \frac{1}{2}\Gamma_n + S)\} \tag{4.142}
$$

This effective transmission function represents the transmission possibility for phonons of different frequencies to get through the nonlinear junction section. It is an important concept in thermal transport and its applications will be discussed in the next chapter.

Chapter 5

NEGF: Implementation and Applications

The nonequilibrium Green's function method is a very general method, which is applicable to systems with arbitrary structures. In this chapter, we will discuss the procedures to solve the Green's function and calculate the thermal conductance. The algorithm to solve the surface Green's function is given. This is followed by a discussion about mean field approximation. Then we will apply the resulted program to study some concrete systems. Most importantly, the program is used to study thermal rectification effect.

5.1 Numerical implementation

5.1.1 Procedures for calculating the thermal conductance

The procedure for implementing a program to calculate the thermal conductance of an arbitrary junction is given below. It is just a guide line for the actual implementation. Some detailed tricks and algorithms are explained later.

1. Initialize the program by reading the input files containing the structure of the intended model, i.e. the interactions between each degree of freedom. For system with nonlinear interactions in the junction, third and fourth order interactions are also needed.

2. Compute the Green's function of the semi-infinite leads, using the equation $g_\alpha(\omega) = (\omega^2 - K_\alpha)^{-1}$ with $\alpha = L, R$. Even though $K_{L,R}$ and thus $g_{L,R}(\omega)$ has many degrees of freedom, only the element at the surface is necessary, as tight-binding approximation is used. Therefore it can be calculated effectively using a decimation method given in Sec. 5.1.2.

3. Calculate the self-energy of both leads with $\Sigma_\alpha = V^{C\alpha} g_\alpha V^{\alpha C}$. For a central junction part with N degrees of freedom, the self-energy Σ_α is an $N \times N$ matrix.

4. Compute the linear junction retarded and advanced Green's function $G_0^{r,a}$ by $G_0^r = G_0^{a\dagger} = ((\omega + i\eta)^2 I - K^C - \Sigma^r)^{-1}$, where $\Sigma^r = \Sigma_L^r + \Sigma_R^r$.

5. Calculate the nonlinear self-energy Σ_n in the junction using Feynman diagrams, as explained in Sec. 4.7. The self-energy is calculated self-consistently until it converges.

6. Obtain the junction part of G^r and $G^<$ with nonlinear interactions by $G^r = (G_0^{r\,-1} - \Sigma_n^r)^{-1}$ and $G^< = G^r(\Sigma^< + \Sigma_n^<)G^a$.

7. Get the thermal flux of the system with

$$J = \frac{1}{4\pi} \int_0^\infty \omega \,\mathrm{Tr}\{(G^r - G^a)(\Sigma_R^< - \Sigma_L^<) + iG^<(\Gamma_R - \Gamma_L)\} d\omega$$

   where $\Gamma_{L,R} = i(\Sigma_{L,R}^r - \Sigma_{L,R}^a)$.

8. Obtain the thermal conductance of the junction from $\kappa = \lim_{\Delta T \to 0} \frac{J}{\Delta T}$, where

ΔT is the temperature difference between the two heat baths that are connected to the junction.

5.1.2 Surface Green's function

The surface Green's function is an essential part in our calculation. We have followed Ref. [107] to present the derivation. The Green's function of the lead is given by Eq. (4.57), i.e. $g^r(\omega) = (\omega^2 - K)^{-1}$, where K is the interaction matrix. The leads are comprised of principal layers. Each principal layer only interacts with its two neighboring layers. This can always be done if the long range interaction is negligible.

The matrix form of Eq. (4.57) is

$$\begin{pmatrix} \omega^2 - K_{00} & -K_{01} & 0 & \dots & \\ -K_{10} & \omega^2 - K_{11} & -K_{12} & 0 & \dots \\ 0 & -K_{21} & \omega^2 - K_{22} & -K_{23} & 0 \ \dots \\ \dots & & & & \end{pmatrix} \begin{pmatrix} g_{00} & g_{01} & g_{02} & \dots \\ g_{10} & g_{11} & g_{12} & \dots \\ g_{20} & g_{21} & g_{22} & \dots \\ \dots & & & \end{pmatrix} = I, \quad (5.1)$$

where I is the unit matrix. It can be written out as a set of equations explicitly, which yields

$$\begin{aligned} (\omega^2 - K_{00})g_{00} &= 1 + K_{01}g_{10}, \\ (\omega^2 - K_{00})g_{10} &= K_{01}^T g_{00} + K_{01}g_{20}, \\ (\omega^2 - K_{00})g_{20} &= K_{01}^T g_{10} + K_{01}g_{30}, \\ &\dots \\ (\omega^2 - K_{00})g_{n0} &= K_{01}^T g_{n-1,0} + K_{01}g_{n+1,0}, \end{aligned} \quad (5.2)$$

where we have used $K_{00} = K_{11} = K_{22} = \dots$, $K_{01} = K_{12} = K_{23} = \dots$ and $K_{10} = K_{01}^T$. For cases where $K_{00} \neq K_{11}$, the result should be similar. Our aim is to calculate g_{00}.

Combine the first two equations of Eq. (5.2), we have

$$(\omega^2 - K_{00} - K_{01}(\omega^2 - K_{00})^{-1}K_{01}^T)g_{00} = 1 + K_{01}(\omega^2 - K_{00})^{-1}K_{01}g_{20}. \tag{5.3}$$

Similarly, any arbitrary layer has

$$\begin{aligned}(\omega^2 - K_{00} - K_{01}(\omega^2 - K_{00})^{-1}K_{01}^T - K_{01}^T(\omega^2 - K_{00})^{-1}K_{01})g_{n0} \\ = K_{01}^T(\omega^2 - K_{00})^{-1}K_{01}^T g_{n-2,0} + K_{01}(\omega^2 - K_{00})^{-1}K_{01}g_{n+2,0}. \quad (n \geq 2)\end{aligned} \tag{5.4}$$

This procedure effectively removes the nearest neighbors from the equation set. To summarize, we have

$$\begin{aligned}(\omega^2 - \epsilon_s)g_{00} &= 1 + \alpha g_{20}, \\ (\omega^2 - \epsilon)g_{n0} &= \beta g_{n-2,0} + \alpha g_{n+2,0} \quad (n \geq 2),\end{aligned} \tag{5.5}$$

with

$$\begin{aligned}\epsilon_s &= K_{00} + K_{01}(\omega^2 - K_{00})^{-1}K_{01}^T, \\ \epsilon &= K_{00} + K_{01}(\omega^2 - K_{00})^{-1}K_{01}^T + K_{01}^T(\omega^2 - K_{00})^{-1}K_{01}, \\ \alpha &= K_{01}(\omega^2 - K_{00})^{-1}K_{01}, \\ \beta &= K_{01}^T(\omega^2 - K_{00})^{-1}K_{01}^T.\end{aligned} \tag{5.6}$$

A subset of Eq. (5.5) gives the even Green's function element, which is

$$\begin{aligned}(\omega^2 - \epsilon_s)g_{00} &= 1 + \alpha g_{20}, \\ (\omega^2 - \epsilon)g_{2n,0} &= \beta g_{2(n-1),0} + \alpha g_{2(n+1),0} \quad (n \geq 1),\end{aligned} \tag{5.7}$$

which has the same form as Eq. (5.2), thus the above procedure can be used again

and we arrive at

$$\begin{aligned}(\omega^2 - \epsilon_i^s)g_{00} &= 1 + \alpha_i g_{2^i n,0}, \qquad (n \geq 1),\\ (\omega^2 - \epsilon_i)g_{2^i n,0} &= \beta_i g_{2^i(n-1),0} + \alpha_i g_{2^i(n+1),0},\end{aligned} \tag{5.8}$$

with

$$\begin{aligned}\alpha_i &= \alpha_{i-1}(\omega^2 - \epsilon_{i-1})^{-1}\alpha_{i-1},\\ \beta_i &= \beta_{i-1}(\omega^2 - \epsilon_{i-1})^{-1}\beta_{i-1},\\ \epsilon_i^s &= \epsilon_{i-1}^s + \alpha_{i-1}(\omega^2 - \epsilon_{i-1})^{-1}\beta_{i-1},\\ \epsilon_i &= \epsilon_{i-1} + \alpha_{i-1}(\omega^2 - \epsilon_{i-1})^{-1}\beta_{i-1} + \beta_{i-1}(\omega^2 - \epsilon_{i-1})^{-1}\alpha_{i-1},\end{aligned} \tag{5.9}$$

and $\epsilon_0^s = \epsilon_0 = K_{00}$, $\alpha_0 = K_{01}$, $\beta_0 = K_{01}^T$. Eq. (5.9) gives an explicit iterative procedure. The iteration can be terminated when α and β are small enough so that $\epsilon_i^s \approx \epsilon_{i-1}^s$ and $\epsilon_i \approx \epsilon_{i-1}$, and we have

$$(\omega^2 - \epsilon_i^s)g_{00} \approx I. \tag{5.10}$$

In the actual calculation, ω is replaced by $\omega + i\eta$. This is to avoid the singularity appeared in Eq. (5.10). A short program to calculate the surface Green's function is included in Appendix A.

5.1.3 Mean field approximation

In the Feynman diagram expansion, there are terms of arbitrary orders. Due to the calculation capacity, only a few of these terms can be calculated. At low temperatures, the higher order diagrams are not important, thus can be safely discarded. However, at high temperatures, the omission of higher order terms will seriously affect the final results. Thus we need to find a way to include higher order terms, and at the

same time, make the problem still solvable. This can be done through mean field approximation. The mean field approximation of self-energy is given in Fig. 5.1, where some of the single lines representing G_0 in Fig. 4.2 are replaced by double lines representing G so that the expansion of the self-energy after replacement provides higher order terms.

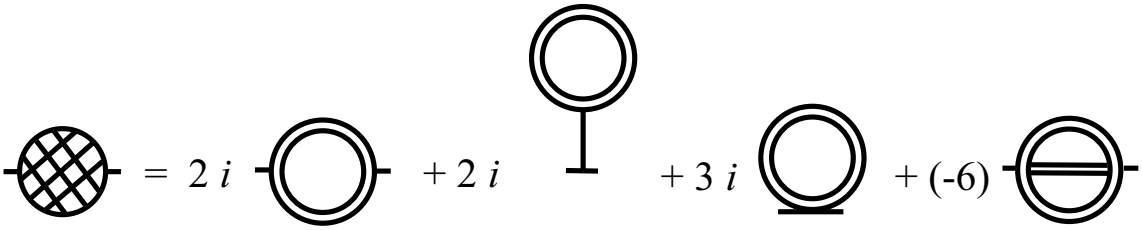

Figure 5.1: Mean field approximation to the self-energy. The double line represents the full Green's function G. The single line denotes G_0

5.2 Results and Discussion

5.2.1 One-dimensional harmonic chain

Firstly, we study a uniform one-dimensional harmonic chain. This simple system can be solved exactly, thus the results of our calculation can be checked easily.

For such a system, there are no resistance for the phonon transmission, thus all the phonons up to a specific frequency can be transmitted as free particles. The result is shown in Fig. 5.2. A direct calculation shows that the maximum frequency for a harmonic chain with force constant K and mass m is $\sqrt{4K/M}$ [2]. For $K = 1$ and $M = 1$, the maximum frequency would be $\omega = 2$, which is the same as what is shown in Fig. 5.2.

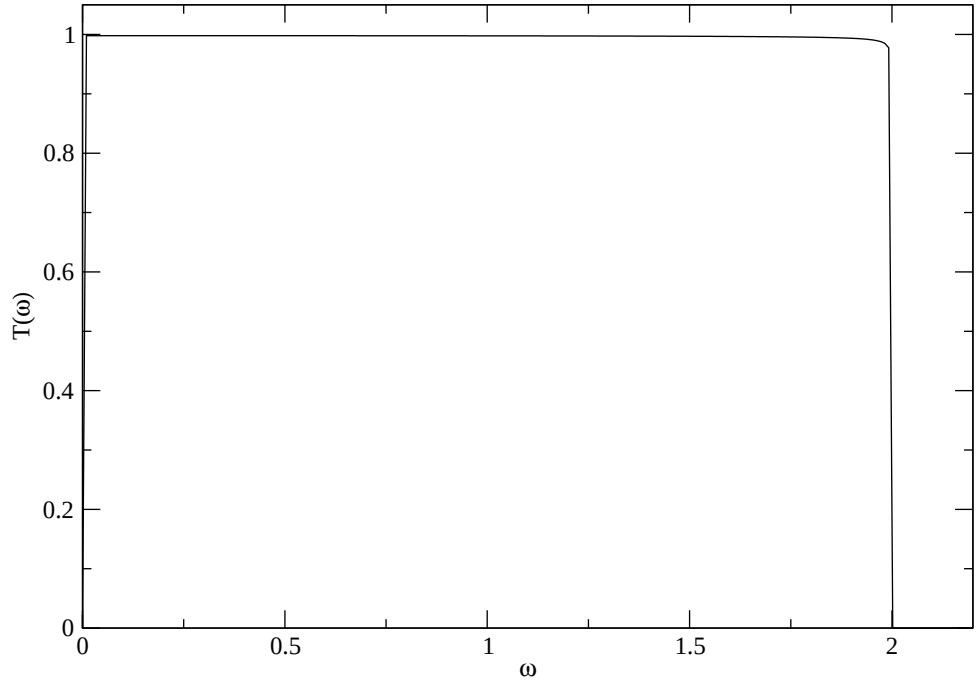

Figure 5.2: Thermal transmission for uniform harmonic one-dimensional chain with $K = 1$ and $m = 1$.

5.2.2 Thermal conductivity with nonlinear interactions

To show the effects of nonlinear interactions on the system's thermal conductivity, we calculated the thermal conductivity of a one-dimensional chain with cubic and quartic interactions. The Hamiltonian of the system is in the form of Eq. (4.1), while the nonlinear term is much simpler in this case. It gives

$$H_n = \sum_{i,j=i\pm1} \frac{1}{3} k_3 (u_i - u_j)^3 + \sum_{i,j=i\pm1} \frac{1}{4} k_4 (u_i - u_j)^4, \tag{5.11}$$

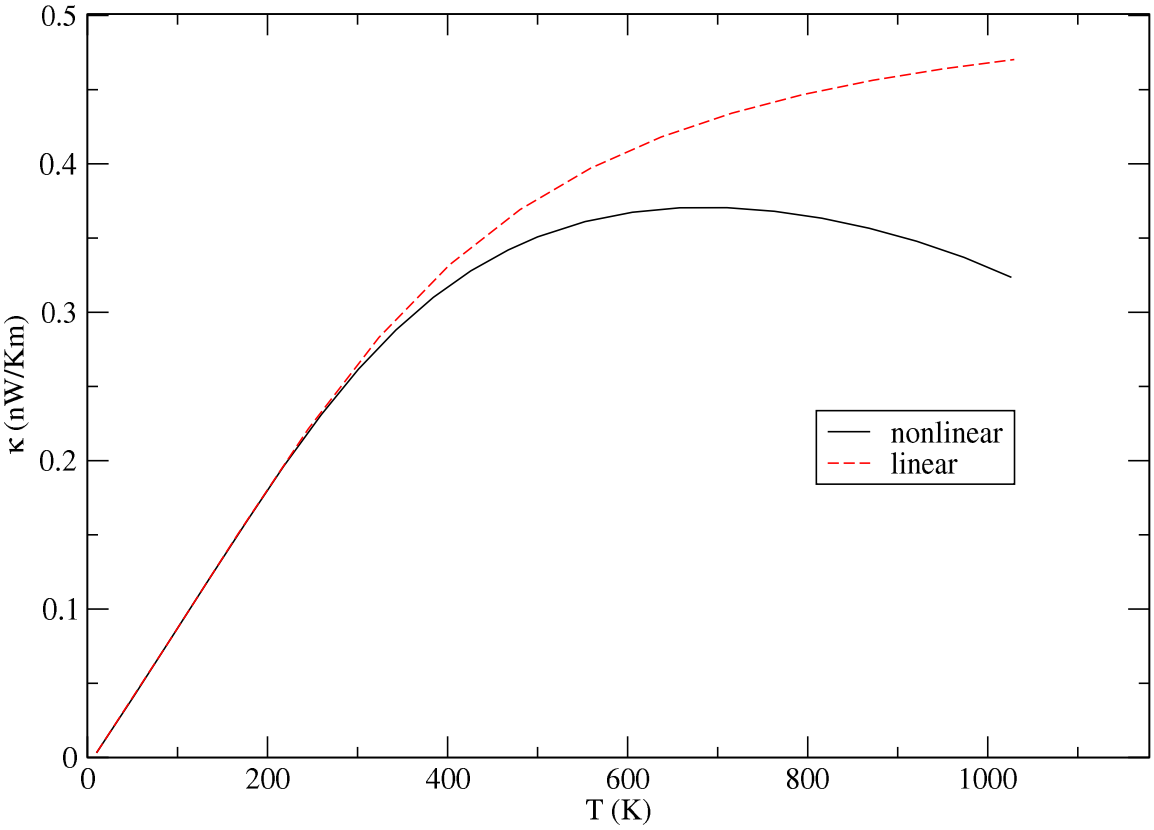

Figure 5.3: Thermal conductivity vs. temperature of one-dimensional chain with and without nonlinear interactions. The solid line denotes the system with nonlinear interactions, and the segmented line represents the results without the nonlinear interactions. $k_2 = 17.3$ ev/Å^2, $k_3 = 116$ ev/Å^3, $k_4 = 605.6$ ev/Å^4, and $m = 12$ g/mol.

where we have only considered interactions between adjacent atoms. Figure 5.3 shows the relation between the thermal conductivity and the temperature for two different cases. The solid line represents the case with the nonlinear interactions switched on, and the segmented line denotes the case without the nonlinear interactions. We have set the linear interactions between adjacent atoms as $k_2 = 17.3$ ev/Å^2. The cubic and quartic force constants have the values $k_3 = 116$ ev/Å^3 and $k_4 = 605.6$ ev/Å^4, respectively. The mass of each atom is $m = 12$ g/mol. There are 10 atoms altogether

in the junction part. From the figure we notice that the thermal conductivity increases linearly at low temperatures. It reaches the maximum around $700K$ and then decreases as the temperature gets higher. This agrees well with our intuition. At low temperatures, the nonlinear interactions are very weak, thus their effects on thermal conduction are not obvious. As the temperature gets higher, the lattice movements become more violent and thus more and more phonons are generated. The phonon mean free path changes from infinity to a finite value, cause the chance of collision has increased. These collisions are caused by the nonlinear interactions. For a pure harmonic model, the system is ballistic, thus no decline should be observed, as is shown by the segmented line in the figure.

5.2.3 Benzene molecule in the junction

Molecular devices have attracted a lot of attentions in recent years, due to their potential to be used in future generation electronics. A lot of theoretical analyses of their electronic and thermal transport properties have been performed [108, 109, 110, 111, 112, 113], and experiments at such a scale are also increasing rapidly [82, 114, 88, 115, 84, 116, 83, 117, 87, 85, 89, 94, 118, 86, 96, 119, 95, 91, 93, 90, 92]

In this subsection, we examine the thermal transport properties of a benzene molecule connected to two polyethylene leads. Two opposite sites of a benzene ring, which are normally the hydrogen atoms, are now bound covalently to carbon atoms, forming a 1,4-dibutyl-benzene molecule representing the whole system. The system has 14 carbon atoms and 22 hydrogen atoms. The model is shown in Fig. 5.4 The interactions are calculated using Gaussian 03 [120]. We use the Hartree-Fock method with the 6-31G basis set. We have also used a convenient new feature of Gaussian, which can calculate anharmonic interactions up to the 4th order.

Figure 5.5 (solid line) shows the effective transmission function $\tilde{T}[\omega]$ of the benzene junction model at a temperature of 300 K calculated using the mean-field theory. The

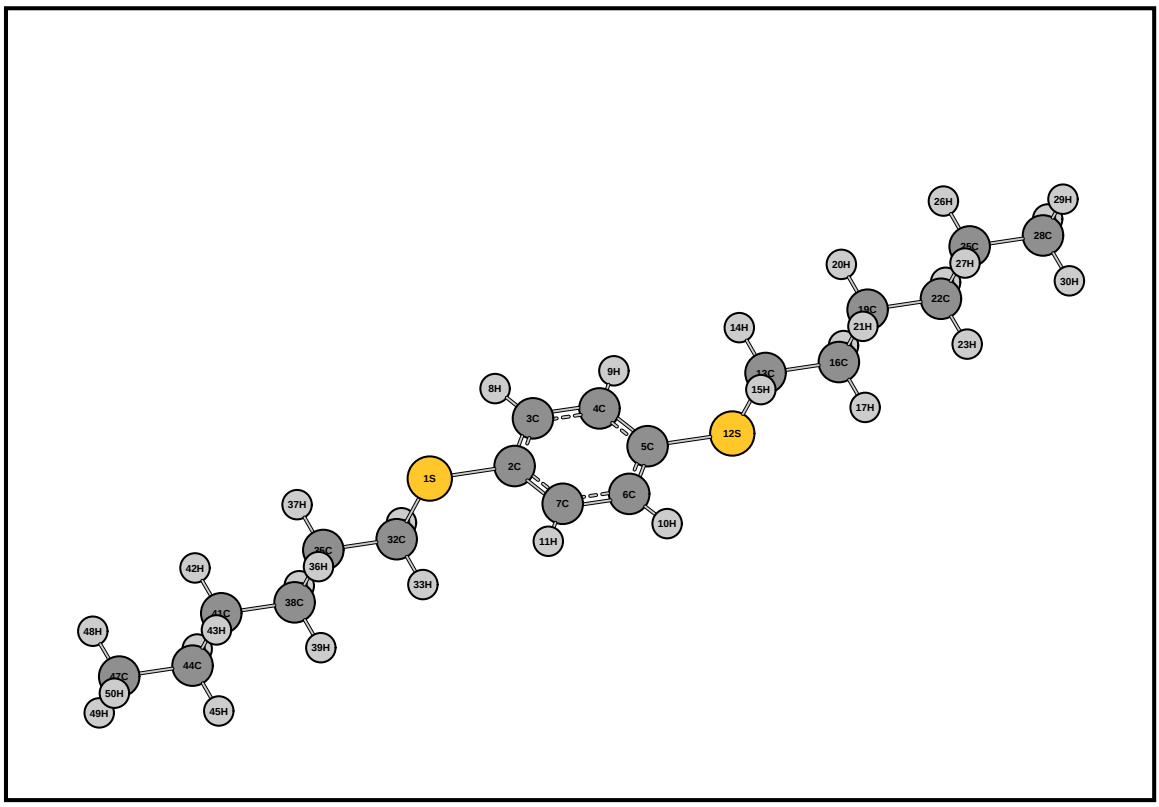

Figure 5.4: Benzene-dithiol molecule connected to polyethylene chain

peak features are complicated, resulting from the vibrational modes of the molecule, the interaction with the leads, and the vibrational spectra of the leads, as well as the temperature effect. To understand the transmission function better, we correlate the peak features with the vibrational spectrum of an isolated benzene molecule calculated from Gaussian, shown in Fig. 5.5 as solid bars. The transmission peaks are roughly located at where the vibrational frequencies appear, but somewhat shifted to low frequencies. It is difficult to identify the peaks with eigenmodes unambiguously.

We notice that the hydrogen atoms do not play much role in the thermal transport. In particular, there are frequencies around $3000\,\mathrm{cm}^{-1}$ associated with the vibrations of H atoms, but there is no transmission in these high frequencies. Vibrations of H atoms have only local effects. We confirm that the H atoms are less important by

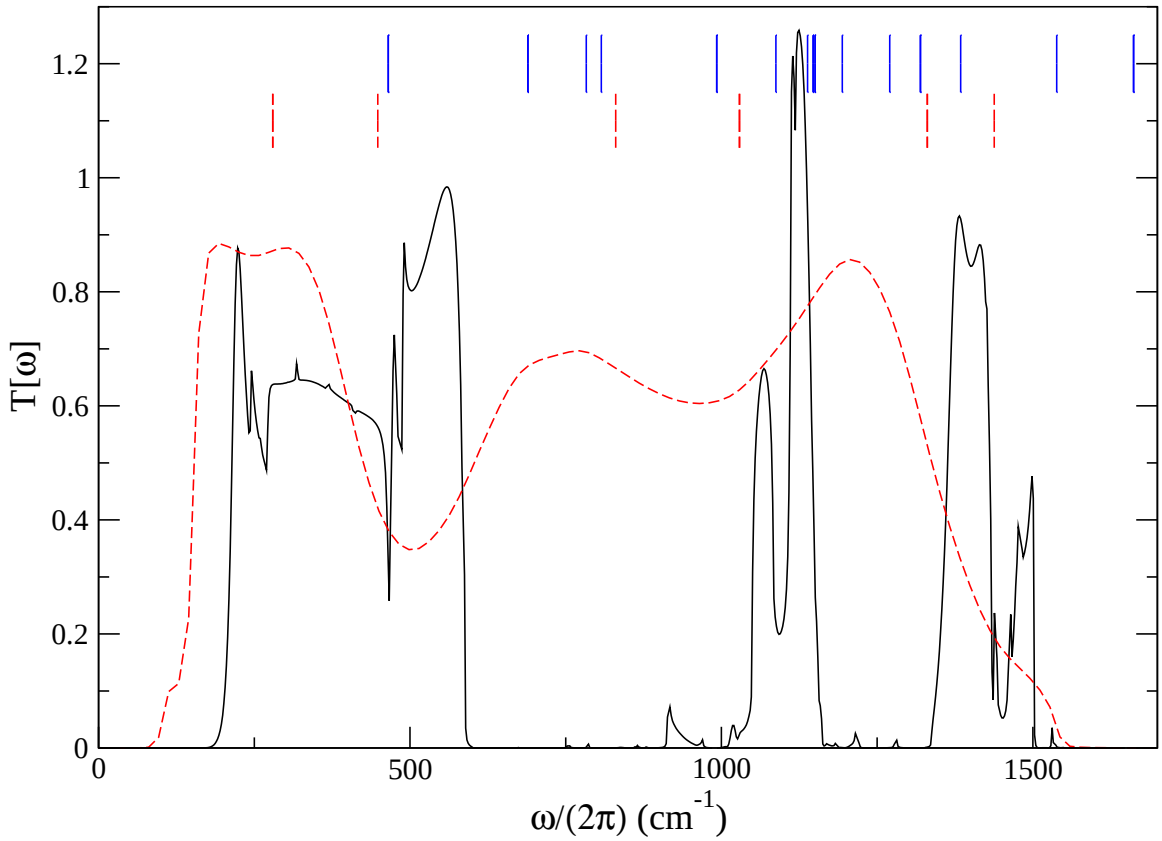

Figure 5.5: Effective transmission of the benzene ring junction at a temperature of 300 K. The solid line is for a full model with force constants calculated from Gaussian, while the dotted line is from a simplified 2D model. The vertical bars indicate the vibrational frequencies of isolated benzene rings of the full model (topmost) and simplified model (dashed), respectively.

a much simplified model retaining only the degrees of freedom of the carbon atoms in a 2D model. The leads are pseudo polyethylene chains; we use an united atom approximation, so the CH_2 group is treated as a single atom. The force constant between each atom is obtained from the DREIDING model [97]. There are only bond interactions in the leads, and we have used the Morse function to calculate the bond potential, which has the form $D(e^{-\alpha(R-R_0)}-1)^2$, where $D = 70\,(\text{kcal/mol})$, $\alpha = \sqrt{5}\,\text{Å}^{-1}$, and $R - R_0$ is the displacement (with the equilibrium bond length $R_0 = 1.4\,\text{Å}$). For the benzene ring, we also include an angular potential, which has the form $\frac{4}{3}\big(\cos(\theta_{ijk})+\frac{1}{2}\big)E$, where $E = 100$ (kcal/mol). We make a Taylor expansion of the potential and calculate the force constants up to the 4th order.

The transmission for the simplified model (dotted line in Fig. 5.5) is smoother due to much reduced degrees of freedom. It is qualitatively in agreement with the full model. In this case, the peaks appear to be in good agreement with the vibrational modes of a hexagonal ring.

5.2.4 Thermal rectification

In this part, we study the thermal rectification effect in nanoscale systems. Although its counterpart in electronics was invented a hundred years ago, the exciting possibility of a thermal rectifier is only now becoming a reality as a result of progress in nanotechnology. The novel electrical and thermal properties of nanoscale systems make them good candidates for solid-state thermal rectifiers. However, to design and optimize useful thermal rectifiers, it is essential to gain an understanding of the fundamental mechanisms behind thermal rectification. Previous work, reviewed below, has shown that two conditions are necessary. The first is that the system must be asymmetric. The second is that there must be nonlinear interactions in the system. While the first condition is obvious, the mechanisms by which the second comes into play are poorly understood.

Terraneo et al. [121] were the first to suggest a possible one-dimensional thermal rectifier model using molecular dynamics simulations. Their model consisted of a chain of particles with harmonic coupling and a Morse on-site potential giving rise to nonlinear interactions. The thermal rectification effect was observed with asymmetrical thermostats. Their explanation using an effective phonon analysis, however, was not very satisfactory, as it did not explain how phonons can transform their frequencies gradually to get through the channel. A different model concentrating on the interface effect was introduced by Li et al.[122, 123, 124, 125]. In their model, two separate nonlinear lattices described by the Frenkel-Kontorova model were joined together with a harmonic chain. Their numerical simulation showed that the heat flow can be controlled by the coupling strength and other system parameters, and the difference in the heat flux in the two directions can be significant. Experiments to measure the thermal conductance of nanowires began to appear in recent years [96]. An experiment measuring the thermal conductance of a nanotube with a coating of increasing mass along the length of the nanotube was carried out by Chang et al. [96], which is the first of this kind. It was noted that thermal flux transmits better in the direction of mass decrement, which cannot be explained by the wave theory and the authors claimed that the observed rectification should be related to solitons. A follow-up study by Yang et al. [126] with a simple one-dimensional model confirmed the rectification effect in such a structure. Simulations to look for thermal rectification in a more complicated nanotube were also carried out [127]. While most of results were obtained from classical molecular dynamics simulations, we also note the work of Segal et al. [128, 112, 129] in which a two level system was analysed quantum mechanically, and in which thermal rectification was also found. [123]

Inspired by the experiment [96], we studied a one-dimensional chain with increasing mass from one end to the other. Changing the mass is effectively equivalent to changing the interaction coefficients, as we can always normalize the coordinates.

The mass gradient provides the necessary asymmetrical structure, and three-body and fourth-body interactions are included to fulfill the second requirement.

Our model is a one-dimensional system which is separated into three parts. The right and left parts are semi-infinite linear leads which are acting as heat baths. The central junction part is coupled to the leads through linear interactions. It can have any structure and it also includes nonlinear interactions, which are our major interest. The Hamiltonian of the system is written as

$$\begin{aligned} \mathcal{H} &= \sum_{\alpha=L,C,R} H_\alpha + u_L^T V_{LC} u_C + u_C^T V_{CR} u_R + H_n \\ H_\alpha &= \sum_i \frac{1}{2}\dot{u}_{\alpha i}^2 + \sum_{i,j=i\pm1} \frac{1}{2} k_{\alpha,ij}(u_{\alpha i} - u_{\alpha j})^2 \\ H_n &= \sum_{i,j=i\pm1} \frac{1}{3} k_3 (u_i - u_j)^3 + \sum_{i,j=i\pm1} \frac{1}{4} k_4 (u_i - u_j)^4 \end{aligned} \tag{5.12}$$

where $u_i = x_i\sqrt{m_i}$ is the normalized displacement for atom i. H_α is the harmonic Hamiltonian of each part, V_{LC} and V_{RC} are the interactions between the junction and the lead, and H_n is the nonlinear interaction in the junction.

In our calculations, the tight-binding approximation is assumed, so the atoms can only interact with their nearest neighbors. The interaction coefficients between adjacent atoms are obtained from the Morse potential $D\{\exp[a(r-r_0)^2]-1\}^2$, where $D = 70$ kcal/mol, $a = \sqrt{5}\text{Å}^{-1}$, and r_0 is the equilibrium distance between adjacent atoms. The values of these parameters were obtained from Ref. [97] for C-C interactions. The third and fourth order coefficients in Eq.(5.12) are obtained by Taylor expansion of the potential around the equilibrium distance. The left lead and the right lead maintain a temperature difference ΔT, which gives $T_L = T + \Delta T/2$ and $T_R = T - \Delta T/2$ for a particular temperature T, or in the reverse order for heat flows in the opposite direction.

In the following part, without specification, the unit of mass is g/mol, the units

of the second, third and fourth order interaction coefficients are eV/Å^2, eV/Å^3 and eV/Å^4 respectively, and the unit of temperature is K as usual. All other quantities have units derived from these.

We start with a one-dimensional chain model with an uneven mass distribution in the junction section. There are 20 atoms in the junction. The mass of each atom is $m_p = m_L(1+0.4p)$ with $p \in [0, 20)$. The second order force constant between adjacent atoms is $k_2 = 17.3$. The third and fourth interaction coefficients are $k_3 = -116$ and $k_4 = 605.6$, respectively. This setup is similar to the experimental conditions for which thermal rectification was measured on a nanotube coated unevenly with heavy molecules [96]. The mass gradient provides the necessary asymmetrical structure for thermal rectification, and three-body and four-body interactions are included to fulfill the requirement of nonlinear interactions.

The thermal transmission probability $T(\omega)$ of phonons with different frequencies is shown in Fig. 5.6. The dot-dot-dashed line represents the result for thermal flux flow from left to right with temperature $T_L = 1100$ and $T_R = 900$. The dashed line shows the results when the direction of thermal flux is reversed. The heat baths at both ends of the junction are identical with a monatomic lattice basis of mass $m_L = m_R = 14$. The plot is divided into two regions by frequency ω_c. From Fig. 5.6 we notice that at low frequencies, where $\omega < \omega_c$, the transmission probability difference between the two curves is small, while at high-frequency region, where $\omega > \omega_c$, the difference is quite noticeable. This indicates that the thermal rectification effect is due to the contribution of high-frequency phonons.

To examine the effect of heat baths on the transmission probability, we change the lattice basis mass of the right heat bath to $m_R = 120.4$ to match the right end of the junction. The results are shown by the solid line and the dot-dashed line in Fig. 5.6. This time, the separation of the low-frequency region and the high-frequency region is more obvious. In fact, the separation frequency ω_c is approximately equal

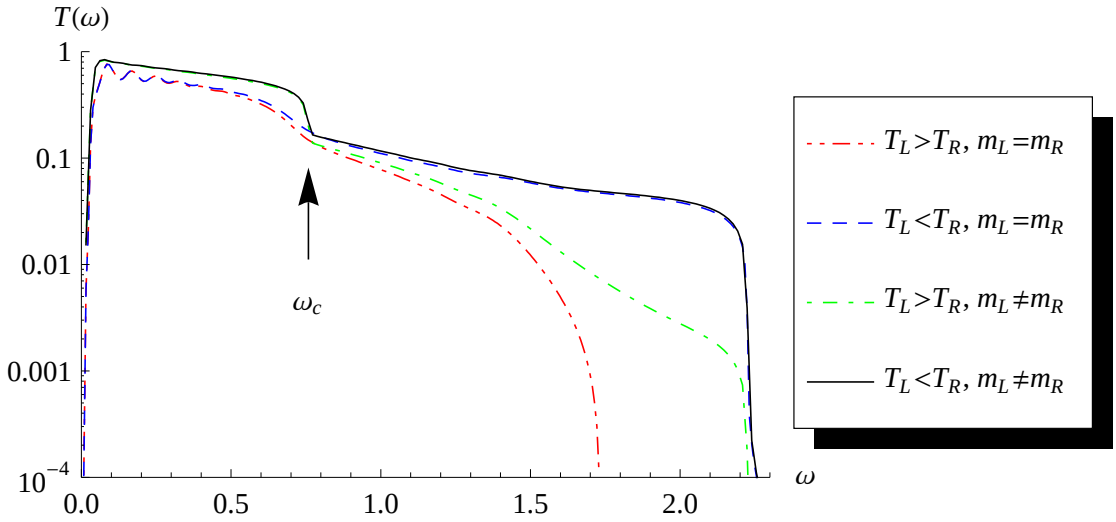

Figure 5.6: (Color Online) Effective thermal transmission vs. phonon frequency, with $n = 20$, $m_p = m_L(1 + 0.4p)$ in the junction region. The dot-dot-dashed line and the dashed line have the same heat baths at each ends with $m_L = m_R = 14$. The dot-dashed line and the solid line have different heat baths at each ends with $m_L = 14$ and $m_R = 120.4$. ω_c is the separation frequency of the high-frequency region and the low-frequency region.

to $\sqrt{4K/M_{max}}$ where K is the force constant, and equal to k_2 here, M_{max} is the maximum atom mass in the chain, which gives $\omega_c = 0.758$. When $\omega > \omega_c$, we notice that the $T(\omega)$'s for phonons flowing from right to left match almost exactly in both heat bath setups. As no high-frequency phonons flow out of the right heat bath due to the filtering at the right interface, this means that the high-frequency phonons flowing into the left heat bath are junction related.

We can define the thermal rectification ratio as

$$\gamma = \frac{|\kappa_{L\to R} - \kappa_{R\to L}|}{\kappa_{L\to R}}, \tag{5.13}$$

where $\kappa_{L\to R}$ is the thermal conductance for heat flows from left to right and $\kappa_{R\to L}$ is the thermal conductance in the opposite direction. Using Eq. (4.129) we obtain the

thermal conductance $\kappa_{L\to R} = 78.0$ pW/K and $\kappa_{R\to L} = 91.2$ pW/K with equal heat baths. Thus the thermal rectification ratio is $\gamma = 0.169$.

To understand the results of Fig. 5.6, we draw the maximum transmittable phonon frequencies across the system as in Fig. 5.7. Different heat baths at the ends are chosen for generality. The left heat bath has a higher cut-off frequency than the right heat bath. The maximum transmittable phonon frequency decreases gradually across the junction section due to the variation of the atom mass. When the thermal flux flows from left to right, phonons with frequency $\omega < \omega_c$ can enter the right lead without problem, while phonons with frequency $\omega > \omega_c$ are blocked at the interface of the junction and the right lead. When the system reaches steady state, the thermal flux across the right interface of the junction and the right lead is proportional to the difference of the number of phonons at both sides, i.e. $J \propto N_L(\omega, T_C) - N_R(\omega, T_R)$, where T_C and T_R is the temperature at the left and right side of the interface, respectively, with frequencies $0 < \omega < \omega_c$. When the thermal flux is reversed, we have the same difference for low-frequency phonons at the left interface. However, there are extra high-frequency phonons flow into the left lead. This is the reason why the thermal conductance is larger when the thermal flux flows from lower cutoff frequency region to higher cutoff frequency region. In this case, the thermal conductance is larger in the mass decrease direction. This is in agreement with Ref. [123, 96, 126].

The extra high-frequency phonons flowing into the left lead originate from low-frequency phonons due to nonlinear interactions in the junction. Without these nonlinear interactions, there would be no high-frequency phonons in the junction when heat flows from right to left, and thus no thermal rectification.

As only high-frequency phonons contribute to the thermal rectification, if the low-frequency phonons are suppressed, the thermal rectification ratio is expected to increase, even though as a consequence the overall thermal flux will also reduce. In

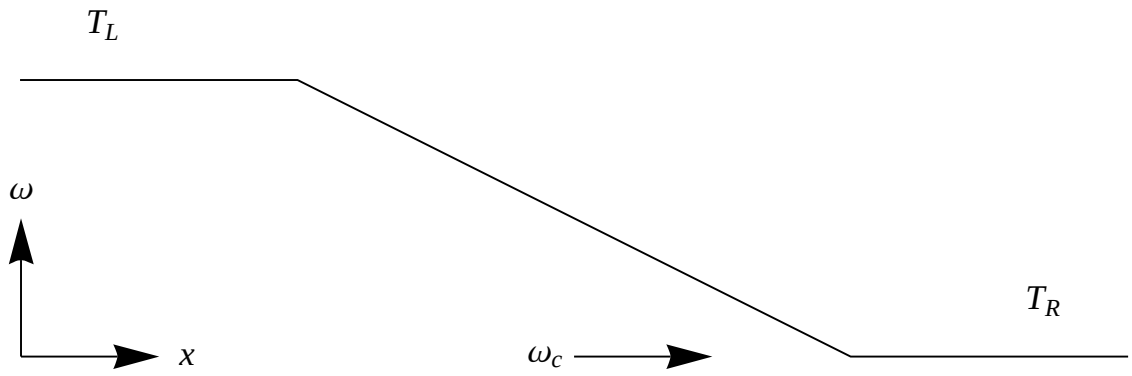

Figure 5.7: Maximum transmittable phonon frequencies for one-dimensional chain with mass varying junction section connected with different heat baths.

other words, the separation frequency ω_c need to be as small as possible. We thus construct a model with even simpler configuration. The atoms in junction section have mass $m_p = m_L = 14$, and the atoms in the right lead have mass $m_R = \beta m_L$ with β ranging from 2 to 1024. Now the only frequency range difference appears at the right interface. The right lead behaves like a high-frequency phonon filter, with only low-frequency phonons allowed to enter. The interaction coefficients are chosen as previously, i.e. $k_2 = 17.3$, $k_3 = -116$ and $k_4 = 605.6$. The results are shown in Fig. 5.8, which gives the dependence of thermal rectification ratio γ on the heat bath mass ratio β. Figure 5.8 shows that as β increases, the thermal rectification ratio γ increases too. The inset of Fig. 5.8 shows the dependence of the thermal conductance difference $\Delta\kappa$ on β. $\Delta\kappa$ becomes a constant when β is sufficiently large. The low-frequency phonons are effectively suppressed, which means that the major contribution to the thermal conductance come from the high-frequency phonons. However, it should also be pointed out that even though the rectification ratio can be very large due to the reduced weight of low-frequency phonons in the conduction, the actual thermal flux is rather small. This is caused by the low density of high-frequency phonons generated in the junction section.

In order to increase the number of high-frequency phonons in the junction, we

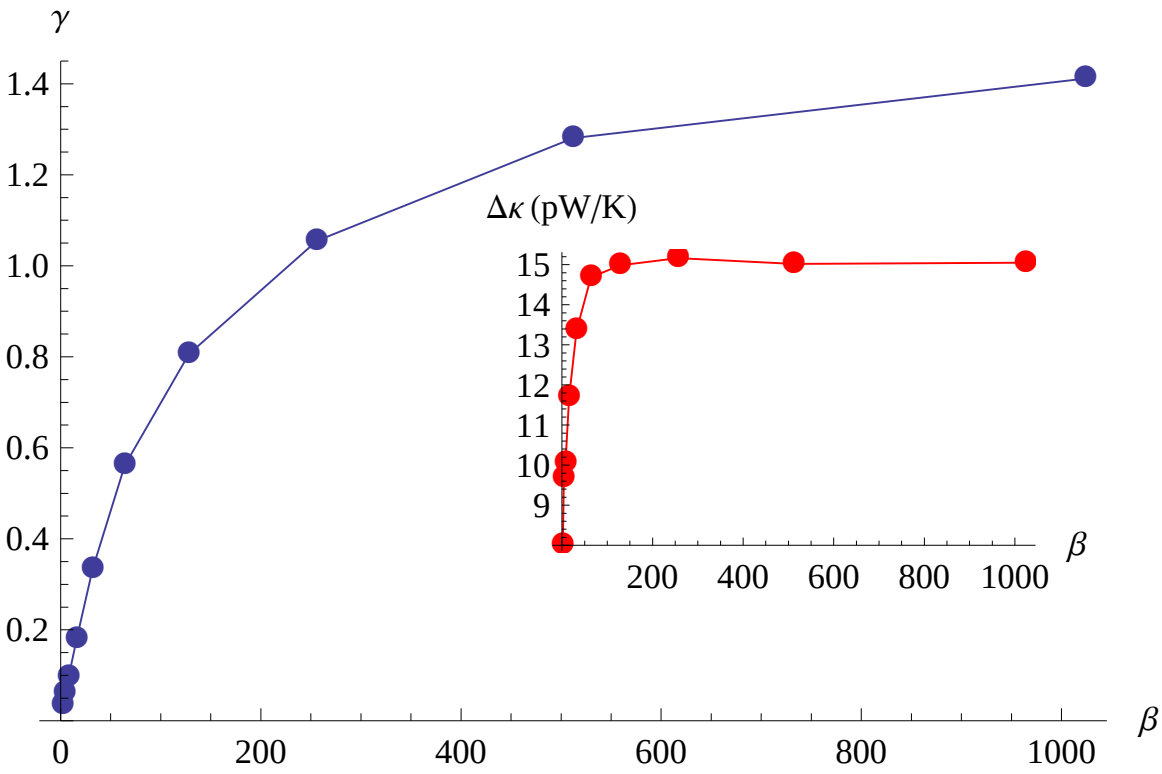

Figure 5.8: Thermal rectification ratio γ vs. heat bath mass ratio $\beta = m_R/m_L$. The inset gives the dependence of the thermal conductance on β for opposite flow directions.

recall that this is temperature related. When the temperature gets higher, more phonons are generated, so the chance of collision is also increased. The relation between the thermal rectification ratio γ and the temperature is illustrated in Fig. 5.9, with the same model parameters in Fig. 5.8 and with β set to 512. Figure 5.9 shows that the thermal rectification ratio increases as the temperature is raised. Ref.[124, 125] using molecular dynamics method also obtained similar results.

In conclusion, we have discussed the thermal rectification effect in a one-dimensional asymmetrical lattice with nonlinear interactions using the nonequilibrium Green's function method. This allowed us to calculate the effective thermal transmission function for phonons. We have shown that thermal rectification is caused by the

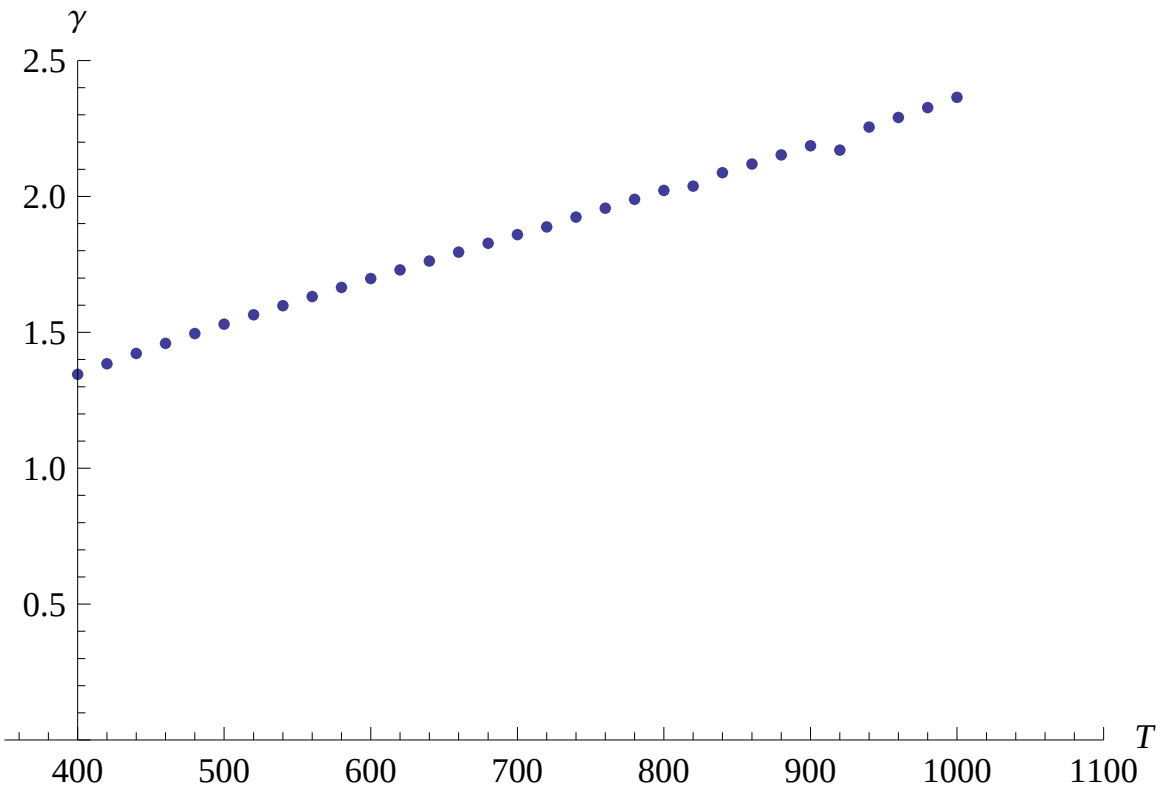

Figure 5.9: Temperature dependence of thermal rectification ratio with $m_L = 14$, $m_R = \beta m_L$, $\beta = 512$, $n = 20$

transmission of high-frequency phonons. These high-frequency phonons are generated from low-frequency phonons by collisions. A thermal rectifier can be realised by designing an effective high-frequency phonon filter at one end of the system so that heat carried by high-frequency phonons are forbidden to enter at one end but freely transmittable at the other end. The thermal rectification ratio can be effectively increased by reducing the weight of low frequency phonons in the entire phonon spectrum. On the other hand, the thermal flux across the system is limited by the conversion rate between low-frequency phonons and high-frequency phonons.

Chapter 6

Conclusion

In this thesis, we have investigated the thermal transport properties of nanoscale systems, where lead-molecule-lead models were studied. Our main focus is on the study of nonlinear effects on the system's thermal conductance.

This thesis is separated into two parts. In the first part, thermal transport is treated from a classical point of view. We studied a quasi one-dimensional polyethylene model using the molecular dynamics method, where the DREIDING force field was used to obtain the force between atoms. We assumed that each atom is in a local equilibrium state, otherwise the temperature will not be well-defined. The relationship between system length and thermal conductivity was studied. We found that the thermal conductivity of this model depends on the tension exerted on its ends. The value of the power index becomes larger as the tension increases. The result explains how different models may have different power index and it suggests a simple way to realize a system with better thermal conductance.

In the second part of the thesis, we studied thermal transport from a quantum point of view. We derived a formalism using nonequilibrium Green's function method,

where we treated the nonlinear interactions explicitly. This is the first time that nonlinear interactions in the nanoscale thermal transport problem is studied using quantum mechanics method. With this formalism, we investigated the thermal transport properties of benzene. The benzene molecule was connected to two semi-infinite polyethylene. We used the DREIDING force field [97] to calculate the energy matrix and the force constants of the system. The force constants up to the 4th order were derived analytically. We then calculated the thermal transmission function using a variational method. A comparison between thermal transmission functions with harmonic interactions and that with anharmonic interactions was made. We noticed that anharmonic interactions greatly reduce the thermal transmission of the system. We also noticed that there is a gap in the transmission function. In order to understand the cause of this, we studied both the spectra of polyethylene and benzene. Compared with the transmission function of the whole system, we found that the gap is caused by the mismatch of phonon dispersion relations of polyethylene and benzene. Another interesting feature we found is that the nonlinear effects are more significant at high temperatures. At low temperatures, their influence is small and generally we can ignore the nonlinear effects. This result agrees with our intuition. When the temperature is very low, there are very few phonons. Thus the phonons can be treated as the ideal gas, where no interactions between phonons exist. As the temperature increases, the density of phonons will also increase, thus the chance of phonon collisions increase too. Phonons can no longer be considered as the ideal gas in this case and the anharmonic interactions need to be considered.

We have also studied thermal rectification effect in one-dimensional chains. In particular, the atoms of the chain have varying mass. It is found that the mass gradient in the central junction plays a role of modifying the phonon transmission frequency band. The asymmetry of the band structure causes thermal rectification. Besides the asymmetry of the structure, nonlinear interactions in the junction is also

necessary, as it provides mechanism for phonons of different frequencies converting between each other. Low frequency phonons in the phonon band overlay region do not contribute to the thermal rectification while high frequency phonons do. Our results present an explicit explanation to the thermal rectification and should enable further investigation on the creation of real solid state thermal rectifiers.

Our NEGF theory is among the first attempts [78, 106, 79] up to now to tackle the nonlinear problems in thermal transport. It sets the ground for further investigations. This first-principles approach enhances our understanding of thermal transport in nanoscale systems. It is both important theoretically and valuable practically.

However, there are some limitations of our formalism that we need to address. Firstly, only phonon-phonon interactions are considered. So our formalism is not applicable to systems whose thermal energy carriers are mainly electrons. We have intentionally omitted the other type of interactions because the materials we are interested in are all insulators. Secondly, we have applied mean field theory in our calculation. Because of this, the results are only qualitatively correct. However, this is not quite critical for our current study, as even a qualitative result is beneficial for our understanding. Thus, a more accurate theory should be developed in the future for this formalism to be widely applicable. Another issue is that no symmetry is considered in the calculation, as this will make the calculation quite complicated. However, because of this, some of the calculations may be redundant, and waste a lot of time. It is desirable to fully utilize the symmetry of the system to make the calculation more efficient.

Up to now, all the research on thermal conductance of nanoscale systems have concentrated on phonon transmission. However, for metals and semiconductors, electrons play an important role in energy transport, which should be studied further. Also, for magnetic and ferromagnetic materials, their thermal transport properties under the magnetic field would be quite different from normal state. A study of the

magnetic effect on the thermal transport would be valuable.

Bibliography

[1] R. E. Peierls. *Quantum Theory of Solids*. Oxford University Press, New York, 1955.

[2] Neil W. Ashcroft and N. David Mermin. *Solid State Physics*. Brooks Cole, college edition, 1976.

[3] P. L. Kapitza. The study of heat transfer in helium ii. *Zh. Eksp. Teor. Fiz.*, 11:1, 1941.

[4] E. T. Swartz and R. O. Pohl. Thermal boundary resistance. *Rev. Mod. Phys.*, 61(3):605–668, Jul 1989.

[5] Z. Rieder, J. L. Lebowitz, and E. Lieb. Properties of a harmonic crystal in a stationary nonequilibrium state. *J. Math. Phys.*, 8(5):1073–1078, 1967.

[6] Hideo Kaburaki and Masahiko Machida. Thermal conductivity in one-dimensional lattices of fermi-pasta-ulam type. *Physics Letters A*, 181(1):85–90, September 1993.

[7] Stefano Lepri, Roberto Livi, and Antonio Politi. Heat Conduction in Chains of Nonlinear Oscillators. *Phys. Rev. Lett.*, 78(10):1896–1899, Mar 1997.

[8] Peter Grassberger, Walter Nadler, and Lei Yang. Heat conduction and entropy production in a one-dimensional hard-particle gas. *Phys. Rev. Lett.*, 89(18):180601, Oct 2002.

[9] Giulio Casati and Toma ž Prosen. Anomalous heat conduction in a one-dimensional ideal gas. *Phys. Rev. E*, 67(1):015203, Jan 2003.

[10] F Mokross and H Buttner. Thermal conductivity in the diatomic toda lattice. *J. Phys. C: Solid State Phys.*, 16(23):4539–4546, 1983.

[11] Takahiro Hatano. Heat conduction in the diatomic toda lattice revisited. *Phys. Rev. E*, 59(1):R1–R4, Jan 1999.

[12] Tomaz Prosen and David K. Campbell. Momentum conservation implies anomalous energy transport in 1D classical lattices. *Phys. Rev. Lett.*, 84(13):2857–2860, Mar 2000.

[13] Onuttom Narayan and Sriram Ramaswamy. Anomalous heat conduction in one-dimensional momentum-conserving systems. *Phys. Rev. Lett.*, 89(20):200601, Oct 2002.

[14] O. V. Gendelman and A. V. Savin. Normal heat conductivity of the one-dimensional lattice with periodic potential of nearest-neighbor interaction. *Phys. Rev. Lett.*, 84(11):2381–2384, Mar 2000.

[15] C. Giardiná, R. Livi, A. Politi, and M. Vassalli. Finite thermal conductivity in 1d lattices. *Phys. Rev. Lett.*, 84(10):2144–2147, Mar 2000.

[16] P. L. Garrido, P. I. Hurtado, and B. Nadrowski. Simple one-dimensional model of heat conduction which obeys fourier's law. *Phys. Rev. Lett.*, 86(24):5486–5489, Jun 2001.

[17] Bambi Hu, Baowen Li, and Hong Zhao. Heat conduction in one-dimensional chains. *Phys. Rev. E*, 57(3):2992–2995, Mar 1998.

[18] Bambi Hu, Baowen Li, and Hong Zhao. Heat conduction in one-dimensional nonintegrable systems. *Phys. Rev. E*, 61(4):3828–3831, Apr 2000.

[19] Kenichiro Aoki and Dimitri Kusnezov. Bulk properties of anharmonic chains in strong thermal gradients: non-equilibrium [phi]4 theory. *Phys. Lett. A*, 265(4):250–256, January 2000.

[20] Emmanuel Pereira and Ricardo Falcao. Normal heat conduction in a chain with a weak interparticle anharmonic potential. *Phys. Rev. Lett.*, 96(10):100601, 2006.

[21] Giulio Casati, Joseph Ford, Franco Vivaldi, and William M. Visscher. One-dimensional classical many-body system having a normal thermal conductivity. *Phys. Rev. Lett.*, 52(21):1861–1864, May 1984.

[22] Nianbei Li, Peiqing Tong, and Baowen Li. Effective phonons in anharmonic lattices: Anomalous vs. normal heat conduction. *Europhys. Lett.*, 75(1):49–55, 2006.

[23] Abhishek Dhar. Heat Conduction in the Disordered Harmonic Chain Revisited. *Phys. Rev. Lett.*, 86(26):5882–5885, Jun 2001.

[24] Baowen Li and Jiao Wang. Anomalous heat conduction and anomalous diffusion in one-dimensional systems. *Phys. Rev. Lett.*, 91(4):044301, Jul 2003.

[25] Jian-Sheng Wang and Baowen Li. Intriguing Heat Conduction of a Chain with Transverse Motions. *Phys. Rev. Lett.*, 92(7):074302, 2004.

[26] Nianbei Li and Baowen Li. Temperature dependence of thermal conductivity in 1d nonlinear lattices. *Europhys. Lett.*, 78(3):34001 (6pp), 2007.

[27] Shigeo Maruyama. A molecular dynamics simulation of heat conduction in finite length swnts. *Physica B: Condensed Matter*, 323(1-4):193–195, October 2002.

[28] Shigeo Maruyama. A molecular dynamics simulation of heat conduction of a finite length single-walled carbon nanotube. *Microscale Thermophysical Engineering*, 7(1):41–50, January 2003.

[29] Gang Zhang and Baowen Li. Thermal conductivity of nanotubes revisited: Effects of chirality, isotope impurity, tube length, and temperature. *J. Chem. Phys.*, 123(11):114714, 2005.

[30] Zhenhua Yao, Jian-Sheng Wang, Baowen Li, and Gui-Rong Liu. Thermal conduction of carbon nanotubes using molecular dynamics. *Phys. Rev. B*, 71(8), 2005.

[31] L. H. Liang and Baowen Li. Size-dependent thermal conductivity of nanoscale semiconducting systems. *Phys. Rev. B*, 73(15):153303, 2006.

[32] I. Ponomareva, D. Srivastava, and M. Menon. Thermal conductivity in thin silicon nanowires: Phonon confinement effect. *Nano Lett.*, 7(5):1155–1159, 2007.

[33] Daniel N. Payton, Marvin Rich, and William M. Visscher. Lattice thermal conductivity in disordered harmonic and anharmonic crystal models. *Phys. Rev.*, 160(3):706–711, Aug 1967.

[34] M. Rich, W. M. Visscher, and D. N. Payton. Thermal conductivity of a two-dimensional two-branch lattice. *Phys. Rev. A*, 4(4):1682–1683, Oct 1971.

[35] Raymond D. Mountain and Rosemary A. MacDonald. Thermal conductivity of crystals: A molecular-dynamics study of heat flow in a two-dimensional crystal. *Phys. Rev. B*, 28(6):3022–3025, Sep 1983.

[36] E A Jackson and A D Mistriotis. Thermal conductivity of one- and two-dimensional lattices. *J. Phys.: Condens. Matter*, 1(7):1223–1238, 1989.

[37] J. Michalski. Thermal conductivity of amorphous solids above the plateau: Molecular-dynamics study. *Phys. Rev. B*, 45(13):7054–7065, Apr 1992.

[38] N Nishiguchi, Y Kawada, and T Sakuma. Thermal conductivity in two-dimensional monatomic non-linear lattices. *Journal of Physics: Condensed Matter*, 4(50):10227–10236, 1992.

[39] Andrea Lippi and Roberto Livi. Heat conduction in two-dimensional nonlinear lattices. *Journal of Statistical Physics*, 100:1147–1172, 2004.

[40] L. Yang, P. Grassberger, and B. Hu. Dimensional crossover of heat conduction in low dimensions. *Phys. Rev. E*, 74(6):062101, 2006.

[41] G. W. Ford, J. T. Lewis, and R. F. O'Connell. Quantum langevin equation. *Phys. Rev. A*, 37(11):4419–4428, Jun 1988.

[42] Dvira Segal, Abraham Nitzan, and Peter Hanggi. Thermal conductance through molecular wires. *J. Chem. Phys.*, 119(13):6840–6855, 2003.

[43] Jian-Sheng Wang. Quantum thermal transport from classical molecular dynamics. *Phys. Rev. Lett.*, 99(16):160601, 2007.

[44] R. Landauer. None. *IBM J. Res. Dev.*, 1:223, 1957.

[45] M. Büttiker. Four-terminal phase-coherent conductance. *Phys. Rev. Lett.*, 57(14):1761–1764, Oct 1986.

[46] David C. Langreth and Elihu Abrahams. Derivation of the landauer conductance formula. *Phys. Rev. B*, 24(6):2978–2984, Sep 1981.

[47] Luis G. C. Rego and George Kirczenow. Quantized thermal conductance of dielectric quantum wires. *Phys. Rev. Lett.*, 81(1):232–235, Jul 1998.

[48] Schwab, Henriksen, Worlock, and Roukes. Measurement of the quantum of thermal conductance. *Nature*, 404(6781):974–977, Apr 2000.

[49] Julian Schwinger. On the green's functions of quantized fields. i. *PNAS*, 37(7):452–455, 1951.

[50] Julian Schwinger. On the green's functions of quantized fields. ii. *PNAS*, 37(7):455–459, 1951.

[51] Paul C. Martin and Julian Schwinger. Theory of many-particle systems. i. *Phys. Rev.*, 115(6):1342–1373, Sep 1959.

[52] Takeo Matsubara. A new approach to quantum-statistical mechanics. *Prog. Theor. Phys.*, 14(4):351–378, 1955.

[53] Gordon Baym and N. David Mermin. Determination of thermodynamic green's functions. *J. Math. Phys.*, 2(2):232–234, 1961.

[54] Gordon Baym and Leo P. Kadanoff. Conservation laws and correlation functions. *Phys. Rev.*, 124(2):287–299, Oct 1961.

[55] Gordon Baym. Self-consistent approximations in many-body systems. *Phys. Rev.*, 127(4):1391–1401, Aug 1962.

[56] S.V. Tyablikov and V.L. Bonch-Bruevich. Perturbation theory for double-time temperature-dependent green functions. *Advances in Physics*, 11(44):317–348, October 1962.

[57] R.A. Cowley. The lattice dynamics of an anharmonic crystal. *Advances in Physics*, 12(48):421–480, October 1963.

[58] L. V. Keldysh. Diagram technique for nonequilibrium processes. *Zh. Eksp. Teor. Fiz*, 47:1515–1527, Oct. 1964.

[59] Leo P. Kadanoff and Gordon Baym. *Quantum Statistical Mechanics*. Benjamin, New York, 1962.

[60] S. Fujita. Thermodynamic evolution equation for a quantum statistical gas. *Journal of Mathematical Physics*, 6(12):1877–1885, 1965.

[61] C Caroli, R Combescot, P Nozieres, and D Saint-James. Direct calculation of the tunneling current. *J. Phys. C: Solid State Phys.*, 4(8):916–929, 1971.

[62] P. Danielewicz. Quantum theory of nonequilibrium processes, i. *Annals of Physics*, 152(2):239–304, February 1984.

[63] Antti-Pekka Jauho. Nonequilibrium green function techniques applied to hot electron quantum transport. *Solid-State Electronics*, 32(12):1265–1271, December 1989.

[64] J. Rammer and H. Smith. Quantum field-theoretical methods in transport theory of metals. *Rev. Mod. Phys.*, 58(2):323–359, Apr 1986.

[65] Mathias Wagner. Expansions of nonequilibrium green's functions. *Phys. Rev. B*, 44(12):6104–6117, Sep 1991.

[66] C Niu, D L Lin, and T-H Lin. Equation of motion for nonequilibrium green functions. *J. Phys.: Condens. Matter*, 11(6):1511–1521, 1999.

[67] Yigal Meir and Ned S. Wingreen. Landauer formula for the current through an interacting electron region. *Phys. Rev. Lett.*, 68(16):2512–2515, Apr 1992.

[68] Raffaele Guido Della Valle and Piero Procacci. Equation of motion for the green's function in anharmonic solids. *Phys. Rev. B*, 46(10):6141–6149, Sep 1992.

[69] Lindor E. Henrickson, Arnold J. Glick, Garnett W. Bryant, and David F. Barbe. Nonequilibrium-green's-function theory of transport in interacting quantum dots. *Phys. Rev. B*, 50(7):4482–4496, Aug 1994.

[70] Antti-Pekka Jauho, Ned S. Wingreen, and Yigal Meir. Time-dependent transport in interacting and noninteracting resonant-tunneling systems. *Phys. Rev. B*, 50(8):5528–5544, Aug 1994.

[71] Supriyo Datta. Nanoscale device modeling: the green's function method. *Superlattices Microstruct*, 28(4):253–278, October 2000.

[72] Stefan Rotter, Jian-Zhi Tang, Ludger Wirtz, Johannes Trost, and Joachim Burgdörfer. Modular recursive green's function method for ballistic quantum transport. *Phys. Rev. B*, 62(3):1950–1960, Jul 2000.

[73] P. S. Damle, A. W. Ghosh, and S. Datta. Unified description of molecular conduction: from molecules to metallic wires. *Phys. Rev. B*, 64(20):201403, Oct 2001.

[74] P.A. Derosa and J.M. Seminario. Electron transport through single molecules: Scattering treatment using density functional and green function theories. *J. Phys. Chem. B*, 105(2):471–481, 2001.

[75] J. G. Kushmerick, D. B. Holt, J. C. Yang, J. Naciri, M. H. Moore, and R. Shashidhar. Metal-molecule contacts and charge transport across monomolecular layers: Measurement and theory. *Phys. Rev. Lett.*, 89(8):086802, Aug 2002.

[76] Prashant Damle, Avik W. Ghosh, and Supriyo Datta. First-principles analysis of molecular conduction using quantum chemistry software. *Chem. Phys.*, 281(2-3):171–187, August 2002.

[77] N. Mingo and Liu Yang. Phonon transport in nanowires coated with an amorphous material: An atomistic green's function approach. *Phys. Rev. B*, 68(24):245406, 2003.

[78] Jian-Sheng Wang, Jian Wang, and Nan Zeng. Nonequilibrium green's function approach to mesoscopic thermal transport. *Phys. Rev. B*, 74(3):033408, 2006.

[79] N. Mingo. Anharmonic phonon flow through molecular-sized junctions. *Phys. Rev. B*, 74(12):125402, 2006.

[80] Tomomi Shimazaki and Koichi Yamashita. Theoretical study of molecular conduction: I. Effective Green's function based on perturbation theory. *Int. J. Quantum Chem.*, 106(4):803–813, 2006.

[81] Takahiro Yamamoto and Kazuyuki Watanabe. Nonequilibrium green's function approach to phonon transport in defective carbon nanotubes. *Phys. Rev. Lett.*, 96(25):255503, 2006.

[82] T. S. Tighe, J. M. Worlock, and M. L. Roukes. Direct thermal conductance measurements on suspended monocrystalline nanostructures. *Appl. Phys. Lett.*, 70(20):2687–2689, 1997.

[83] W. Fon, K. C. Schwab, J. M. Worlock, and M. L. Roukes. Phonon scattering mechanisms in suspended nanostructures from 4 to 40 k. *Phys. Rev. B*, 66(4):045302, Jul 2002.

[84] P. Kim, L. Shi, A. Majumdar, and P. L. McEuen. Thermal transport measurements of individual multiwalled nanotubes. *Phys. Rev. Lett.*, 87(21):215502, Oct 2001.

[85] Li Shi, Deyu Li, Choongho Yu, Wanyoung Jang, Dohyung Kim, Zhen Yao, Philip Kim, and Arunava Majumdar. Measuring thermal and thermoelectric properties of one-dimensional nanostructures using a microfabricated device. *Journal of Heat Transfer*, 125(5):881–888, 2003.

[86] C. Yu, L. Shi, Z. Yao, D. Li, and A. Majumdar. Thermal conductance and thermopower of an individual single-wall carbon nanotube. *Nano Lett.*, 5(9):1842–1846, 2005.

[87] Deyu Li, Yiying Wu, Philip Kim, Li Shi, Peidong Yang, and Arun Majumdar. Thermal conductivity of individual silicon nanowires. *Appl. Phys. Lett.*, 83(14):2934–2936, 2003.

[88] W. Yi, L. Lu, Zhang Dian-lin, Z. W. Pan, and S. S. Xie. Linear specific heat of carbon nanotubes. *Phys. Rev. B*, 59(14):R9015–R9018, Apr 1999.

[89] Tae Y. Choi, Dimos Poulikakos, Joy Tharian, and Urs Sennhauser. Measurement of thermal conductivity of individual multiwalled carbon nanotubes by the 3-omega method. *Appl. Phys. Lett.*, 87(1):013108, 2005.

[90] Zhao Liang Wang, Da Wei Tang, Xiao Bo Li, Xing Hua Zheng, Wei Gang Zhang, Li Xin Zheng, Yuntian T. Zhu, Ai Zi Jin, Hai Fang Yang, and Chang Zhi Gu. Length-dependent thermal conductivity of an individual single-wall carbon nanotube. *Appl. Phys. Lett.*, 91(12):123119, 2007.

[91] Olivier Bourgeois, Thierry Fournier, and Jacques Chaussy. Measurement of the

thermal conductance of silicon nanowires at low temperature. *J. Appl. Phys.*, 101(1):016104, 2007.

[92] M. N. Ou, T. J. Yang, S. R. Harutyunyan, Y. Y. Chen, C. D. Chen, and S. J. Lai. Electrical and thermal transport in single nickel nanowire. *Appl. Phys. Lett.*, 92(6):063101, 2008.

[93] C. Dames, S. Chen, C. T. Harris, J. Y. Huang, Z. F. Ren, M. S. Dresselhaus, and G. Chen. A hot-wire probe for thermal measurements of nanowires and nanotubes inside a transmission electron microscope. *Rev. Sci. Instrum.*, 78(10):104903, 2007.

[94] Motoo Fujii, Xing Zhang, Huaqing Xie, Hiroki Ago, Koji Takahashi, Tatsuya Ikuta, Hidekazu Abe, and Tetsuo Shimizu. Measuring the thermal conductivity of a single carbon nanotube. *Phys. Rev. Lett.*, 95(6):065502, 2005.

[95] E. Pop, D. Mann, Q. Wang, K. Goodson, and H. Dai. Thermal conductance of an individual single-wall carbon nanotube above room temperature. *Nano Lett.*, 6(1):96–100, 2006.

[96] C. W. Chang, D. Okawa, A. Majumdar, and A. Zettl. Solid-state thermal rectifier. *Science*, 314(5802):1121–1124, 2006.

[97] Stephen L. Mayo, Barry D. Olafson, and William A. Goddard III. DREIDING: a generic force field for molecular simulations. *J. Phys. Chem*, 94:8897 – 8909, 1990.

[98] Andrew R. Leach. *Molecular modelling principles and applications*. Pearson Education, 2 edition, 2001.

[99] Shuichi Nose. A unified formulation of the constant temperature molecular dynamics methods. *J. Chem. Phys.*, 81(1):511–519, 1984.

[100] William G. Hoover. Canonical dynamics: Equilibrium phase-space distributions. *Phys. Rev. A*, 31(3):1695–1697, Mar 1985.

[101] Glenn J. Martyna, Michael L. Klein, and Mark Tuckerman. Nos[e-acute]–Hoover chains: The canonical ensemble via continuous dynamics. *J. Chem. Phys.*, 97(4):2635–2643, 1992.

[102] Stefano Lepri, Roberto Livi, and Antonio Politi. Thermal conduction in classical low-dimensional lattices. *Phys. Rep.*, 377(1):1–80, April 2003.

[103] Alexander L Fetter and John Dirk Walecka. *Quantum theory of many-particle systems*. San Francisco, McGraw-Hill [1971], 1971.

[104] D. C. Langreth. Linear and non-linear response theory with applications. In J. T. Devreese and V. E. van Doren, editors, *Linear and Nonlinear Electron Transport in Solids*. Plenum Press, New York and London, 1976.

[105] H. Haug and AP Jauho. *Quantum Kinetics in Transport and Optics of Semiconductors*. Springer, 1996.

[106] Jian-Sheng Wang, Nan Zeng, Jian Wang, and Chee Kwan Gan. Nonequilibrium green's function method for thermal transport in junctions. *Phys. Rev. E*, 75(6):061128, 2007.

[107] M P Lopez Sancho, J M Lopez Sancho, J M L Sancho, and J Rubio. Highly convergent schemes for the calculation of bulk and surface green functions. *J. Phys. F: Metal Physics*, 15(4):851–858, 1985.

[108] A. Buldum, DM Leitner, and S. Ciraci. Thermal conduction through a molecule. *Europhys. Lett.*, 47(2):208–212, 1999.

[109] Jeremy Taylor, Hong Guo, and Jian Wang. Ab initio modeling of open systems: Charge transfer, electron conduction, and molecular switching of a C_{60} device. *Phys. Rev. B*, 63(12):121104, Mar 2001.

[110] J. Heurich, J. C. Cuevas, W. Wenzel, and G. Schön. Electrical Transport through Single-Molecule Junctions: From Molecular Orbitals to Conduction Channels. *Phys. Rev. Lett.*, 88(25):256803, Jun 2002.

[111] M. Di Ventra, S. T. Pantelides, and N. D. Lang. First-Principles Calculation of Transport Properties of a Molecular Device. *Phys. Rev. Lett.*, 84(5):979–982, Jan 2000.

[112] Dvira Segal and Abraham Nitzan. Heat rectification in molecular junctions. *J. Chem. Phys.*, 122(19):194704, 2005.

[113] Sebastian G. Volz and Gang Chen. Molecular-dynamics simulation of thermal conductivity of silicon crystals. *Phys. Rev. B*, 61(4):2651–2656, Jan 2000.

[114] J. Hone, M. Whitney, C. Piskoti, and A. Zettl. Thermal conductivity of single-walled carbon nanotubes. *Phys. Rev. B*, 59(4):R2514–R2516, Jan 1999.

[115] S. U. S. Choi, Z. G. Zhang, W. Yu, F. E. Lockwood, and E. A. Grulke. Anomalous thermal conductivity enhancement in nanotube suspensions. *Appl. Phys. Lett.*, 79(14):2252–2254, 2001.

[116] David G. Cahill, Kenneth Goodson, and Arunava Majumdar. Thermometry and thermal transport in micro/nanoscale solid-state devices and structures. *Journal of Heat Transfer*, 124(2):223–241, 2002.

[117] Scott T. Huxtable, David G. Cahill, Sergei Shenogin, Liping Xue, Rahmi Ozisik, Paul Barone, Monica Usrey, Michael S. Strano, Giles Siddons, Moonsub Shim,

and Pawel Keblinski. Interfacial heat flow in carbon nanotube suspensions. *Nat Mater*, 2(11):731–734, November 2003.

[118] Y. Sungtaek Ju. Phonon heat transport in silicon nanostructures. *Appl. Phys. Lett.*, 87(15):153106, 2005.

[119] T.-Y. Choi, D. Poulikakos, J. Tharian, and U. Sennhauser. Measurement of the thermal conductivity of individual carbon nanotubes by the four-point three-omega method. *Nano Lett.*, 6(8):1589–1593, 2006.

[120] M. J. Frisch, G. W. Trucks, H. B. Schlegel, G. E. Scuseria, M. A. Robb, J. R. Cheeseman, J. A. Montgomery, Jr., T. Vreven, K. N. Kudin, J. C. Burant, J. M. Millam, S. S. Iyengar, J. Tomasi, V. Barone, B. Mennucci, M. Cossi, G. Scalmani, N. Rega, G. A. Petersson, H. Nakatsuji, M. Hada, M. Ehara, K. Toyota, R. Fukuda, J. Hasegawa, M. Ishida, T. Nakajima, Y. Honda, O. Kitao, H. Nakai, M. Klene, X. Li, J. E. Knox, H. P. Hratchian, J. B. Cross, V. Bakken, C. Adamo, J. Jaramillo, R. Gomperts, R. E. Stratmann, O. Yazyev, A. J. Austin, R. Cammi, C. Pomelli, J. W. Ochterski, P. Y. Ayala, K. Morokuma, G. A. Voth, P. Salvador, J. J. Dannenberg, V. G. Zakrzewski, S. Dapprich, A. D. Daniels, M. C. Strain, O. Farkas, D. K. Malick, A. D. Rabuck, K. Raghavachari, J. B. Foresman, J. V. Ortiz, Q. Cui, A. G. Baboul, S. Clifford, J. Cioslowski, B. B. Stefanov, G. Liu, A. Liashenko, P. Piskorz, I. Komaromi, R. L. Martin, D. J. Fox, T. Keith, M. A. Al-Laham, C. Y. Peng, A. Nanayakkara, M. Challacombe, P. M. W. Gill, B. Johnson, W. Chen, M. W. Wong, C. Gonzalez, and J. A. Pople. Gaussian 03, Revision C.02. Gaussian, Inc., Wallingford, CT, 2004.

[121] M. Terraneo, M. Peyrard, and G. Casati. Controlling the energy flow in nonlinear lattices: A model for a thermal rectifier. *Phys. Rev. Lett.*, 88(9):094302, Feb 2002.

[122] Baowen Li, Lei Wang, and Giulio Casati. Thermal diode: Rectification of heat flux. *Phys. Rev. Lett.*, 93(18):184301, 2004.

[123] Baowen Li, Jinghua Lan, and Lei Wang. Interface thermal resistance between dissimilar anharmonic lattices. *Phys. Rev. Lett.*, 95(10):104302, 2005.

[124] Jinghua Lan and Baowen Li. Thermal rectifying effect in two-dimensional anharmonic lattices. *Phys. Rev. B*, 74(21):214305, 2006.

[125] Jinghua Lan and Baowen Li. Vibrational spectra and thermal rectification in three-dimensional anharmonic lattices. *Phys. Rev. B*, 75(21):214302, 2007.

[126] Nuo Yang, Nianbei Li, Lei Wang, and Baowen Li. Thermal rectification and negative differential thermal resistance in lattices with mass gradient. *Phys. Rev. B*, 76(2):020301(R), 2007.

[127] Gang Wu and Baowen Li. Thermal rectification in carbon nanotube intramolecular junctions: Molecular dynamics calculations. *Phys. Rev. B*, 76(8):085424, 2007.

[128] Dvira Segal and Abraham Nitzan. Spin-boson thermal rectifier. *Phys. Rev. Lett.*, 94(3):034301, 2005.

[129] Dvira Segal. Heat flow in nonlinear molecular junctions: Master equation analysis. *Phys. Rev. B*, 73(20):205415, 2006.

Appendix A

Surface Green's functions

```
"""Calculating surface green functions of a quasi one dimensional system"""
from scipy import *

def sgf(omega, H_00, H_01):
    # initialize
    E = Es = H_00
    alpha, beta = H_01, H_01.H
    eta, eps = 1e-14, 1e-10
    m, n = H_00.shape
    assert(m == n)
    omega_matrix = (omega**2 + eta * 1j) * mat(identity(n))

    while True:
        temp = (omega_matrix - E).I
        alpha_new = alpha * temp * alpha
        beta_new = beta * temp * beta
        E_new = E + alpha * temp * beta + beta * temp * alpha
        Es_new = Es + alpha * temp * beta

        if abs(max(asarray(E_new - E).flat.real)) < eps:
```

```
            break
        else:
            alpha = alpha_new
            beta = beta_new
            E = E_new
            Es = Es_new

    return (omega_matrix − Es).I
```

Appendix B

Recursive expansion of Green's functions

The following gives Mathematica code to compute the expansion of Green's functions according to the recursive rules discussed in Sec. 4.6. The coupling $T[i, j, k]$ is denoted by λ, which controls the order of expansion. Maxorder is the highest order to compute, Grn[{a,b,c},n] is the Green's function with leg [a,b,c]. n indicates the number of λ generated so far in the final graph. At the highest (top) level, we take n=0. Two terminating conditions for the grand recursion are first set. Grn[] implements the resursive rules and also symmetries with respect to the arguments with the orderless attributes.

```
Clear[maxorder, Grn, G, ts, permuterules];
maxorder = 4
SetAttributes[G, Orderless];
Grn[{}, n_]:= - I;
Grn[arg_List, n_]:=0/;n > maxorder
Grn[arg_List, n_Integer]:=
Module[{len, k, j, newarg, res, tdummy},
```

```
len = Length[arg];
tdummy = ToExpression["t" <> ToString[n]];
res = 0;
For[k = 1, k ≤ len, ++k,
newarg = Insert[ReplacePart[arg, tdummy, k],
tdummy, k];
res+=(1/len) * λ * G[arg[[k]], tdummy]*
Grn[newarg, n + 1];
For[j = 1, j ≤ len, ++j,
If[j ≠ k,
res+=(1/len) * I * G[arg[[k]], arg[[j]]]*
Grn[Delete[arg, {{k}, {j}}], n];
];
];
];
res//Simplify//Expand
]
g12 = Grn[{1, 2}, 0];
```

Canonize[] takes a term, puts it into the canonical form by permuting all the dummy indices t_n and chooses a particular one.

```
ts = Table[ToExpression["t" <> ToString[k]],
{k, 0, maxorder − 1}];
permuterules = Map[Thread[ts → #]&, Permutations[ts]];

canonize[fyn_]:=Module[{flist},
flist = Sort[fyn/.permuterules];
Return[flist[[1]]]
```

]

canonize/@g12

Draw Feynman diagrams from the above results: (1) draw n vertexes if there is a λ^n, label the vertexes as t_0, t_1, ..., t_{n-1}, plus two extra terminals 1 and 2, connect with lines if there is a Green's function G[a,b]. G[a,b] is the Green's function without the cubic interaction, still nonequilibrium (contour ordered) Green's functions. The numerical factors are the same as in the above formula. Finally, the dummy indices t_k=(j,t) have to be summed (for lattice site indices) and integrated (for time on the contour).